Applied Battery Research for Transportation
(B&R No. VT-1102000)

Progress Report
for
First Quarter FY 2013

Contributions from
Argonne National Laboratory
Army Research Laboratory
Brookhaven National Laboratory
Idaho National Laboratory
Jet Propulsion Laboratory
Lawrence Berkeley National Laboratory
National Renewable Energy Laboratory
Oak Ridge National Laboratory
Sandia National Laboratories

March 2013

Applied Battery Research for Transportation Program
First Quarter Progress Report for FY 2013

This quarterly progress report describes the activities being conducted in support of DOE's Applied Battery Research for Transportation (ABR) Program. This program focuses on helping the industrial developers to overcome barriers for Li-Ion batteries for use in plug-in hybrid electric vehicles (PHEVs). In its goal of developing low-emission high fuel economy light-duty HEVs and PHEVs, the DOE and U.S. DRIVE established requirements for energy storage devices in these applications. The Vehicle Technologies Program at DOE has focused the efforts of this applied battery R&D program on the PHEV application.

Through the U.S. DRIVE Partnership, DOE is currently supporting the development of advanced Li-Ion batteries with industry for HEV, PHEV, and EV applications. The industrial developers have made significant progress in developing such batteries for HEV applications and there are new challenges associated with developing viable battery technologies for the PHEV application, especially when targeting the 40-mile all electric range. In addition to the calendar life, abuse tolerance, and cost challenges that exist for Li-Ion batteries in the HEV application, now the issue of providing sufficient energy within the weight and volume requirements becomes a huge challenge, as does cycle life. Also, the abuse tolerance and cost challenges become even greater. The Applied Battery Research for Transportation program is directed at assisting the industrial developers to identify the major factors responsible for the technical barriers and to find viable cost-effective solutions to them. The goal is to facilitate the development of low-cost cell chemistries that can simultaneously meet the life, performance, abuse tolerance, and cost goals that have been established by the U.S. DRIVE Partnership.

The ABR Program is organized to identify and develop advanced electrochemical couples, and further to efficiently move promising electrochemical couples from the research environment to industrial developers for evaluation. An overview of this process is given in Figure 1. Argonne has joined with other national laboratories, universities, and industry to create an integrated team to accomplish the program goals. There is a significant effort within the program to develop promising advanced electrochemical couples. As these electrochemical couples or others identified from outside the program exhibit reproducible cutting-edge results in small lab cells, the component materials are scaled-up as needed by the Materials Engineering Research Facility (MERF) and prototype cells are built by the Cell Fabrication Facility (CFF). The advanced prototype cells are thoroughly tested, examined, and characterized by a broad spectrum of studies, including utilizing the Electrochemical Analysis and Diagnostic Laboratory (EADL) and the Post-Test Facility (PTF). This information is fed back to the material researchers, and further offered to industrial developers along with prototype cells and scaled materials.

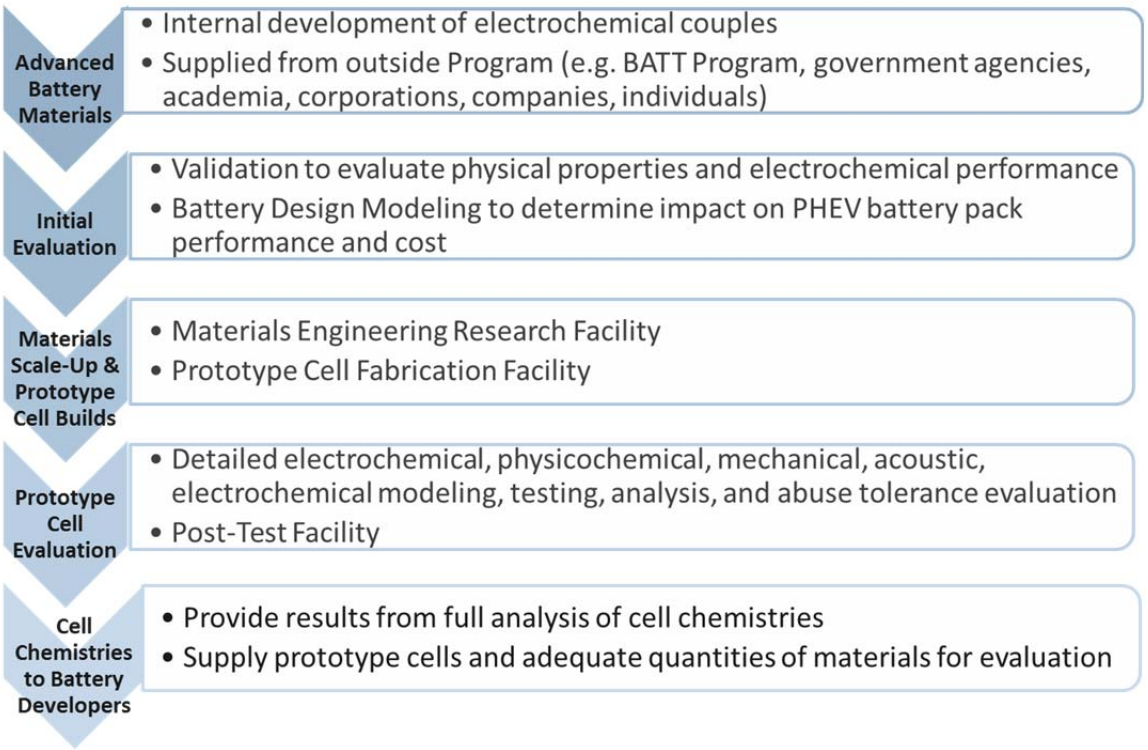

Figure 1. High level view of ABR program.

Initially, the ABR Program was organized into three main technical task areas to address the challenges for PHEVs:

(1) Battery Cell Materials Development—focuses on research, development, and engineering of advanced materials and cell chemistries that simultaneously address the life, performance, abuse tolerance, and cost issues.
(2) Calendar & Cycle Life Studies—deals with understanding the factors that limit life in different Li-Ion cell chemistries, which are used as feedback to Task 1. This task also deals with the establishment and operation of in-program cell fabrication capabilities for use in these life studies.
(3) Abuse Tolerance Studies—deals with understanding the factors that limit the inherent thermal and overcharge abuse tolerance of different Li-ion cell materials and chemistries, as well as developing approaches for enhancing their abuse tolerance.

The ABR Program is currently going through a major reorganization. The broad range of projects is being further integrated into core facility teams and efforts, along with larger electrochemical couples and electrolyte development projects. As part of the restructuring a crosscutting project focused on enabling the Argonne high energy composite layered cathode $xLi_2MnO_3 \bullet (1-x)LiMO_2$ (M = Ni, Mn, Co), also referred to as lithium and manganese rich NMC material (LMR-NMC), for the 40-mile PHEV (PHEV-40) application. This class of materials offers the potential for capacities exceeding

250mAh/g, excellent cycle and calendar life, and outstanding abuse tolerance. However, the material currently possesses a voltage fade issue (and other related issues) that affects its long-term cycle life and needs to be resolved. The voltage fade project results are reported under Task 1 although they cover activities in Task 2 also.

The list of current projects is given in the table, with the individual reports compiled in the Appendix.

Organization	AMR Project ID	AOP Project ID	Title	PI/Contact Point	Page Number
			Task 1: Battery Cell Materials Development		
ANL	ES161	1.2	Voltage Fade in the LMR-NMC Materials	Anthony Burrell	6
ANL	ES167	IV. E.1.1	Process Development and Scale up of Advanced Cathode Materials	Gregory Krumdick	33
ANL	ES168	IV. E.1.2	Process Development and Scale up of Advanced Electrolyte Materials	Gregory Krumdick	37
ARL	ES024		High Voltage Electrolytes for Li-ion Batteries	Kang Xu and Richard Jow	41
JPL	ES026		Electrolytes for Use in High Energy Li-Ion Batteries with Wide Operating Temperature Range	Marshall Smart	49
INL	ES027		Novel Phosphazene Compounds for Enhancing Electrolyte Stability and Safety of Lithium-ion Cells	Kevin Gering	57
LBNL	ES029	1.2.2	Scale-up and Testing of Advanced Materials from the BATT Program	Vincent Battaglia	66
ORNL	ES164	18502	Overcoming Processing Cost Barriers of High Performance Lithium Ion Battery Electrodes	David Wood	69
NREL	ES162		Development of Industrially Viable Battery Electrode Coatings	Robert Tenent	77
NREL	ES196	25194	Evaluate ALD Coatings of LGCPI Cathode Materials and Electrodes	Shriram Santhanagopalan	81

Organization	AMR Project ID	AOP Project ID	Title	PI/Contact Point	Page Number
			Task 2: Calendar & Cycle Life Studies		
ANL	ES030	1.1	Cell Fabrication Facility Team Production and Research Activities	Andrew Jansen	84
LBNL	ES033	1.1.1 and 2.4	Strategies to Enable the Use of High-Voltage Cathodes and Diagnostic Evaluation of ABRT Program Lithium Battery Chemistries	Robert Kostecki	105
BNL	ES034	1.1, 2.4, and 3.3	Life and Abuse Tolerance Diagnostic Studies for High Energy Density PHEV Batteries	Xiao-Qing Yang	108
ORNL	ES165	18502	Roll-to-Roll Electrode Processing NDE and Materials Characterization for Advanced Lithium Secondary Batteries	David Wood	111
			Task 3: Abuse Tolerance Studies		
SNL	ES036	3.2	Abuse Tolerance Improvements	Chris Orendorff	119
LBNL	ES037	3.3	Overcharge Protection for PHEV Batteries	Guoying Chen	123

APPENDIX

Individual Project Progress Reports

TASK 1
Battery Cell Materials Development

Project Number: 1.2 (ES161)

Project Title: Voltage Fade in the LMR-NMC Materials

Project PI, Institution: Anthony Burrell, Argonne National Laboratory

Collaborators (include industry): Ali Abouimrane, Daniel Abraham, Khalil Amine, Mahalingam Balasubramanian, Javier Bareno Garcia-Ontiveros, Ilias Belharouak, Roy Benedek, Ira Bloom, Zonghai Chen, Dennis Dees, Kevin Gallagher, Hakim Iddir, Brian Ingram, Christopher Johnson, Wenquan Lu, Nenad Markovic, Dean Miller, Yan Qin, Yang Ren, Michael Thackeray, Lynn Trahey, and John Vaughey all from Argonne National Laboratory

Project Start/End Dates: March 2012 / September 2014

Objectives: The objective of the work is to enable the Argonne high energy composite layered cathode $xLi_2MnO_3 \bullet (1-x)LiMO_2$ (M = Ni, Mn, Co), also referred to as lithium and manganese rich NMC material (LMR-NMC), for the 40-mile PHEV (PHEV-40) application. This class of materials offers the potential for capacities exceeding 250mAh/g, excellent cycle and calendar life, and outstanding abuse tolerance. This material currently possesses a voltage fade issue (and other related issues) that effects its long-term cycle life and this issue needs to be resolved.

Approach: Bring together a diverse technical team that will share data and expertise to "fix" voltage fade in the LMR-NMC cathode materials. This will be a single team effort – not multiple PI's working independently on the same problem.

- Definition of the problem and limitations of the composite cathode materials.
- Data collection and review of compositional variety available using combinatorial methods.
- Modeling and Theory.
- Fundamental characterization of the composite cathode materials.
- Understand the connections between electrochemistry and structure.
- Synthesis.
- Post treatment/system level fixes.

Milestones:

(a.) Determine if coatings have a positive effect on voltage fade – go/no-go on coatings within this project. May, 2013 (On schedule)

(b.) Determine the origin of the enhanced capacity in the LMR-NMC materials. September, 2014 (On schedule)

(c.) Determine the effect of synthesis (if any) on voltage fade. September, 2013 (On schedule)

(d.) Establish the connection between voltage fade and the hysteresis in the LMRNMC materials. September, 2013 (On schedule)
(e.) Synthesize, characterize and optimize the composition of 'layered-layered-' and 'layered-layered-spinel' electrodes and to determine the causes for, and to counter, the voltage fade phenomenon. September, 2014 (On schedule)
(f.) Investigate the addition of dopants such as Ni to the xLi_2MnO_3•$(1-x)LiCoO_2$ 'layered-layered' system. September, 2014 (On schedule)
(g.) Using first principles identify strategies for designing high-capacity VF-free cathode materials, and calculate properties of candidate materials that implement these strategies. September, 2014 (On schedule)
(h.) Analyze the atomic order in NMR-NMC materials to predict Fermi-contact NMR shifts for different Li atomic environments and assist of the characterization work. September, 2014 (On schedule)

Financial data: $4000K/year

PROGRESS TOWARD MILESTONES

Energy density is a critically important characteristic for energy storage devices, as it not only describes the energy stored per unit mass or volume but also scales well with the predicted real-world battery costs. Practical high-energy lithium-ion cells, in which a high potential positive electrode material is cycled against a low-potential graphitic negative electrode over a fixed voltage window, face almost inevitably a loss in deliverable energy when repeatedly charged and discharged. This energy loss can typically be traced back to three major causes: i) chemical trapping and loss of mobile lithium within the cell, ii) loss of available lithium-hosting sites, and iii) rising cell resistances. That is, lithium can be trapped in parasitic electrochemical or chemical side reactions throughout entire cell; particle isolation and structural changes can reduce the total number of accessible lithium-hosting sites in the active materials; and cell resistances increase due to growing surface films, a degrading electrolyte, or degrading electrodes slowing down charge carrier diffusion and migration.

There exists yet another mechanism causing the cell's energy output to decrease under certain conditions: a drop in the electrochemical potential of the positive electrode over time and/or cycle number. This phenomenon, referred to as voltage fade, or decay, occurs only for certain material chemistries and/or under specific cycling conditions. As we will show, this phenomenon is a major contributor to the cell's energy fade when a Li-rich layered oxide is cycled beyond ~4.3V versus Li/Li^+ - and all other degradation mechanisms are minimized. To quantify the relative contribution of voltage fade, we have taken a lithium- and manganese-rich transition metal layered-oxide (LMR-NMCs) and compare its performance in two different cell configurations.

Materials and experimental details

For both configurations, the active oxide is the same. It is an LMR-NMC, $0.5Li_2MnO_3$•$0.5LiMn_{0.375}Ni_{0.375}Co_{0.25}O_2$, and is supplied by Toda according to

specifications provided by Argonne. It is commonly referred to as "TodaHE5050". The first cell configuration is what we call our baseline: its specifications are given in Table 1. The second configuration, consisted of an improved positive electrode, provided by Argonne's Cell Fabrication Facility (CFF), and a modified Gen 2 electrolyte. The new electrode was designed to have a longer cycle life through the removal of the graphitic additive, SFG-6. In addition, the electrolyte was modified by adding 2.0 wt. % LiDFOB to the Gen2 electrolyte to also increase cycle life of the positive electrode by decreasing its impedance rise as discussed in several publications. Additional electrode specifications are given in Table 1. It summarizes chemistries and electrode formulations of the positive electrodes tested. Galvanostatic cycling is conducted in 2032-type coin cells (1.6 cm^2 area electrodes) with Li-metal counter electrodes. They are assembled in an Ar-atmosphere glove box (O_2 < 10 ppm, H_2O < 1 ppm) and cycled at exactly 30°C. A standard cycling protocol is used to allow all future work to be directly comparable. This protocol uses moderate charge and discharge rates of ~C/10 to reduce electrode polarization. Electrochemical cycling is carried out over a 2.0 and 4.7 V vs. Li^+/Li voltage window. The protocol also measures cell resistances via a current interrupt technique at various cell voltages during charging and discharging. The current is stopped for 10 minutes and voltages are recorded before and after the stopping period to estimate the cell resistance. This value is then used to estimate the "near equilibrium" average voltage, also referred to as resistance-corrected average voltage.

Table 1. Positive electrodes evaluated for energy and voltage fade

Description	Baseline electrode (by Saft)	Improved electrode (by ANL-CFF)
Active material	86 wt.% $Li_{1.2}Ni_{0.15}Mn_{0.55}Co_{0.1}O_2$ (Toda HE5050)	92 wt.% $Li_{1.2}Ni_{0.15}Mn_{0.55}Co_{0.1}O_2$ (Toda HE5050)
Binder	8 wt.% PVdF (Solvay 5130)	4 wt.% PVdF (Solvay 5130)
Additives	4 wt.% SFG-6 graphite (Timcal) 2 wt.% SuperP (Timcal)	- - 4 wt.% SuperP (Timcal)
Current collector	Al, 15 µm	Al, 20 µm
Electrolyte	1.2 M $LiPF_6$ in ethylene carbonate : ethyl methyl carbonate (3:7 by wt.)	1.2 M $LiPF_6$ in ethylene carbonate : ethyl methyl carbonate (3:7 by wt.) with 2 wt.% LiDFOB
Separator	25 µm thick (Celgard 2325)	
Active loading density	6.64 mg-cm^{-2}	6.57 mg-cm^{-2}
Laminate thickness	35 µm	42 µm

Contribution of voltage fade

Figure 1 shows the energy loss during cycling for the two half-cell configurations. The measured energies as a function of cycle are given by the black solid curves. The average loss per cycle (based on the 20th cycle after the initial activation cycle) was then modeled in a simple and straight forward manner by taking the capacity losses of the electrode, cell resistance effects, and voltage fade of the oxide separately into account. Capacity losses in a half-cell vs. Li metal are caused by oxide particle separation from the electrode's conducting network, but also by loss of active sites within the oxide particles

due to chemical and structural changes in bulk and surface. Resistance effects are the sum of various electrochemical and ohmic polarization losses. The sum of these polarizations typically tends to increase, as cycling continues, due to thickening surface films and a degrading electrolyte. We have recently shown that even the baseline electrode contributes significantly to the overall cell resistance due to a degrading electronic network within the electrode. A simple linear model is then used to quantify the relative contributions for each loss mechanism. The capacity losses are quantified through separate half-cell measurements in which the capacity is measured after the Li metal counter electrode, separator, and electrolyte were replaced with fresh ones to exclude any resistance effects from those components for the capacity measurement. Voltage fade effects were calculated from the resistance-corrected average voltages that were calculated for each cycle using the information obtained by the Argonne cycling protocol. In fact, we found, in a separate investigation, that the electrode formulation and the use of the LiDFOB additive did not impact voltage fade. Resistance effects were quantified by subtracting those two independently calculated effects from the overall energy density.

The results are shown in Figure 1: Resistance increase is very strong in the baseline and therefore makes up for the most of the energy losses. In the improved configuration, resistance effects are much smaller due to the described improvements. The energy losses due to voltage fade are the same for both cell configurations. However, they dominate all other effects in the improved cell configuration. The results show clearly that the contribution of voltage fade to energy output cannot be neglected and significant improvements can be achieved if voltage fade is mitigated.

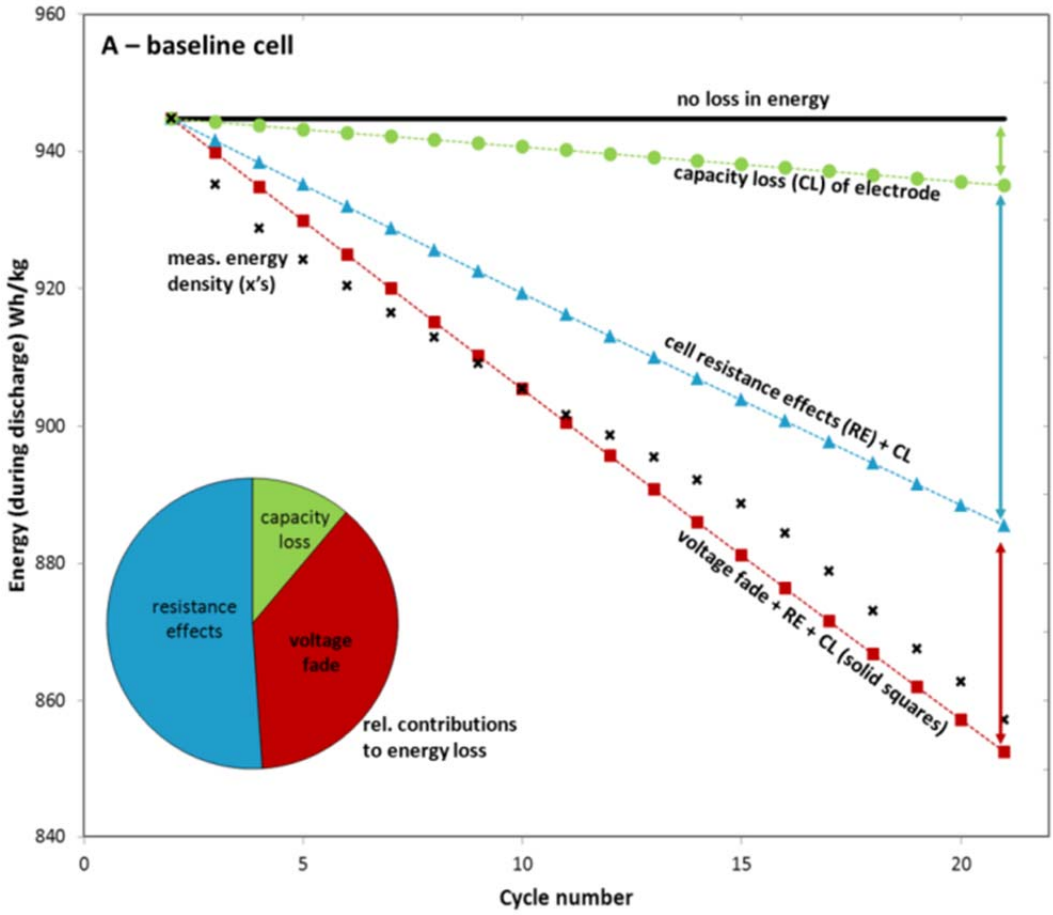
A – baseline cell
no loss in energy
capacity loss (CL) of electrode
meas. energy density (x's)
cell resistance effects (RE) + CL
voltage fade + RE + CL (solid squares)
capacity loss
resistance effects
voltage fade
rel. contributions to energy loss
Energy (during discharge) Wh/kg
Cycle number
960
940
920
900
880
860
840
0
5
10
15
20

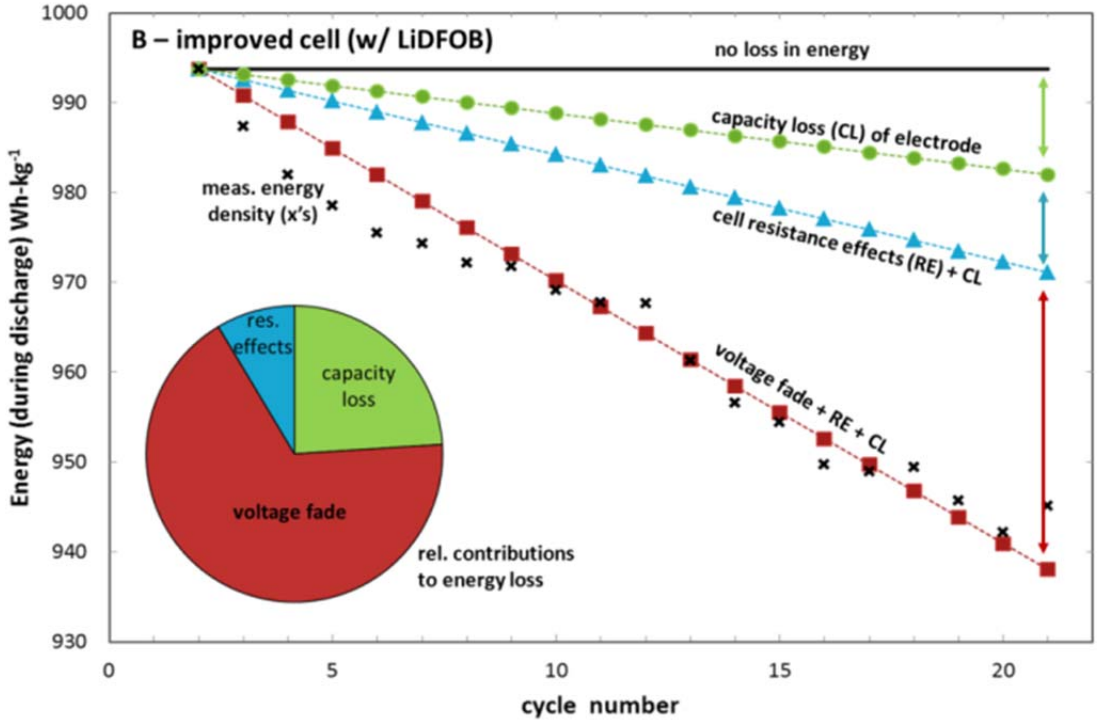
B – improved cell (w/ LiDFOB)
no loss in energy
capacity loss (CL) of electrode
meas. energy density (x's)
cell resistance effects (RE) + CL
voltage fade + RE + CL
res. effects
capacity loss
voltage fade
rel. contributions to energy loss
Energy (during discharge) Wh-kg-1
cycle number
1000
990
980
970
960
950
940
930
0
5
10
15
20

Figure 1. Discharge energy densities as a function of cycle number for (A) baseline and (B) improved cell configurations. The contributions from electrode capacity loss, cell resistance effects, and voltage fade, that cause the energy to decrease, are also plotted according to an average rate of degradation. Details are given in the text. The pie chart displays their relative contributions to the overall loss in energy (solid black curves). The measured energy density after 20 cycles after activation is indicated by the black rectangle. The improved cell configuration shows a significantly reduced contribution from cell resistance effects. As a result, the relative loss in energy density for the improved configuration is only half of that of the baseline one (0.25% vs. 0.5% per cycle). Once the cell performance is optimized, voltage fade is clearly the major cause energy loss.

Testing

A voltage window study was undertaken to tease out the accelerating factors relating to voltage fade. In other words, what electrochemical exposures make voltage fade worse? This study used the baseline material Toda HE5050 in the form of the SAFT fabricated electrodes with Gen2 electrolyte and Celgard 2325 separator against a lithium metal negative electrode. 2032 coin cells were assembled and tested in an oven controlled to 30°C. The testing protocol was a variant on the standardized testing protocol to ensure the average voltage was measured in the same manner in this test as it is in all other studies.

Test protocol:
•1st cycle (activation), 2-4.7 V at 10 mA/g
•2nd cycle, 2-4.7 V at 20 mA/g with current interrupts to measure average voltage
•20 cycles in truncated voltage window at 20 mA/g
•23rd cycle, 2-4.7 V at 20 mA/g with current interrupts to measure average voltage

The cycling windows chosen for the truncated voltage window cycling all included 4.7 V as the high voltage to utilize a high fraction of the lithium content. The lower voltage window potential was varied among different samples to map out the mechanistic space. Figure 1 (left) displays the drop in average IR corrected voltage on discharge between the 23rd and 2nd cycle as a function of lower voltage cutoff during the truncated cycles. The error bars were calculated based on the 95% confidence limits determined from the spread of average voltage measured on the 2nd cycle for all samples.

Two interactions are observable in Figure 2 (top). Voltage fade clearly worsens as the lower voltage cutoff is moved to smaller values in the truncated cycling. The second observation is that a maximum voltage fade appears to exist between 3.0 and 3.3 V. The existence of a maximum is interesting and a hypothesis exists to explain that behavior. However, more experimental studies are necessary to prove the statistical significance of the observation and characterization efforts need to support the current hypothesis. We maintain our focus on the trend that the greatest voltage happens when cycling from a high voltage such as 4.7 V to a lower voltage. This is a somewhat curious trend and raises the question of the importance of calendar time effects in this decay mechanism. To

explore the calendar time dependence, the cycling data was transformed to a calendar time plot and additional data points were measured. The earlier test protocol was repeated on the same samples to put up to 65 cycles on the same coin cell. New coin cells were also made and tested with a hold at 4.7 V for 120, 240, 360, or 480 hours rather than cycling in a truncated window.

Figure 2 (bottom) displays the calendar time behavior of all of the different samples. Once again, it is shown that cycling between 4.7 V and 3.0-3.3 V accelerates voltage fade faster than any other electrochemical exposure. The calendar time study shows a greater extent of voltage fade for the 120 hour hold than the equivalent 2-4.7 V cycling data; however, holding the electrode material at 4.7 V for longer periods of time does not appear to contribute much more to the voltage fade. From this observation, we may conclude that while calendar time is important, cycling to low voltages is necessary to significantly accelerate voltage fade.

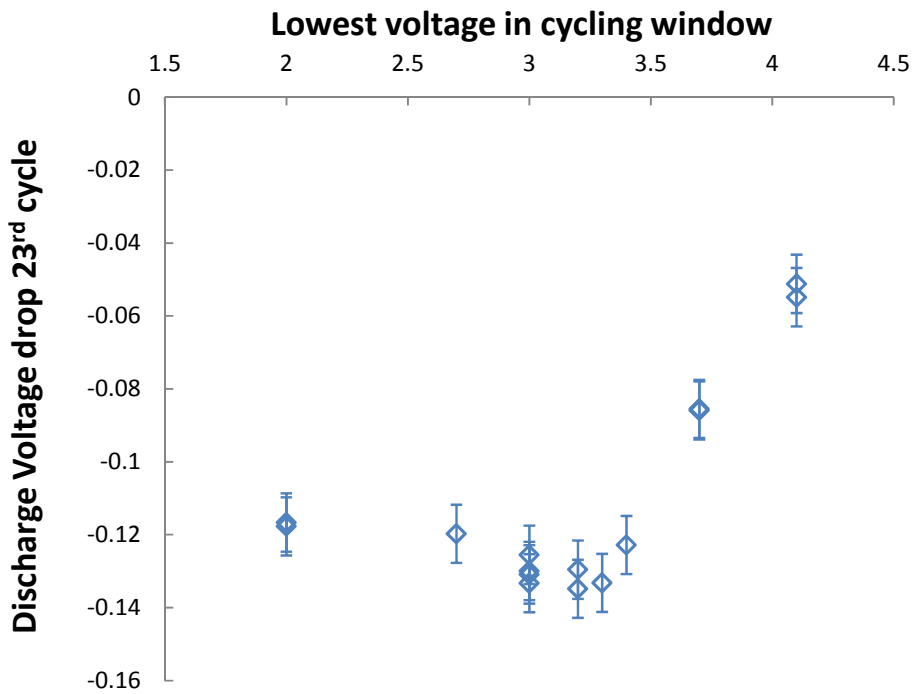

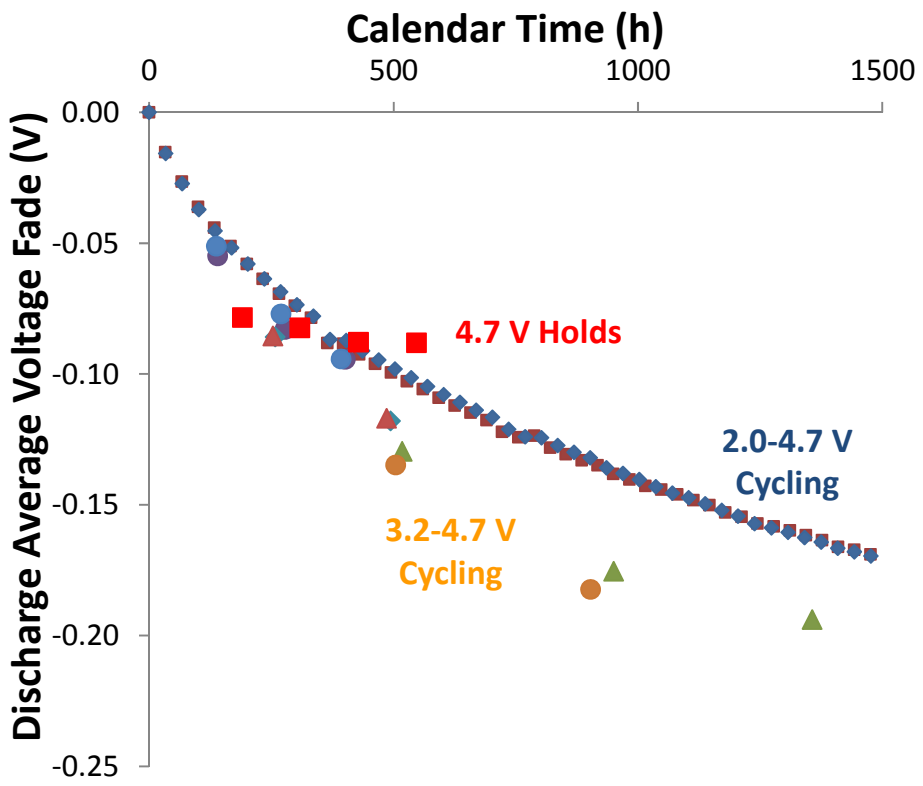

Figure. 2. (top) Drop in IR corrected average voltage on discharge between the 23rd and 2nd cycle. (bottom) Drop in IR corrected average voltage on discharge transformed to calendar time of the test.

These observations can lead us to some mechanistic insight and in-turn a phenomenological voltage fade model. Figure 3 (top) is a cartoon that was derived from the scanning curves of open-circuit voltage measurements to probe hysteresis in LMR-NMC materials. That study, reported in the 2012 annual report, put forth an argument wherein 10-15% of the lithium capacity is responsible for the hysteresis in these materials while the remainder of the material behaves in a manner similar to standard layered intercalation materials. The work (also detailed in J. Croy et al Submitted to JPC-C 2012) also postulates that the migration of transition metals ions into a Li^{+}---M^{z+} dumbbell may be responsible for this behavior. The migration of transition metals, sometimes reversible oftentimes irreversible, has been documented for many layered lithium-based intercalation compounds (Thackeray, Bruce, Ceder, Balasubramanian).

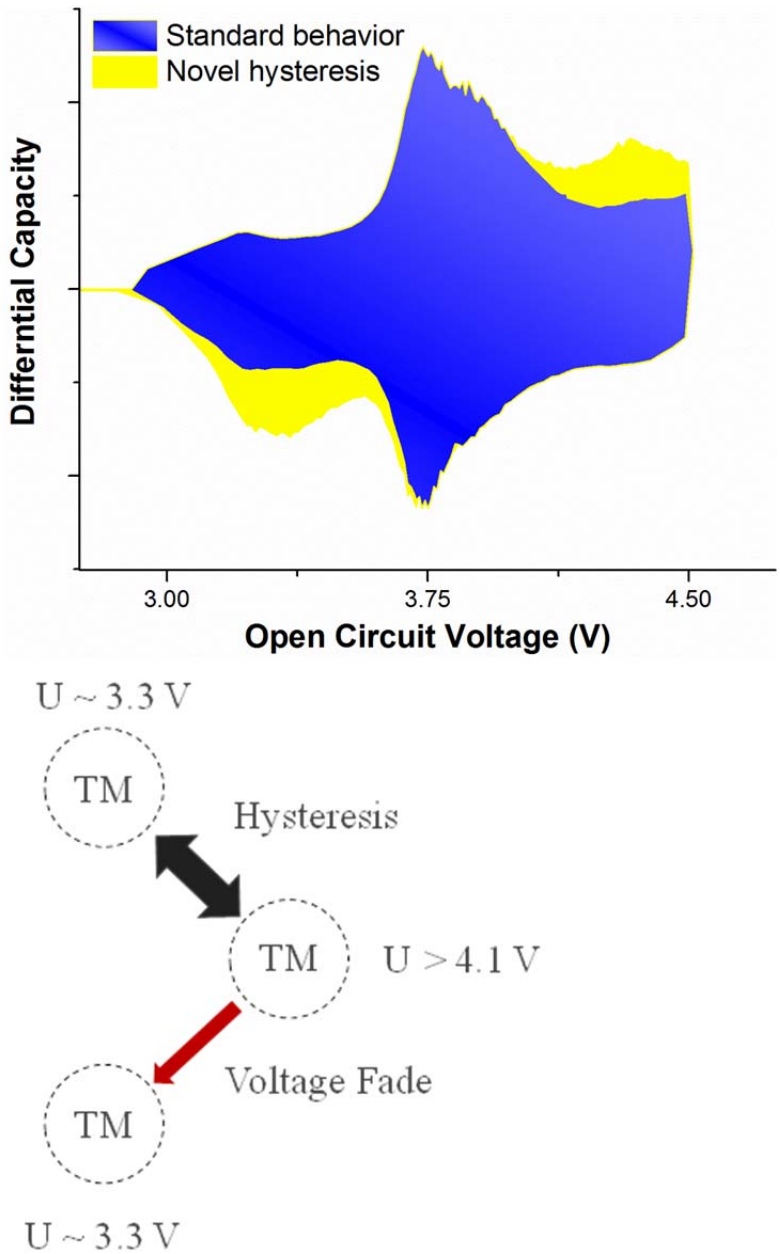

Figure 3. (top) cartoon of hysteresis behavior wherein 10-15% of the lithium content displays a 1V hysteresis (bottom) mechanism displaying the interrelation of hysteresis and voltage fade in LMR-NMC

The formation of a dumbbell defect directly affects at least three nearest neighbor lithium vacancies and could easily change the energy for lithium site occupancy thus resulting in the observed hysteresis. This dumbbell would then be annihilated when a sufficient driving force for the reduction of the transition metal was present, as is the case near 3.3 V. As the cartoon in Figure 3 (bottom) depicts, the hysteresis process is relatively reversible compared to the voltage fade pathway. Both mechanisms would be time dependent and a function of the vacancies surrounding the transition metal ion. Thus the

cartoon is consistent with the experimental cycling and calendar testing observations described above.

Theory

We perform first-principles density functional theory (DFT) at the GGA+U level. Computational cells including up to two hundred atoms in the periodic unit are employed. Extensions of DFT are being employed, such as cluster-expansion techniques (collaboration with J. Bhattacharya, C. Wolverton, NU), which enable calculation of temperature dependent properties. This work is being coordinated with experimental efforts, including particularly the synthesis and NMR groups.

(a) Three strategies for developing VF-free materials have been identified: (i) Shift the redox of the $Li_2M'O_3$ component of the layered-layered composites from O onto M', by substitution of transition elements with higher-valent as well as tetravalent oxidation states (Cr, V, Fe, etc.) for Mn; (ii) Explore materials with alternatives to the usual O3 stacking, such as O2, which are resistant to spinel formation upon cycling; (iii) explore layered-spinel composites without Li-excess, to avoid the irreversibility of the 4.5 V plateau. Theoretical efforts related to these strategies are being coordinated with the synthesis program. Pursuant to strategy (i), calculations are in progress for lithium manganite, $Li_2M'O_3$. We are considering two limits: dilute concentrations of tetravalent M' substitutions for Mn in Li in Li_2MnO_3 and $Li(Ni_{0.5}Mn_{0.5})O_2$ and comparison of the energies of pure $Li_2M'O_3$ in the C2/m and R-3m structures. Preliminary results (Figure. 4, below) show a small preference (hundredths of an eV/ fu) of tetravalent dopants for the monoclinic over the layered structure. For pure $Li_2M'O_3$, the C2/m is predicted to be more stable than the R-3m structure, except perhaps for Cr. Calculations related to strategies (ii) and (iii) are planned, but have not commenced.

(b) A set of effective cluster interaction (ECI) coefficients has been determined for the layered composition NMC333, based on fits to DFT calculations for about three dozen low energy atomic arrangements in the transition metal layer. With the ECI coefficients, Monte Carlo simulations of atomic ordering at relevant temperatures are now being started. Results will be analyzed to predict NMR spectra for pristine specimens.

(c) Progress has been made in the development of a code to apply a heuristic model analysis of Fermi contact shifts to Li NMR spectra, based on DFT predictions of the local environment of Li in relevant cathode materials. Preliminary comparisons with experiment will be made in the next quarter.

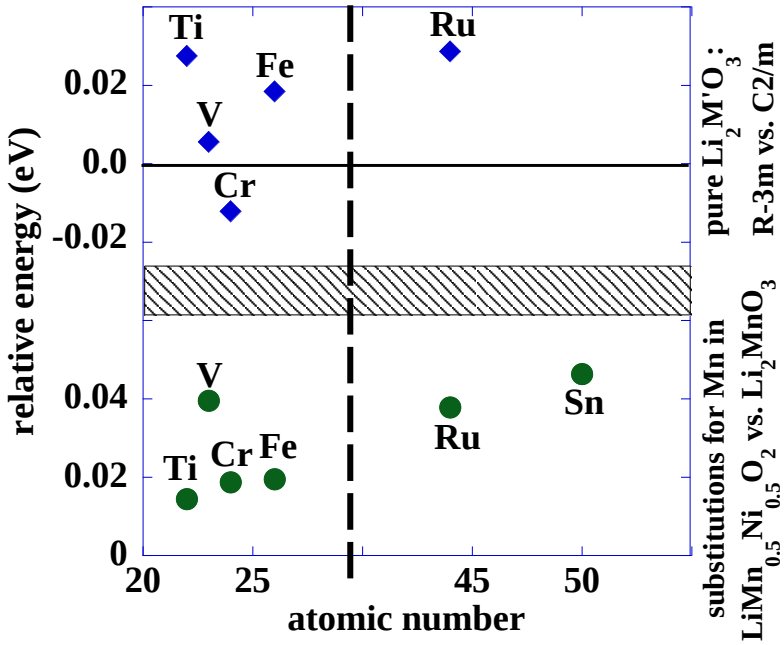

Figure. 4. DFT predictions for TM substitutions for Mn in monoclinic and layered structures. See text for discussion.

Synthesis

We are working on arresting voltage fade (VF) in 'layered-layered' $xLi_2M'O_3$●$(1-x)LiMO_2$ composite electrodes through synthesis that is theory driven. In the previous annual report we focused on the domain structure of Li_2MnO_3 as the $Li_2M'O_3$ model compound. We used acid-treatment to convert the layer stacking from O3 to P3. It is possible to readily convert P3 to P2 then O2 and thus ultimately we want to synthesize an O2-[$xLi_2M'O_3$●$(1-x)LiMO_2$] composite phase that won't convert to spinel. Recent theory work by Benedek and Iddir (2013) suggests that if the M' in $Li_2M'O_3$ can achieve an oxidation state above 4+, then it may be possible to eliminate the voltage plateau and avoid the massive structural rearrangement of $xLi_2M'O_3$●$(1-x)LiMO_2$ to a generic O3-$Li(M_{1-z}M'_z)O_2$ layered phase that is capable of converting to spinel during cycling . As an electroactive compound, we chose Li_2RuO_3, that has the same crystal structure as Li_2MnO_3 and can achieve oxidation states above Ru(IV). Note that in these Li_2MnO_3 materials the oxidation of Mn(IV) is prohibitively high voltage and will not be expected to occur. Li_2RuO_3, $Li_2Zr_{0.1}Ru_{0.9}O_3$ and $Li_2Mn_{0.5}Ru_{0.5}O_3$ were synthesized by a combustion method to ensure single phase products. The electrochemistry of these materials is shown in Figure 5. Briefly the Li_2RuO_3 compound shows no pronounced flat voltage plateau during Ru oxidation which supports the supposition that redox active M' elements will add capacity but not experience a phase change. It still remains to be seen from XRD analysis if this is the case. The mixed $Li_2Mn_{0.5}Ru_{0.5}O_3$ has a plateau that is

shorter and a lower voltage than Li_2MnO_3. Thus, $Li_2Mn_{0.5}Ru_{0.5}O_3$ may be written as a composite: $0.5Li_2MnO_3 \bullet 0.5Li_2RuO_3$. The capacity expected from removal of two lithiums is approximately 340 $mAhg^{-1}$; nearly identical to what is experimentally observed. Theory is in agreement with experiment in this case. Finally, the voltage does fade (average discharge voltage change with cycle number) for $0.5Li_2MnO_3 \bullet 0.5Li_2RuO_3$ but the mechanism of fade is different than conventional $xLi_2M'O_3 \bullet (1-x)LiMO_2$ (M'=Mn; M= Ni, Mn, and Co), that suggests that electroactive M' plays a role in altering voltage fade. Theory has suggested other electroactive M' elements such as V, Cr, and Mo that have a similar ionic radii and CN for Mn, and energetically, prefer to form the monoclinic $Li_2M'O_3$ C2/c instead of $LiMO_2$ rhombohedral R-3m. Future studies will rely on sol-gel synthesis to make homogeneous composite materials which will enable us to compare and evaluate the role of dopants and substitutions to theory predictions.

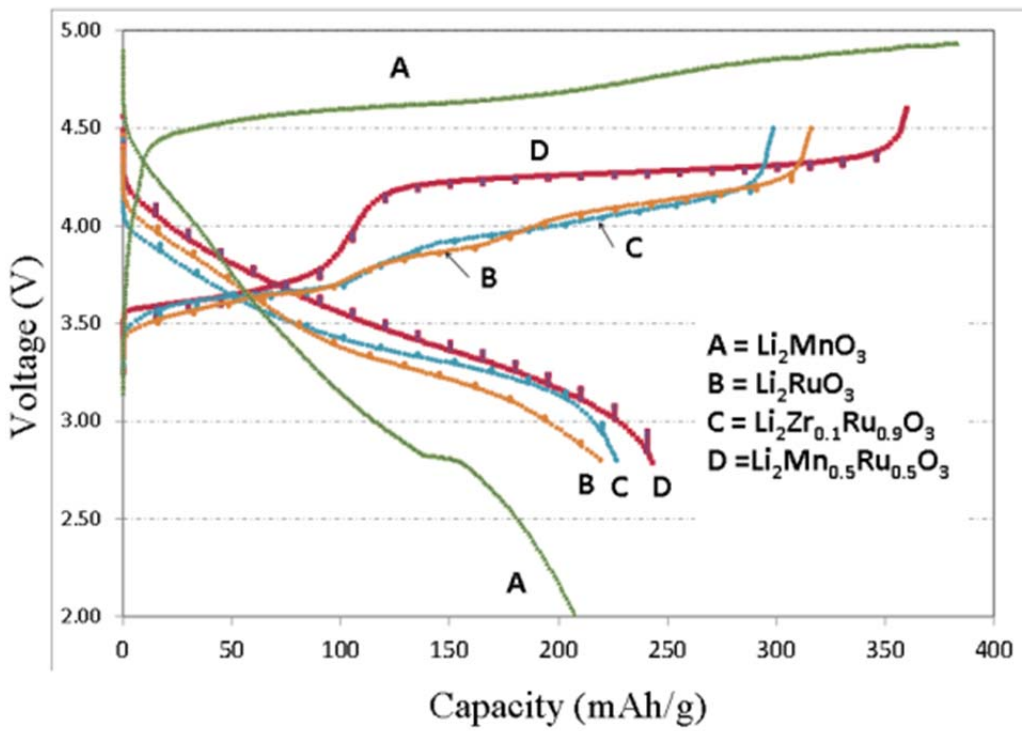

Figure. 5. $Li/Li_2M'O_3$ cells.

The continuous voltage fade during cycling of the LMR-NMC cathode is an obstacle to practical applications of this family of materials. During formation, the activation of the Li_2MnO_3 component increases the capacity of the material; however, this activation may also be responsible for the voltage fade. To enhance the understanding of the effect composition on voltage fade and of the relationships in the low-Co portion of the Li_2MnO_3-$LiCoO_2$-$LiNiO_2$-$LiMnO_2$ phase diagram, we took advantage of the combinatorial equipment in CSE to synthesize 147 samples to explore wide range of LMR-NMC compositions. The nominal compositions for this study are given in Table 1, with the Li stoichiometry varying from 1 to 1.6 in steps of 0.1 in each group, labeled A, B,…, and G, respectively. TODA HE5050, $0.5(Li_2MnO_3)\bullet 0.5(LiNi_{0.375}Mn_{0.375}Co_{0.25})O_2$

or $(Li_2MnO_3)0.5(LiNiO_2)_{0.1875}(LiMnO_2)_{0.1875}(LiCoO_2)_{0.125}$, was included in the study for reference.

Each synthesized sample was characterized by a combination of X-ray diffraction (XRD), inductively-coupled-plasma mass spectrometry (ICP-MS), scanning electron microscopy (SEM) to study overall crystal structure, elemental composition, and particle/laminate morphology. Half-cell of selected compositions were made and tested to characterize energy density, capacity retention and the voltage fade response.

Table 2. List of nominal compositions produced from the combinatorial syntheses.

Group	**Li**	**Ni**	**Co**	**Mn**	**Group**	**Li**	**Ni**	**Co**	**Mn**
1	1~1.6	0.15	0	0.85	**12**	1~1.6	0.25	0.2	0.55
2	1~1.6	0.15	0.05	0.85	**13**	1~1.6	0.3	0	0.7
3	1~1.6	0.15	0.1	0.75	**14**	1~1.6	0.3	0.05	0.65
4	1~1.6	0.2	0	0.8	**15**	1~1.6	0.3	0.1	0.6
5	1~1.6	0.2	0.05	0.75	**16**	1~1.6	0.3	0.15	0.55
6	1~1.6	0.2	0.1	0.7	**17**	1~1.6	0.35	0	0.65
7	1~1.6	0.2	0.15	0.65	**18**	1~1.6	0.35	0.05	0.6
8	1~1.6	0.25	0	0.75	**19**	1~1.6	0.35	0.1	0.55
9	1~1.6	0.25	0.05	0.7	**20**	1~1.6	0.4	0	0.6
10	1~1.6	0.25	0.1	0.65	**21**	1~1.6	0.4	0.05	0.55
11	1~1.6	0.25	0.15	0.6					

Phase relationships. Elemental analysis of these compositions showed that the Li content was lower than expected. As a result, the X-ray diffraction (XRD) patterns of compositions in Groups 4, 5, 6, 7, 13, 16, 17, and 21 showed that the low-Li-stoichiometry compositions were two-phase mixtures. An example XRD pattern is given in Figure 6a and showed evidence of a spinel phase and/or excess Li_2MnO_3 being present. The reflection at 2θ~3.0^o, instead being a single peak, consisted of multiple peaks. These phases were hard to resolve by XRD. At higher Li stoichiometry, the reflection at 2θ~3.0^o became a single peak (Figure 6b), indicating composite-structure formation.

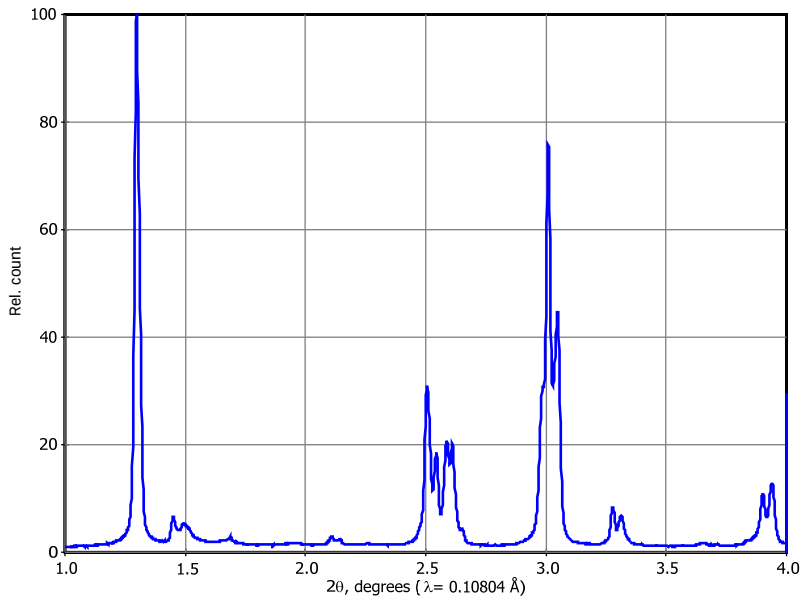

Figure 6a. XRD pattern in the 1.0 to 4.0 range of $LiNi_{0.4}Mn_{0.55}Co_{0.05}O_{2.075}$ (nominal). The complex pattern around 2θ~3.0^{o} is consistent with the presence of multiple phases.

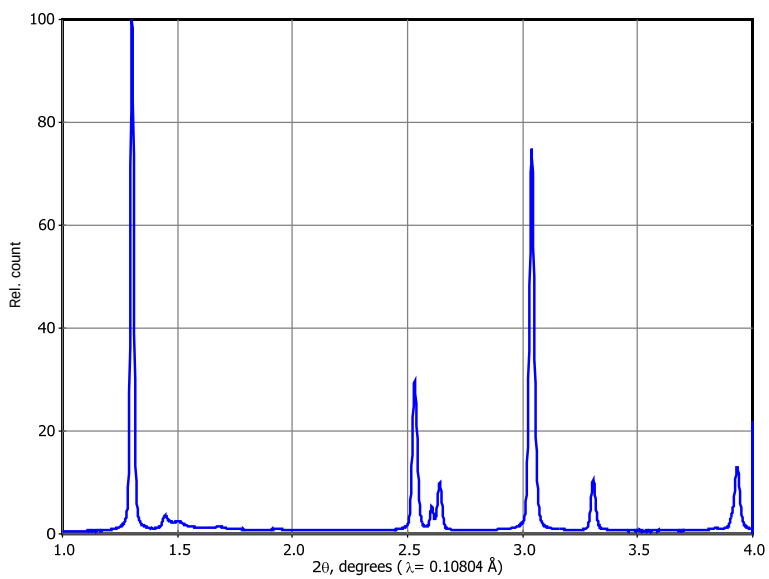

Figure 6b. XRD pattern in the 1.0 to 4.0 range of $Li_{1.6}Ni_{0.4}Mn_{0.55}Co_{0.05}O_{2.375}$ (nominal). The pattern around 2θ~3.0^{o} is consistent with the presence of a composite phase.

Although the integration of $LiMO_2$ and Li_2MnO_3 phases is proposed in the layered-layered composite material, the presence of multiple peaks at $2\theta \sim 3.0^o$ show that the phase relations of these composite materials is very complicated. Figure 7a shows that the XRD patterns for $LiMO_2$ (R3m), Li_2MnO_3 (C2/m), and spinel phase (Fd3m) are very similar to each other, but can be distinguished by using synchrotron X-rays with their higher spatial resolution. Figure 7b shows the XRD patterns for a series of materials in Group 21, with the Li stoichiometry increasing in the vertical direction. With increasing Li stoichiometry, Figure 7b shows that reflection of the spinel (Fd3m) impurity was reduced, and the reflections due to Li_2MnO_3 (C2/m) and $LiMO_2$ (R3m) were broadened, shifted, and, eventually, merged into each other. The data may indicate that interphase of domains of Li_2MnO_3 (C2/m) and $LiMO_2$ (R3m) exist in the composite material as the domains size were reduced and more integrated with each other.

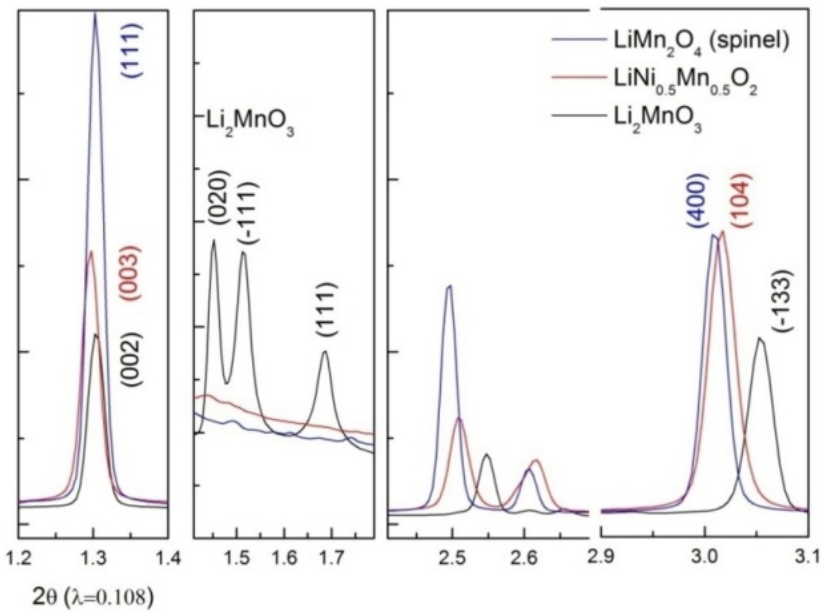

Figure 7a. XRD patterns for $LiMO_2$, Li_2MnO_3, and $LiMn_2O_4$ (spinel).

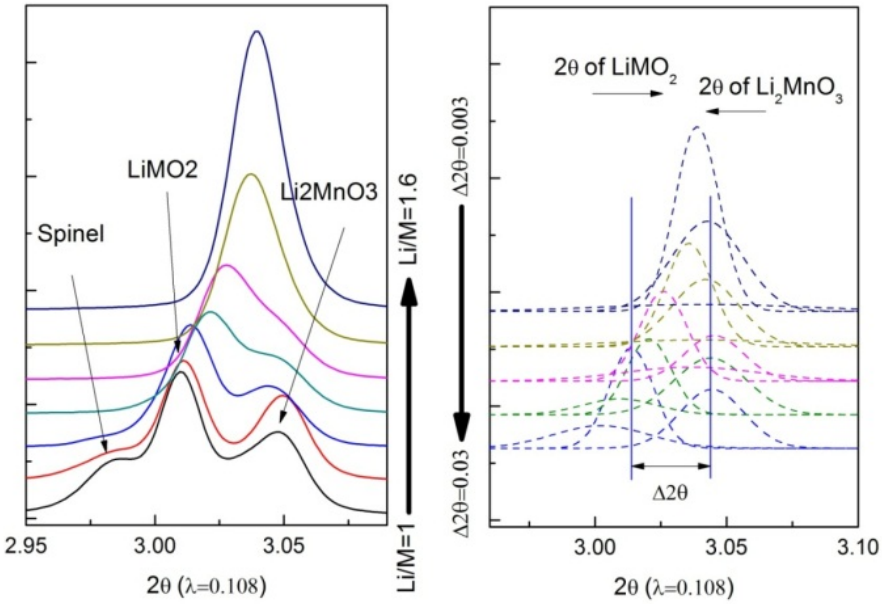

Figure 7b. XRD reflections of Group 21 (Ni=0.4, Mn=0.55, and Co=0.05).

Performance.

The performance parameter, average voltage, was used as the metric in this study. Here, the term 'average voltage' was defined as energy divided by capacity (Wh/Ah) for a given charge or discharge subcycle. As expected, composition directly affected the extent to which the average voltage decreased with cycling, as shown in Figure 8.

Curve fitting was performed on data from a number of discharge and charge cycles to determine the kinetic law for the observed, average-voltage fade. It was found that all average-voltage data could be fit to a paralinear kinetic rate law,

$$x = \frac{K_p}{K_l} \ln \frac{K_p}{K_p - K_l(x - K_l t)}$$

where x is the change in relative average voltage, K_p is the parabolic reaction rate constant, K_l is the linear reaction rate constant and t is time. In general, the regression coefficients, r2, were high, > 0.99, indicating a good fit. As expected, since the average voltage fade was sensitive to composition, the values of K_p and K_l were also (see Figure 8). These kinetic data will be used in further modeling of the average voltage response in the LMR-NMC system.

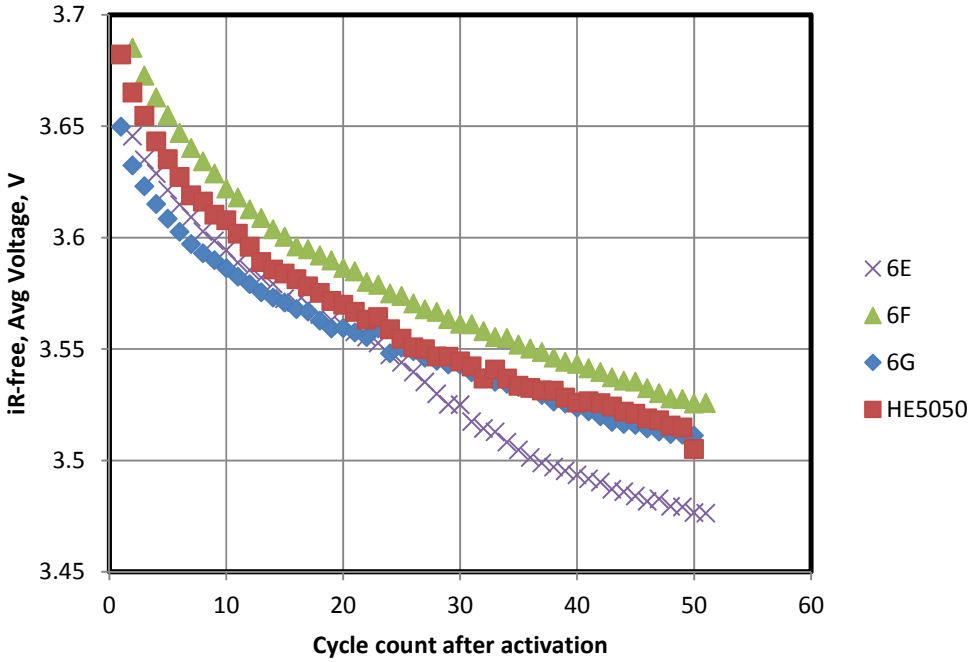

Figure 8. Discharge average voltage (Wh/Ah) vs. cycle count for typical compositions in this study.

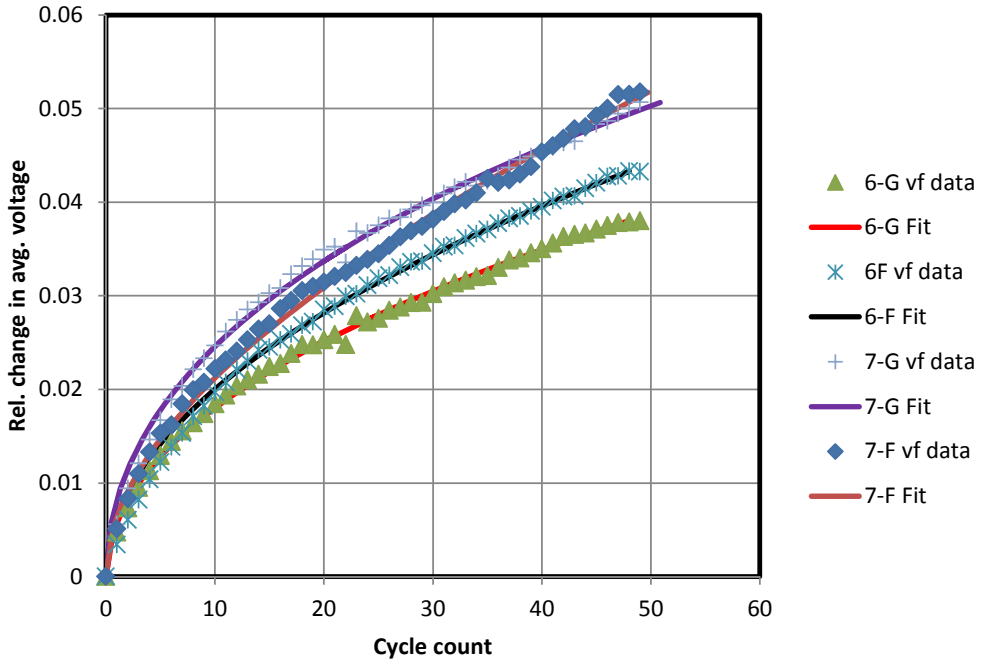

Figure 9. Rel. change in average voltage vs. cycle count. The symbols represent the voltage fade data and the solid curve, the nonlinear fit to the data.

The effect of composition on the capacity has been investigated. The effect of Li stoichiometry on the capacity in the 3rd discharge is shown in Figure 10a. Here, there are two distinguishable regions. The materials with lower capacities also contain less Co. In order to further study the effect Co concentration, the capacities were plotted versus the Co/(Co+Mn+Ni) ratio. Figure 10b shows that the capacity of cathode materials increase more than 2 times as the Co fraction increases from 0 to 0.15. The low capacity could be due to incomplete activation of the Li_2MnO_3 component. Figure 11 shows that there is no marked rate effect on capacity below 4.5 V in half-cells containing $Li_{1.5}Ni_{0.25}Mn_{0.75}O_{2.5}$ (8-F); the capacities below 4.5 V are about the same when charged with currents of 20 mA/g or 4 mA/g. But, the capacity between 4.5 and 4.7 V is sensitive to charging rate. Here, there was a six-fold increase in capacity as the charge currents were reduced from 20 to 4 mA/g. The data may indicate that Co amount affects the conductivity of composite materials or that the activation process of Co-lean materials are sensitive to charging rate.

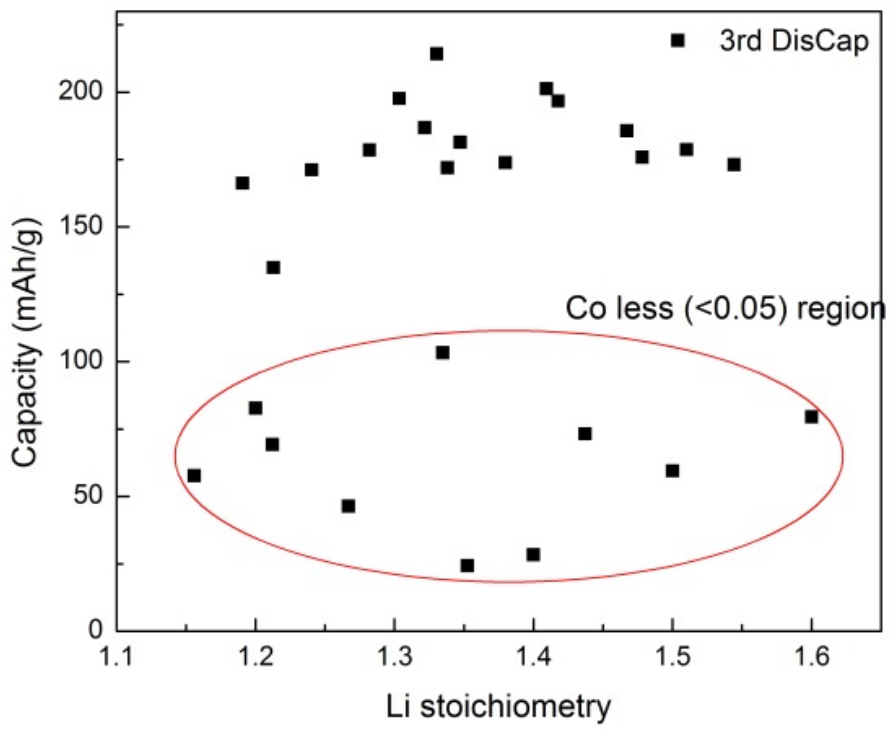

Figure 10a. The effect of nominal Li stoichiometry on capacity of the 3rd discharge.

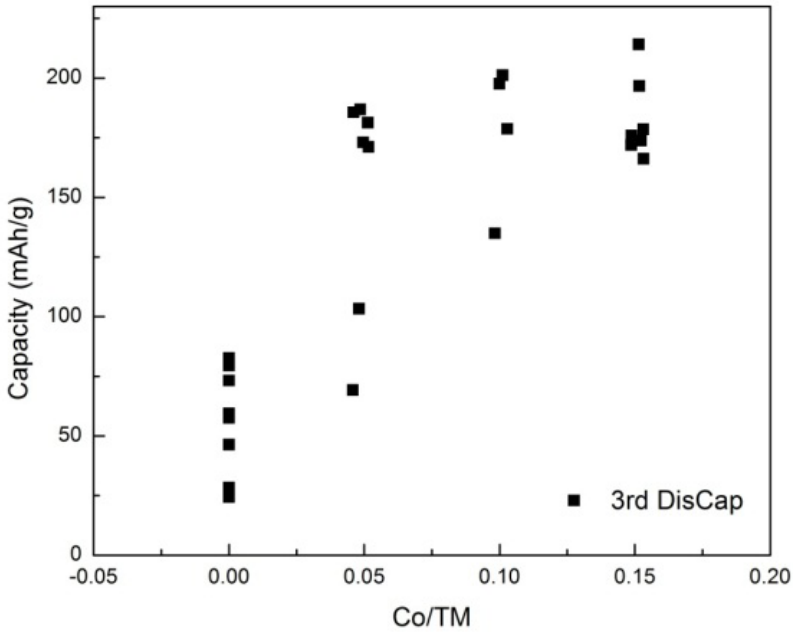

Figure 10b. The effect of Co/(Ni+Mn+Co) on 3rd discharge capacity. In the figure, TM=(Ni+Co+Mn) and equals 1.

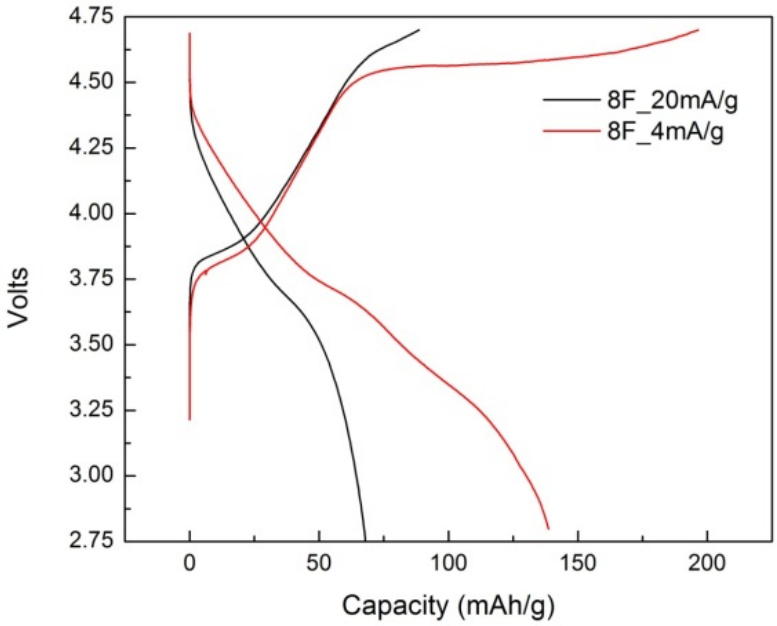

Figure 11. Charge-discharge profile of $Li_{1.5}Ni_{0.25}Mn_{0.75}O_{2.5}$ (8-F) at different cycle currents, 20mA/g and 4mA/g.

Electrochemical Models

Now that a strong correlation has been established between the hysteresis phenomenon and voltage fade, a kinetic model for examining the migration of transition metals and lithium transport will be developed to aid in characterizing the observations.

The concept of increasing the Li_2MnO_3 component in composite x Li_2MnO_3•(1-x)$LiMO_2$ (M=Mn, Ni, Co) 'layered-layered' structures is being explored in order to fully realize the advantages of high manganese content cathode materials. During the past quarter, emphasis was placed on the preparation of electrodes with the general formula x Li_2MnO_3•(1-x)$LiMn_{0.5}Ni_{0.5}O_2$ with x > 0.5 synthesized via oxalate precursors and annealed at various temperatures. It was found that a value of x = 0.7 combined with annealing at 850°C resulted in excellent electrochemical performance. Figure 12a shows the XRD pattern of a 0.7 Li_2MnO_3•0.3$LiMn_{0.5}Ni_{0.5}O_2$ material annealed at 850°C. The data are typical of 'layered-layered' composite materials, showing strong superstructure peaks at ~22° 2θ due to Li and Mn ordering in the transition metal planes. Figure 12b shows a representative SEM micrograph of the final product. The particles take on a rectangular shape and have an average size of roughly 15 µm. In addition, the formation of cleaved crystallites allow for fast lithium ion diffusion.

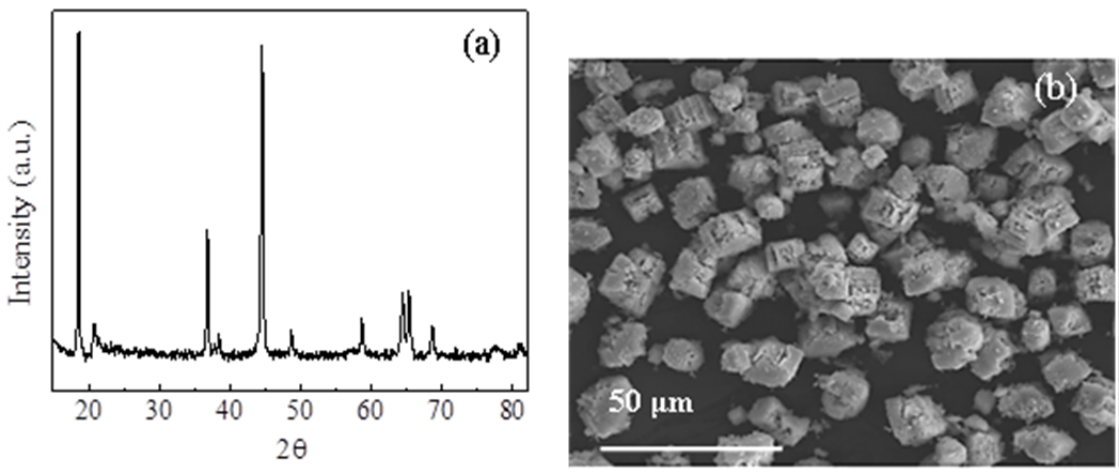

Figure 12. a) XRD pattern for 0.7Li_2MnO_3•0.3$LiMn_{0.5}Ni_{0.5}O_2$ cathode particles prepared via an oxalate precursor and annealed at 850°C. b) SEM micrograph of the final product.

The electrochemical data of a Li/0.7Li_2MnO_3•0.3$LiMn_{0.5}Ni_{0.5}O_2$ cell cycled between 4.6 – 2.0 V at 15 mAh/g, are provided in Figure 13. The cycling data in Figure 13a shows that the Li_2MnO_3 component is activated during the first 2 cycles before reaching a steady capacity of ~260 mAh/g. The voltage profile in Figure. 13b shows that in addition to exceptional overall capacity, the cell delivered ~240 mAh/g above 3.0 V for ~10 cycles. Figure 13c shows the dQ/dV data derived from the voltage curves in Figure 13b for cycles 1, 2, 10, and 31. By cycle 10, an apparent, sharp peak begins to form in the charge process just above 3.0 V (arrow in Figure 13c) with the continued increase in capacity below 3.0 V, forming a spinel-like couple in the cycled material.

The evaluation of metal substitution of the $LiMO_2$ component of the Li_2MnO_3-rich composite electrodes, for example with Co or Mg, is on-going.

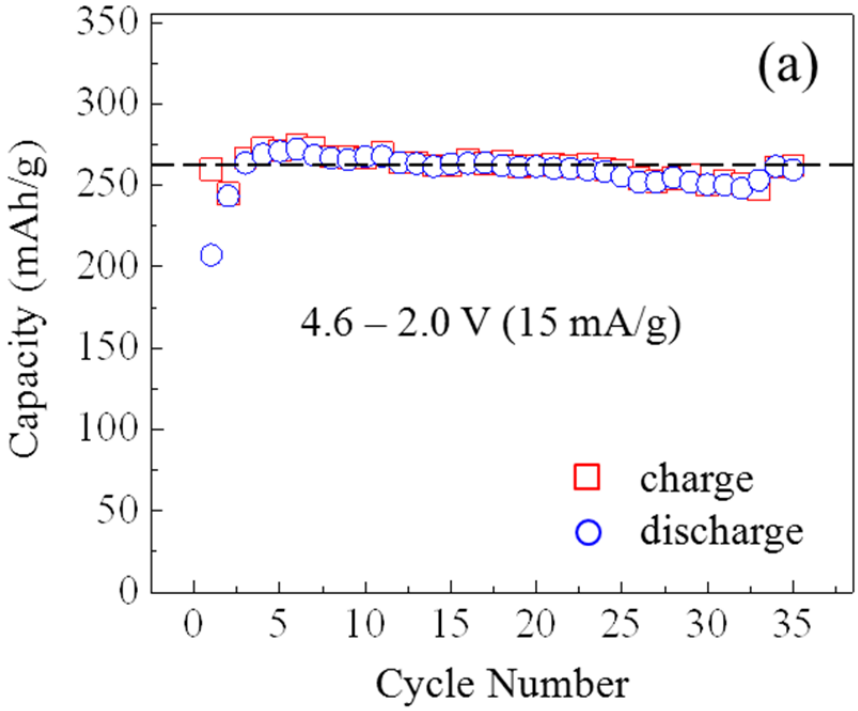

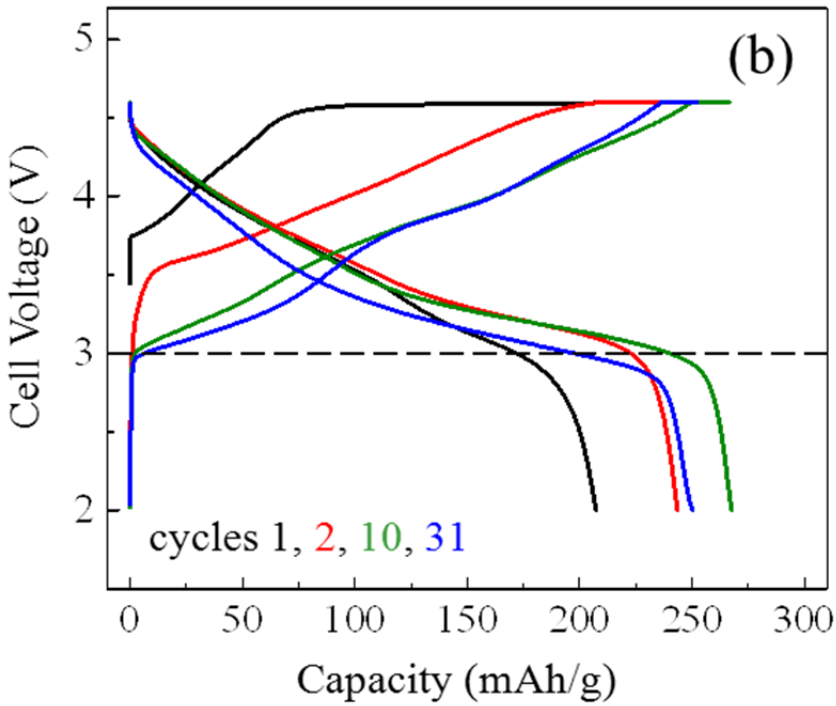

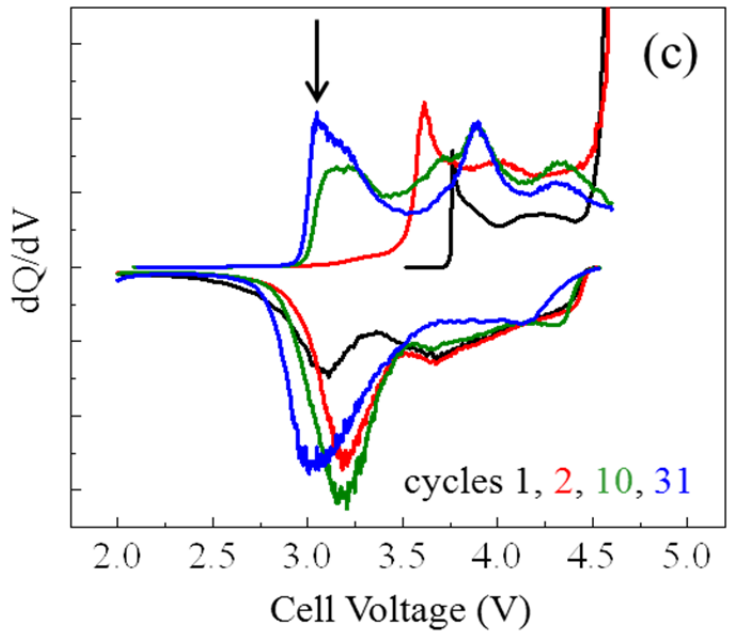

Figure 13. Electrochemical data of a Li/0.7Li_2MnO_3•0.3$LiMn_{0.5}Ni_{0.5}O_2$ cell: a) capacity vs. cycle number plot with dashed line showing 260 mAh/g, b) charge/discharge voltage profiles with the dashed line at 3 V, and c) corresponding dQ/dV plots derived from the data in b).

The addition of a stabilizing Li_2MnO_3 component, which can also act as a reserve for Li, and Ni substitution to conventional $LiCoO_2$ cathode materials is being studied from an electrochemical and structural standpoint. In general, efforts are being focused on the preparation of xLi_2MnO_3•(1-x)$LiCo_yNi_{1-y}O_2$ electrodes by increasing the Ni content during the co-precipitation synthesis of the oxalate precursors. Figure 3 shows initial electrochemical results comparing a 0.1Li_2MnO_3•0.9$LiCoO_2$ electrode with an electrode having a nominal composition of 0.1Li_2MnO_3•0.9$LiCo_{0.5}Ni_{0.5}$O2 to show the effect of Ni incorporation into the 0.1Li_2MnO_3•0.9$LiCoO_2$ material. The addition of Ni significantly improves the first cycle efficiency from 74% ((Figure 14a) to 87% (Figure 14b). Furthermore, the cycling stability is improved with Ni addition, as highlighted by the capacity retention during the first 10 cycles. Extended cycling studies with systematic formulations, including Mn-rich compositions, are in progress.

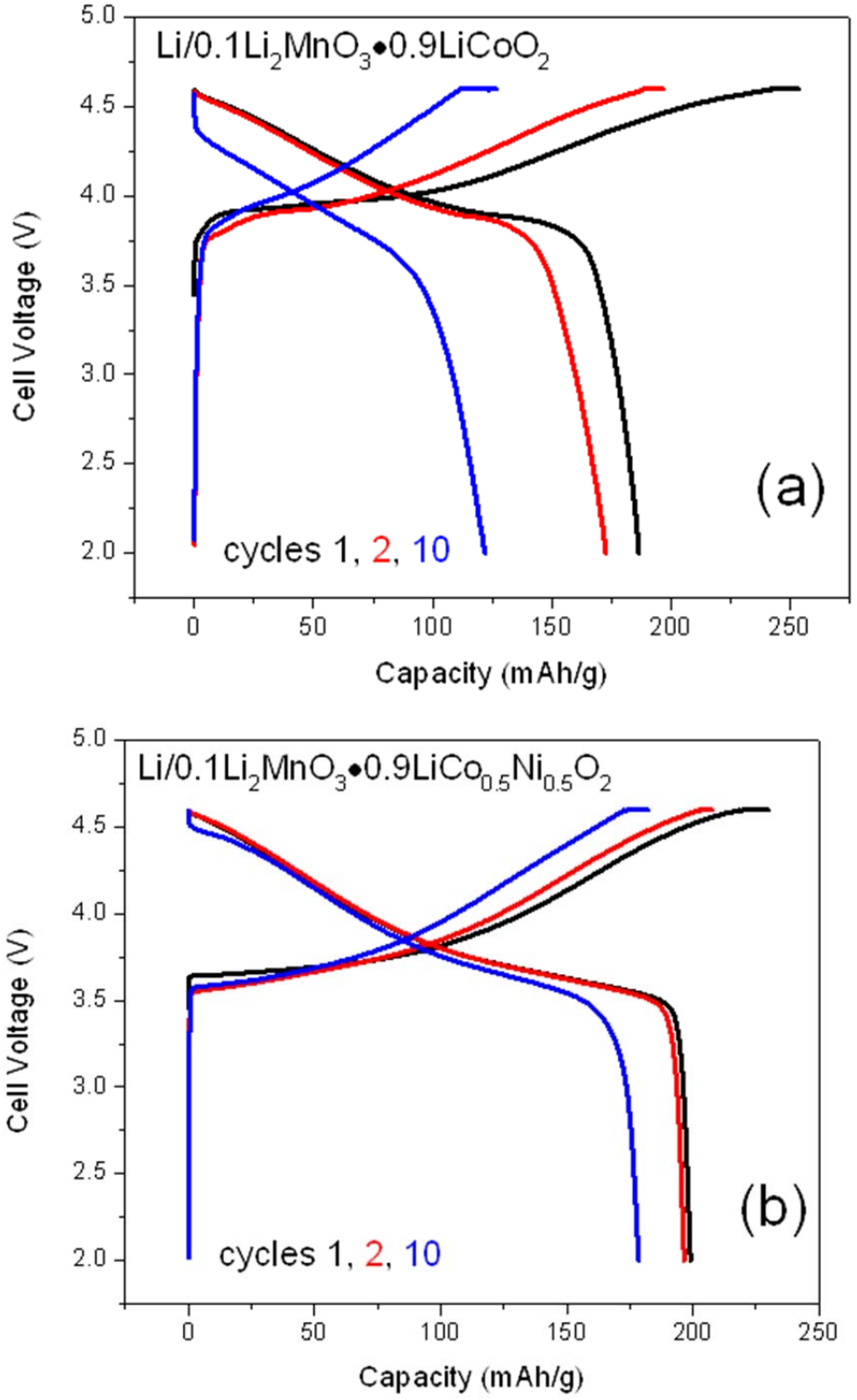

Figure 14. Voltage profiles of a) Li/0.1Li2MnO3•0.9LiCoO2 and b) Li/0.1Li2MnO3•0.9LiCo0.5Ni0.5O2 between 4.6 - 2.0 V at 15 mA/g.

Coatings and Additives

Li-Mn rich oxide cathode materials such as HE5050 are of great interest as potential candidates to replace $LiCoO_2$ in commercial applications because of their higher battery energy densities. However, one of their major drawbacks is their voltage decay. These materials degrade in electrolyte solvents by dissolution of cathode particles, especially at potentials ≥4.0 V. To improve the material electrochemical performance, a surface coatings using 3-H thiophene electrolyte additive is proposed. This additive electrolyte demonstrated some improvement in the capacity retention and the cycling at high temperature. We studied the impact of this electrolyte additive the cathode material decay. In this study, 3HT was added at 0.1wt% concentration to a carbonate-based electrolyte (Gen II electrolyte). For battery cycling tests, we analyzed Li/HE5050 half cells with and without electrolyte additive at room temperature (Figure 15). At high voltage and during battery charging, the electrolyte additive oxidizes into conductor polymer. The use of conjugated polymers as conductive matrices for the cathode material has resulted in reduced voltage fade (Figures 15 & 16). This voltage fade cannot be completely eliminated as it is also a structural phenomenon.

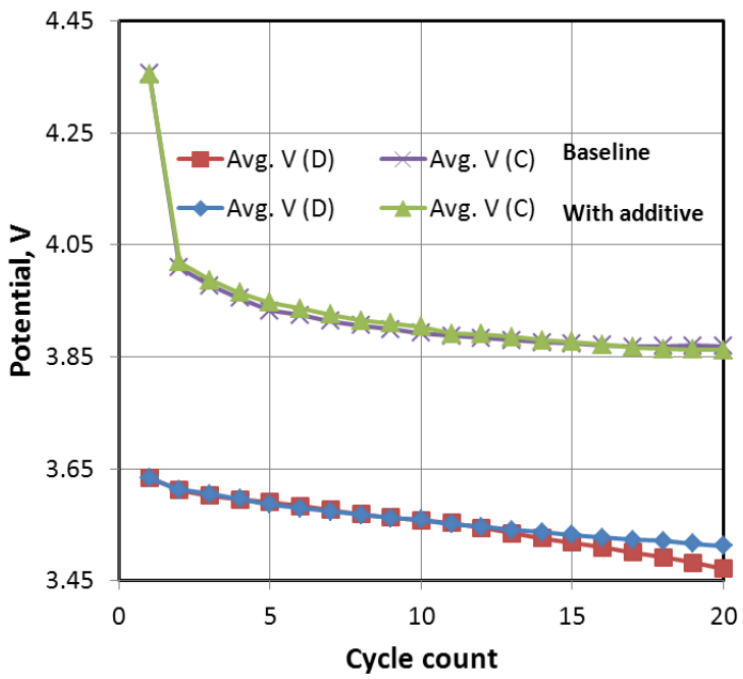

Figure 15: Variation in the voltage of Li/HE5050 cell with cycling.

IR spectra have been reported for oxide cathodes using 3 H-thiophene at 10%wt concentration. It showed the formation a C-S stretch in an aromatic ring at 1100 cm-1 and the peaks at 1408 and 1480 cm−1 are expected locations of CH2 and CH3 bending modes. An additional band at 860 cm−1 can be assigned to the CH out-of-plane deformations of the thiophene ring. With low amount of 0.1 wt% electrolyte additive and after cycling HE5050, we see only some difference in the C=O region near 1750-1800

cm-1. Perhaps the formation of a protective polymer lead to the formation of stable carbonyl group based solid electrolyte interphase layer (SEI) (Figure 16).

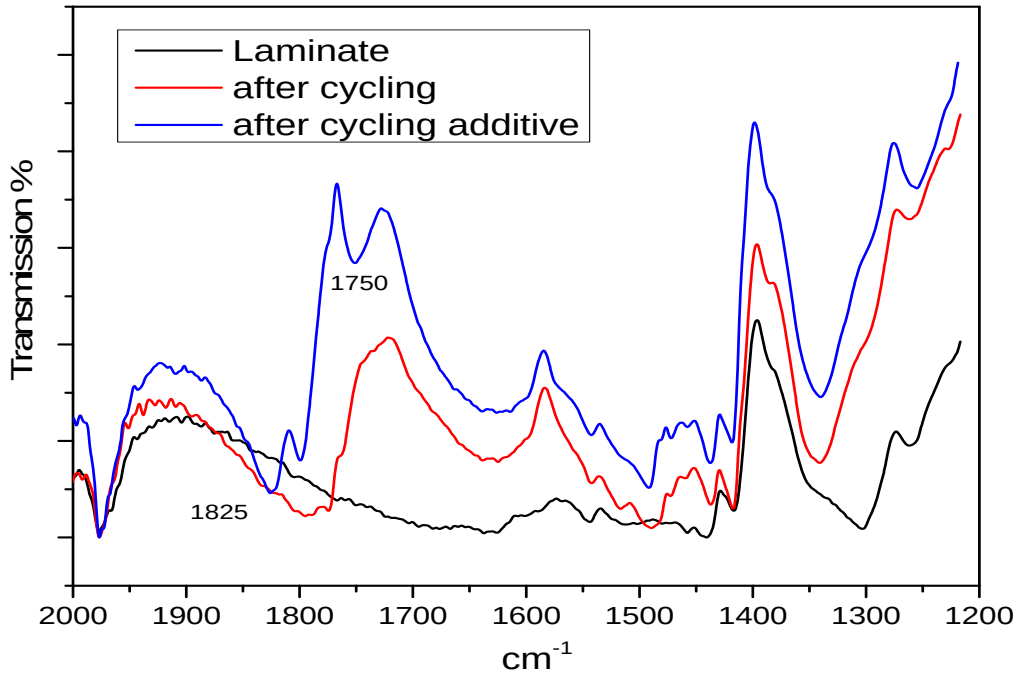

Figure 16: FTIR spectra of the cathode laminate before and after cycling.

One the key issues in understanding these materials is the cause of the enhanced capacity in these materials. Understanding mass changes in the cathode will help in this process. An electrochemical quartz crystal microbalance (EQCM) has been established in an inert glove box atmosphere. The experiments on bare aluminum are being used as baseline studies to familiarize us with the EQCM before modifying the surface with cathode particles. These experiments will be repeated on aluminum crystals treated in a variety of ways for comparison to literature precedent. Ultimately the crystals will be modified with Toda 5050 and other LMR-NMC particles. The instrument consists of the electrochemistry module and baseline QCM (E1) from Q-Sense. Aluminum-coated quartz crystals (5 MHz), mimicking aluminum current collectors in laminate composite cathodes, are used as the sensors/working electrodes. The aluminum surface was cleaned with deionized water, acetone, ethanol, and again acetone. Lithium is electroplated onto a platinum counter electrode plate, and serves as both the counter and reference electrode. Gen 2 electrolyte has been used.

The cell for measurement of SEI on Al was assembled in an argon glovebox and cyclic voltammetry (CV) was performed in the positive direction from OCP to 4.8 V at a scan rate of 10 mV/s sweeping back to 2.0 V (all potentials vs. Li+/Li0). The shape of the CVs acquired to date have been found typical of Gen 2 on lightly passivated aluminum (Figure 17). It can be seen in the first positive scan that the oxidative current rises sharply at 3.2 V. The current passed on first sweep from 3.2 to 4.0 V is assigned to the formation of AlF3 on the aluminum surface. The anodic current remains high until it reaches a maximum at the cutoff potential (4.8 V). Electrolyte oxidation and corrosion are expected

to accelerate at higher potential. The current during the negative direction of the first cycle is lower than that during the positive scan, which suggests surface deactivation, consistent with the formation of a protective film. On subsequent cycles the magnitude of the anodic current is dramatically reduced and there is no S-shaped curve, revealing that the Al became passivated with the formation of a surface film. Oxidative current rises due to electrolyte oxidation from 4.0 – 4.8 V on the second and third scans.

Prior to CV measurement, the QCM was started to get a baseline response. Surprisingly, we found the frequency of the crystal decreases during this process. Correspondingly the mass increased on the Al electrode approximately 500ng/cm2. During this time the cell open circuit potential slightly drops (20 mV to 2.38 V) indicating an ordering of the electrolyte at the aluminum surface and spontaneous surface changes. It seems that without applied bias, the aluminum reacts with the electrolyte resulting in the formation of a thin film on the electrode surface which causes the initial open circuit potential changes and mass changes. As shown in Figure 18, a sharp decrease in the frequency (a) and increase in mass (b) occurs in the first cycle once the CV is on. This can be attributed to the electrochemical passivation on the Al surface. The consecutive cycles show increasing mass, although much less than during the first sweep. At the end of the CVs the frequency measured levels off and stops dropping (mass on Al stops increasing) after several minutes.

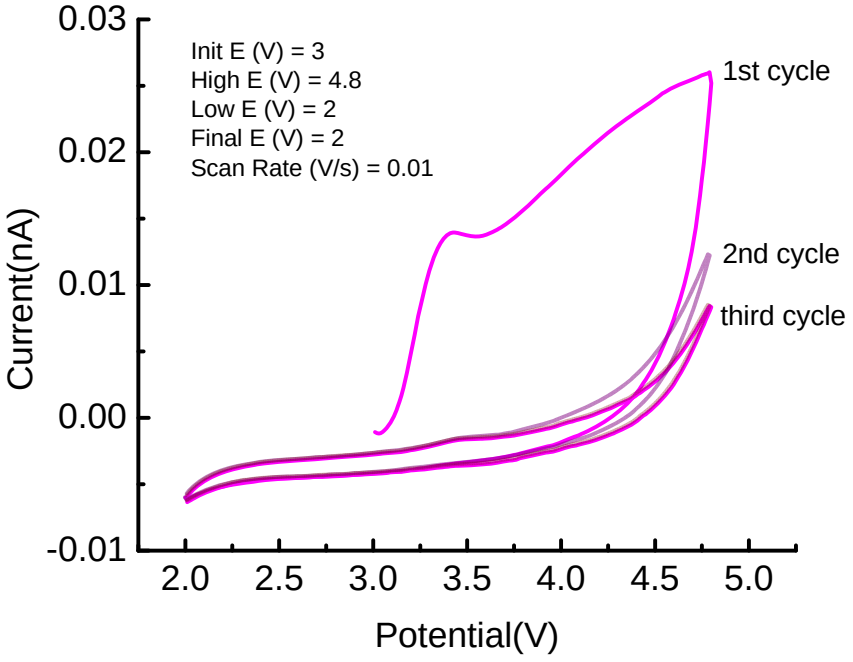

Figure 17. Cyclic voltammograms of the first three consecutive cycles of the Al thin film electrode in Gen 2 electrolyte. Scan rate: 10 mV/s.

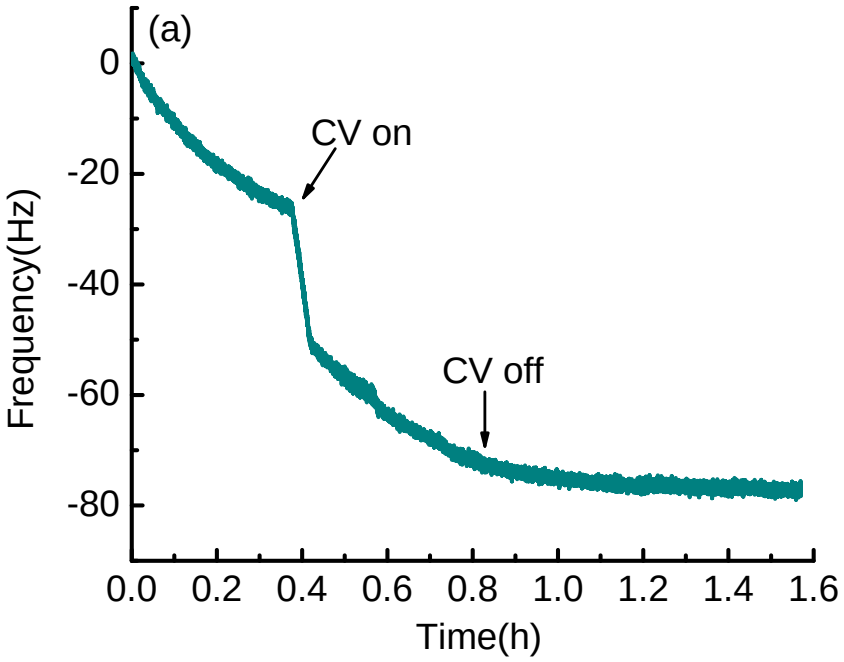

Figure 18. Simultaneously recorded frequency change (a) and corresponding mass change (b) with CV on the Al thin film electrode in Gen 2.

TASK 1
Battery Cell Materials Development

Project Number: IV.E.1.1 (ES167) **2013 Q1 update**

Project Title: Process Development and Scale up of Advanced Cathode Materials

Project PI, Institution: Gregory Krumdick, Argonne National Laboratory

Collaborators (include industry):
Young-Ho Shin, Argonne National Laboratory
Ozgenur Kahvecioglu Feridun, Argonne National Laboratory
Gerald Jeka, Argonne National Laboratory (analytical)
Mike Kras, Argonne National Laboratory (analytical)
Bryant Polzin, Argonne National Laboratory (Cell Fabrication Facility)
Kumar Bugga, Jet Propulsion Laboratory

Project Start/End Dates: start: 10/1/2012; end: 9/30/2013

Objectives: Next generation cathode materials have been developed at the bench scale by a number of researchers focusing on developing advanced lithium ion battery materials. Process engineers will work with these researchers to gain an understanding of the materials and bench-scale processes used to make these materials and then scale–up and optimize the processes.

The objective of this task is to conduct process engineering research for scale-up of Argonne's next generation high energy cathode materials. These materials will be based on NMC chemistries and may include lithium rich technology, layered–layered and layered–spinel classes of cathode materials. The current bench scale processes, using a 4L reactor capable of generating 100-200 grams of precursors per hour (carbonate method) will be optimized and scaled up. Scaling up the process involves modification of the bench-scale process chemistry to allow for the semi–continuous production of material, development of a process engineering flow diagram, design of a pre-pilot scale system layout, construction of the experimental system and experimental validation of the optimized process. The design basis for the pre-pilot scale will be based on a 20L reactor, capable of generating 1 kilogram of precursors per hour (carbonate method). The electrochemical properties of the material will be validated by the Materials Screening group to confirm a performance match to the original materials. Synthesized materials will then be made available to industry for evaluation or to researchers for experimentation.

Approach: Much of FY12 was spent on the scale-up and process optimization of the synthesis of $Li_{1.14}Mn_{0.57}Ni_{0.29}O_2$ using the carbonate process. After several engineering issues were resolved and an optimization study completed, high quality cathode material was produced with a tap density of 1.89 with a 1C rate of 195mAh/g and C/3 held 190mAh/g for 100 cycles in coin cell testing. However, when this material was

calendared it cracked, yielding unpredictable results. This particle fracturing issue seems to be an inherent problem with the carbonate process as it has also been reported from bench scale researchers. Our approach is to first attempt to synthesize the same material using the hydroxide process and compare the results to the carbonate process to determine the best place to focus our efforts.

We will also be comparing a hydroxide process generated material from Jet Propulsion Lab $Li_{1.20}Mn_{0.54}Ni_{0.13}Co_{0.13}O_2$ and Toda's HE5050 (2009): $Li_{1.20}Mn_{0.55}Ni_{0.15}Co_{0.1}O_2$ for reference.

Schedule and Deliverables: Deliverables will include scaled materials for independent testing, publications and a topical report.

Financial data:
Total project duration: 12 mo.
Staff and M&S: $1.3M

Progress towards deliverables: Two hydroxide synthesis pre-pilot scale runs have been completed (Figure 1). The first run (lot #ES-130108) had a particle growth issue which was resolved in the second run (lot #ES-130110). A comparison of cathode materials was done with this preliminary scaled-up material.

Coin cells were produced with the following materials of similar chemical composition and evaluated under identical conditions:

- Bench scale carbonate synthesis (101217B)
- Pre pilot scale, optimized carbonate synthesis (120905)
- Bench scale hydroxide synthesis (110801)
- Pre pilot scale, preliminary hydroxide synthesis (130110)

Two additional hydroxide synthesized materials containing cobalt were also compared:

- Bench scale hydroxide synthesis (JPL material)
- Commercial scale hydroxide synthesis (Toda HE5050-2009)

The rate performance comparison can be seen in figure 2 and a cycle life (C/3) comparison can be seen in figure 3. Figure 4 has SEM images and analytical data for the materials.

As can be seen by the rate and cycle life comparisons, the fully optimized, pre-pilot scale carbonate synthesized cathode material had the highest capacity and had a high tap density. The bench scale JPL NMC material also had a high tap density, although the capacity was not as good. The commercial scale Toda HE5050-2009 performed better than the similar JPL NMC but not as good as the cobalt free carbonate synthesized material. Other than the JPL bench scale NMC, the tap density of the other hydroxide synthesized materials were low, all around 1. These results have prompted us to revisit the carbonate the process and to try a few techniques to attempt to minimize the particle fracturing issue. We also plan to continue to optimize pre pilot scale cobalt free material synthesized by the hydroxide process in an attempt to increase capacity and tap density.

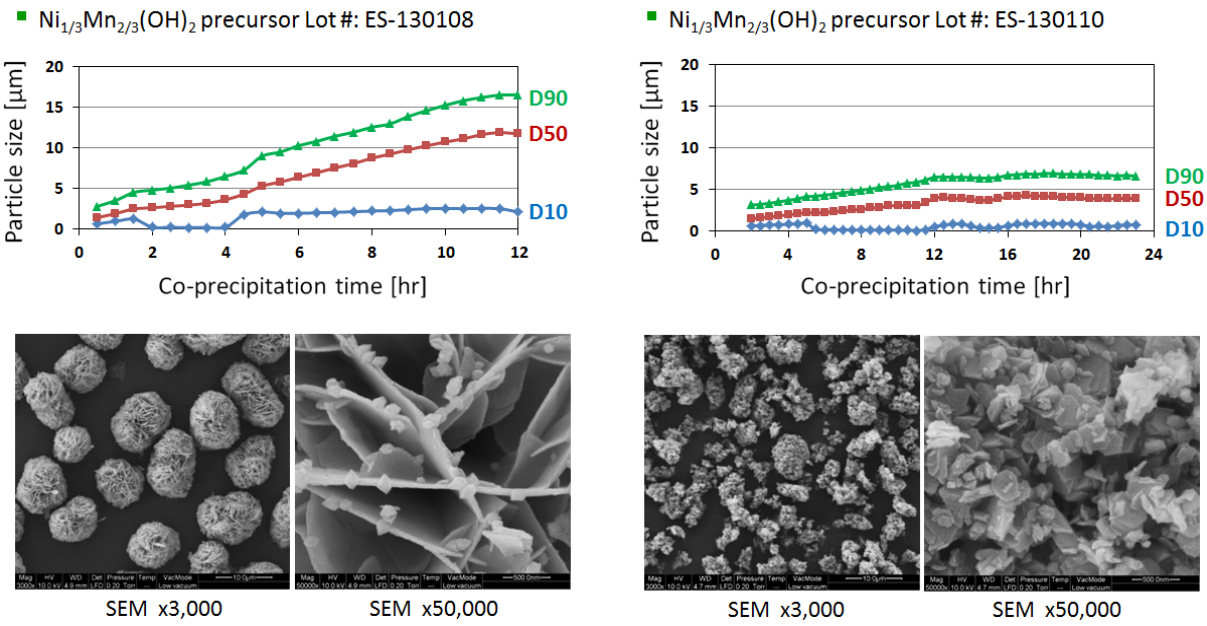

Figure 1. Preliminary scaled hydroxide cathodes ($Li_{1.39}Ni_{0.33}Mn_{0.67}O_y$)

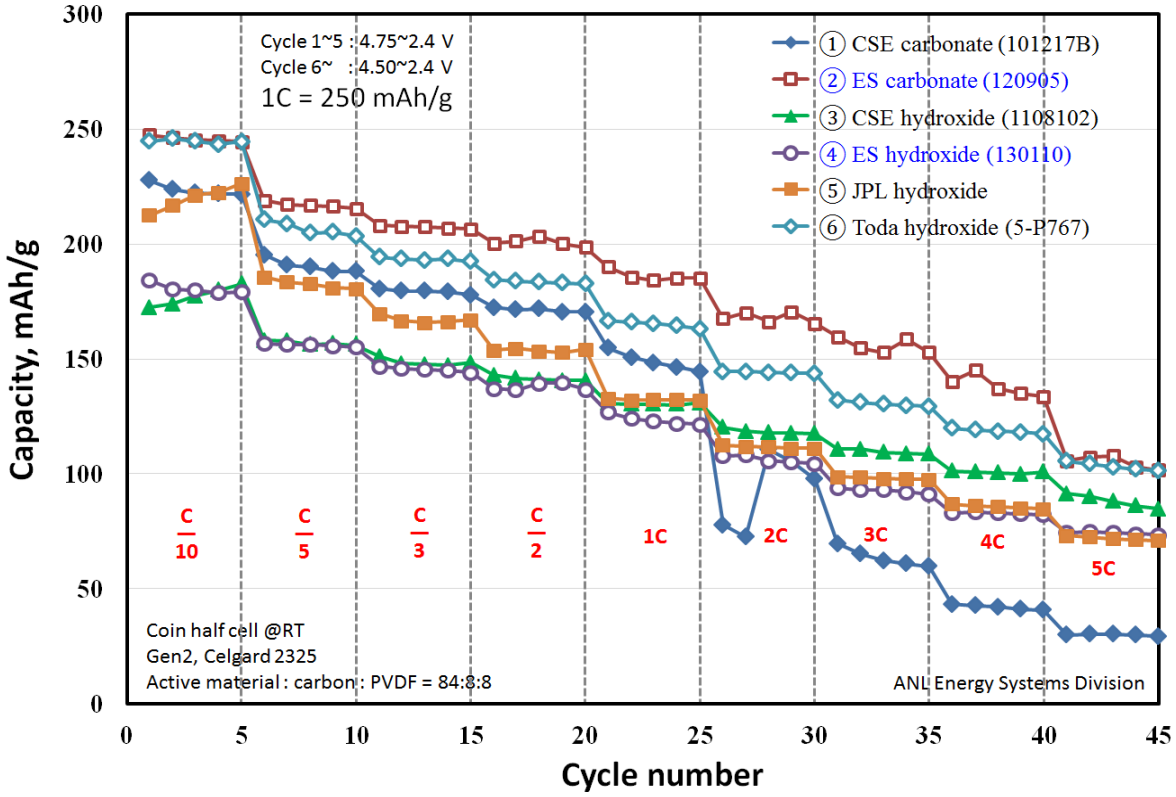

Figure 2. Rate performance comparison

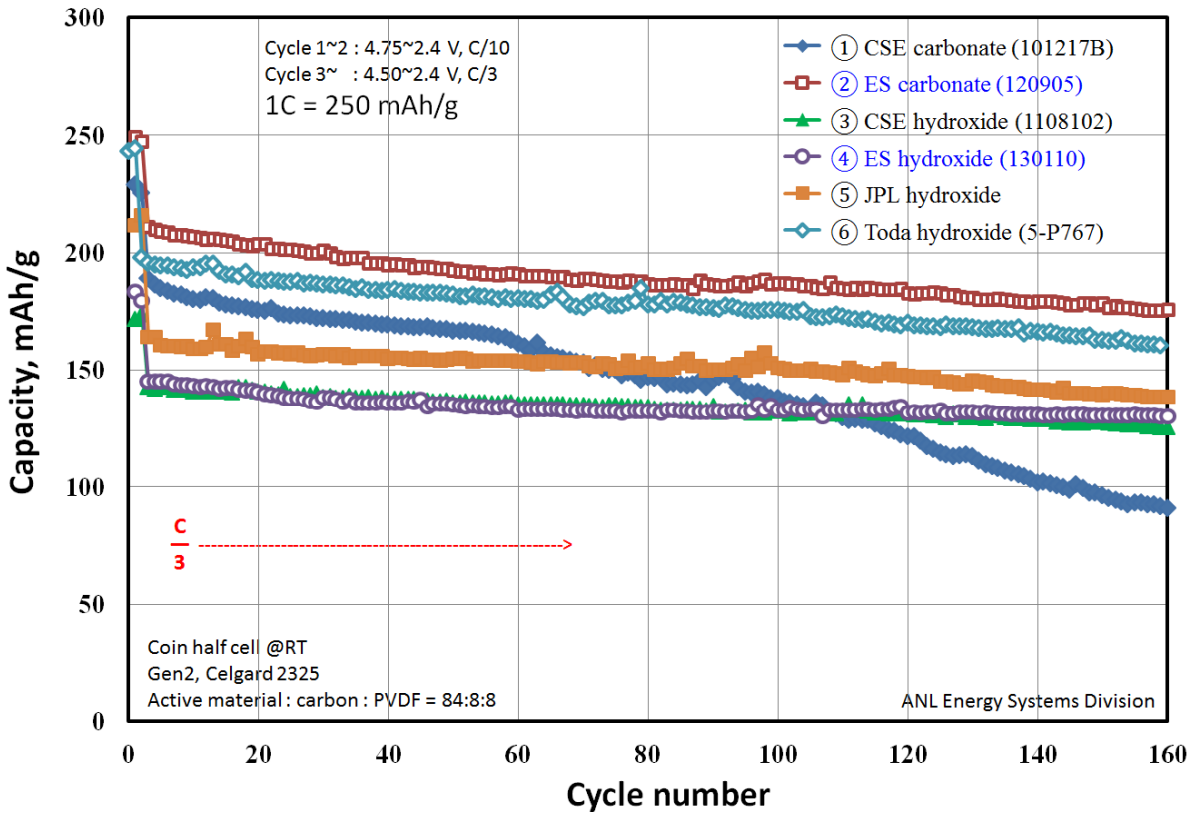

Figure 3. Cycle life (C/3) comparison

	Carbonate cathode		Hydroxide cathode			
Lot #	① CSE-101217B	② ES-120905	③ CSE-1108102	④ ES-130110	⑤ JPL	⑥ Toda-5-P767
Scale	Bench scale	Pre-pilot scale Optimized	Bench scale	Pre-pilot scale Preliminary	Bench scale	Commercial
SEM x3,000	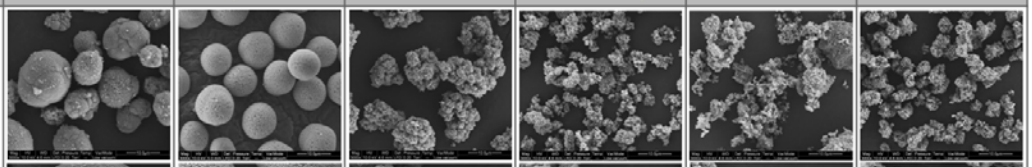					
SEM x8,000	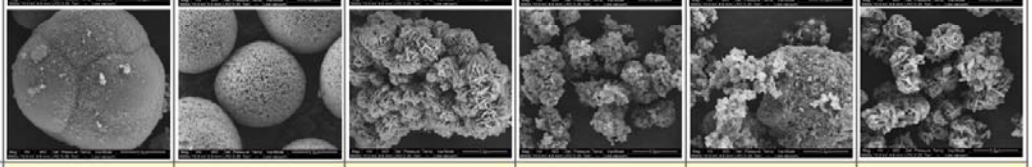					
ICP analysis	$Li_{1.35}Ni_{0.32}Mn_{0.68}O_y$	$Li_{1.37}Ni_{1/3}Mn_{2/3}O_y$	$Li_{1.31}Ni_{1/3}Mn_{2/3}O_y$	$Li_{1.35}Ni_{1/3}Mn_{2/3}O_y$	$Li_{1.61}Ni_{0.16}Mn_{0.71}Co_{0.13}O_y$	$Li_{1.52}Ni_{0.16}Mn_{0.71}Co_{0.13}O_y$
D10/D50/D90 [μm]	7.6 / 12.7 / 21.0	6.9 / 11.1 / 18.4	7.7 / 13.2 / 22.1	2.4 / 4.7 / 8.9	1.2 / 11.1 / 29.3	3.1 / 5.3 / 9.2
Tap density [g/cc]	**1.41**	**1.70**	**0.98**	**1.02**	**1.70**	**1.03**

Figure 4. Comparison of carbonate and hydroxide synthesized cathodes materials

TASK 1
Battery Cell Materials Development

Project Number: IV.E.1.2 (ES168) **2013 Q1 update**

Project Title: Process Development and Scale up of Advanced Electrolyte Materials

Project PI, Institution: Gregory Krumdick, Argonne National Laboratory

Collaborators (include industry):
Krzysztof Pupek, Argonne National Laboratory
Trevor Dzwiniel, Argonne National Laboratory
Wenquan Lu, Argonne National Laboratory
Kang Xu, Army Research Lab

Project Start/End Dates: start: 10/1/2012; end: 9/30/2013

Objectives: The objective of this task is to conduct process engineering research for the scale-up of next generation electrolyte solvents and additive materials. Advanced electrolytes materials are being developed to improve battery safety and to stabilize the interface of lithium ion batteries by forming a very stable passivation film at the carbon anode. Stabilizing the interface has proven to be key in significantly improving the cycle and calendar life of lithium ion batteries for HEV and PHEV applications. Scaling up the process involves modification of the bench-scale procedure and selection of the optimized chemical route that allows for the semi–continuous production of materials, development of a process engineering flow diagram, design of a mini-scale system layout, construction of the experimental system and experimental validation of the optimized process. Electrolyte materials will be produced at the kilogram scale and will be analyzed to confirm material properties and for quality assurance. The electrochemical properties of the material will be validated to confirm a performance match to the original materials. Synthesized materials will then be made available to industry for evaluation or to researchers for experimentation.

Approach: A formal approach for the scale-up of electrolyte materials has been defined. This approach starts with the initial discovery of a new electrolyte material and an initial electrochemical evaluation. This determines if the material is to be added to the inventory spreadsheet, ranked and prioritized. At this point, the scale-up process begins with the initial feasibility study, proof of concept testing, 1st stage scale-up and 2nd scale scale-up. Go/No go decisions are located after feasibility determination and electrochemical validation testing. Scaled materials distributed to industry or to collaborating researchers are tracked in a materials distribution spreadsheet which includes intended use and results obtained.

Schedule and Deliverables: The schedule of electrolyte materials to scale is determined by the prioritized ranking of the scale-up spreadsheet. Materials currently being scaled are reflected in the project milestones. Deliverables will include scaled materials for

evaluation or experimentation and a technology transfer package of information on each material scaled. We expect to complete the scale-up of 3-5 electrolyte materials in FY13.

Financial data:
Total project duration: 12 mo.
Staff and M&S: $1.2 M

Progress towards deliverables:

Completed the scale-up of the electrolyte solvent ANL-1NM2. Initial process development and scale-up of this material took place in FY12; the pilot scale-up was completed in FY13. Pilot scale synthesis yielded 9,715g of material, which has been sampled to ANL-CSE Division and PNNL for experimental use. Completed the scale-up of the electrolyte redox shuttle ANL-RS21. A patent filing on this material is pending; therefore structure detail is currently withheld. Pilot scale synthesis yielded 2,320g of material. Work on the scale-up of the electrolyte additive PFTBP for the Army Research Lab has been initiated.

Since the start of the electrolyte scale-up program, 38 samples have been provided to industry and various national labs for evaluation and experimentation (4 samples in FY11, 25 samples in FY12 and 9 samples in FY13-Q1).

MILESTONE	DATE	STATUS	COMMENTS
ANL-1NM2			
Assess scalability of disclosed process	7/20/12	Completed	
WP&C documentation approved	8/1/12	Completed	
Develop and validate scalable process chemistry (10g scale)	8/20/12	Completed	
First process scale-up (100g bench scale)	9/17/12	Completed	
Second process scale-up (1000g pilot scale)	10/09/12	Completed	9,715g produced in single batch
ANL- RS21			
Assess scalability of disclosed process	9/28/12	Completed	
WP&C documentation approved	9/28/12	Completed	
Develop and validate scalable process chemistry (10g scale)	10/30/12	Completed	
First process scale-up (100g bench scale)	11/30/12	Completed	
Second process scale-up (1000g pilot scale)	01/10/13	Completed	2,320 g produced in single batch

ARL-PFTBP			
Assess scalability of disclosed process	11/21/12	Completed	
WP&C documentation approved	9/28/12	Completed	Covered under existing WP&C document
Develop and validate scalable process chemistry (10g scale)	12/21/12	Completed 2/14/2013	This task took longer than anticipated due to an issue with the target material, which will be detailed in the FY13-Q2 report
First process scale-up (100g bench scale)	2/28/13	Pending	Date revised due to material issue
Second process scale-up (1000g pilot scale)	3/15/13	Pending	Date revised due to material issue

Table 1 – Electrolyte Materials Milestones

Argonne NATIONAL LABORATORY	ANL-1NM2
Description	2,2-dimethyl-3,6,9-trioxa-2-siladecane
CAS #	62199-57-9
Formula	$C_8H_{20}O_3Si$
FW	192.33
LOT #	TD3-129
Purity	>99.9%[1]
Quantity	9715 g
Manufactured	10/09/2012
Other	N/A

Analysis	Instrument/Method	Results	Analysis By:
GC/FID	Agilent 7890A Agilent HP-5MS, 0.25 um, 30m x 0.250 mm, 40 to 300 °C, 30 °C /min	99.917% [1,2]	T. Dzwiniel
GC/MSD	Agilent 7890A/5975C Triple-Axis Agilent DB-5MS, 0.25 um, 30m x 0.250 mm, 40 to 300 deg, 30 deg/min	99.979% [1,2]	T. Dzwiniel
Boiling Point	Buchi M-565 Automatic, 0.6 Hz corrected to standard pressure	190-191 °C	T. Dzwiniel
KF Moisture Titration	KEM MCU-610 Coulometric, WaterMark 1612/1613	40ppm	K. Pupek
FTIR	Bruker Vertex 70 Attenuated Total Reflection	Consistent with Structure	G. Jeka
NMR	Bruker 500 MHz ^1H observed in $CDCl_3$ solution	Consistent with Structure	K. Pupek

[1] By area integration. [2] Average from three analyses.

Table 2 – Spec sheet on ANL-1NM2

Argonne NATIONAL LABORATORY	ANL-RS21
Description	<confidential, patent filing pending>
CAS	<confidential, patent filing pending>
Formula	<confidential, patent filing pending>
FW	<confidential, patent filing pending>
LOT #	TD4-073
Purity	>99.9% [1, 2]
Quantity	2320 g
Manufactured	1/11/2013
Other	N/A

Analysis	Instrument/Method	Results	Analysis By:
HPLC	Agilent Eclipse Plus C18, 3.5 um, 4.6x100, UV 225, water/ACN gradient	>99.9% [2]	T. Dzwiniel
GC/FID	Agilent 7890A Agilent HP-5MS, 0.25 um, 30m x 0.250 mm, 40 to 300 °C, 30 °C /min	99.992% [1,2]	T. Dzwiniel
GC/MSD	Agilent 7890A/5975C Triple-Axis Agilent DB-5MS, 0.25 um, 30m x 0.250 mm, 40 to 300 deg, 30 deg/min	>99.9% [1,2]	T. Dzwiniel
Melting Point	Buchi M-565 Automatic, range method	76-77 °C	T. Dzwiniel
FTIR	Bruker Vertex 70 Attenuated Total Reflection	Consistent with Structure	G. Jeka
NMR	Bruker 500 MHz ^{1}H, ^{13}C observed in $CDCl_3$ solution	Consistent with Structure	T. Dzwiniel

[1] Average of three injections.
[2] By area integration.

Table 3 – Spec sheet on ANL-RS21

TASK 1
Battery Cell Materials Development

Project Number: ES024

Project Title: High Voltage Electrolytes for Li-ion Batteries

Project PI, Institution: Arthur Cresce, Kang Xu, Jan Allen, Oleg Borodin, Samuel Delp, T. Richard Jow, U.S. Army Research Laboratory

Collaborators (include industry): K. Gaskell (U. of Maryland); K. Amine, D. Dees, G. Krumdick (ANL); X. Yu and X. Yang (BNL)

Project Start/End Dates: June 2011 / May 2014

Objectives: Develop high voltage electrolytes that enable the operation of 5 V Li Ion Chemistry. With a 5-V high voltage electrode materials and a capacity similar to that of the state-of-the-art cathode, the energy density will be increased more than 25% than that of the-state-of-the-art Li-ion batteries for HEV/PHEV. Our other objective is to understand the surface chemistry at the high voltage cathode and electrolyte interface through surface characterization and computational effort. With better understanding, better electrolyte components and cathode materials can be developed.

Approach: Three approaches were taken.

1. **Design and Synthesis of New Additives**
   a. Rationale of electron deficient center
   b. Synthesis, purification and structural characterization by NMR and FTIR
2. **Electrochemical Evaluation**
   a. CC and CC-CV cycling in half and full cells at various temperatures
   b. Impedance analysis
3. **Characterize Interfacial Chemistry at the Elecrode/electrolyte Interface**
   a. Use high resolution XPS, NMR and AFM
4. **Computational Evaluation**
   a. Understand oxidative stability of solvents/electrolytes
   b. Understand reactive pathways of additives and electrolytes
   c. Understand how electron-deficiency would impact on the oxidation stability of additives

Milestones:

(a) Continued testing of new additives (June 2013)
(b) Postmortem diagnostic studies: surface characterization and SEI chemistry (Oct 2013)
(c) Erratum and re-characterization of additive structure (Dec 2012)
(d) Test and evaluate electrolytes with additives in LNMO/graphite, doped-LCP/graphite and other cell couples (Oct 2013)

Financial data: $250,000/year

PROGRESS TOWARD MILESTONES

(a) Additives Design and Synthesis Rationale (Arthur Cresce, Kang Xu)

Previously we have synthesized a series of perfluorinated additives. The tests in full Li ion cells using LMNO/A12 electrochemical couple proved that perfluorination does improve capacity utilization as compared with partially-fluorinated counterparts.

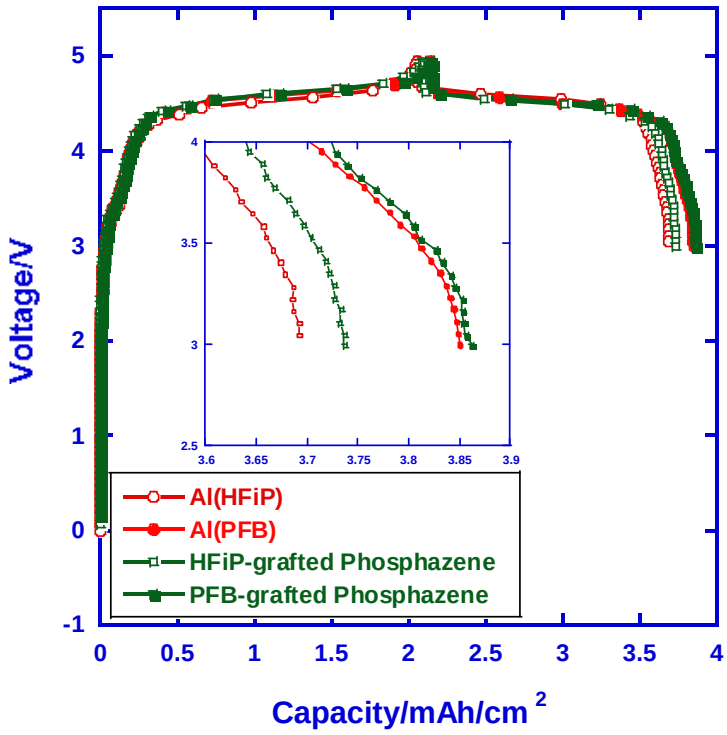

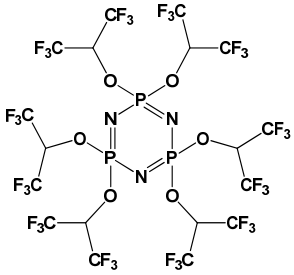

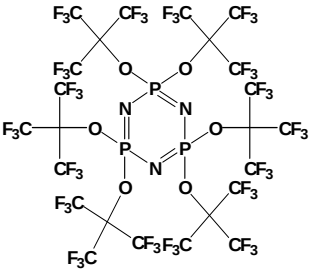

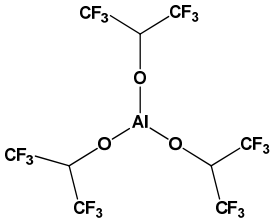

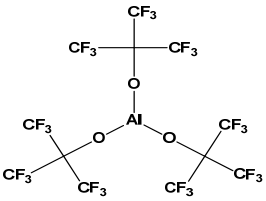

(b) Post-mortem Diagnostics of High-temperature Failure (Arthur Cresce, Kang Xu)

Cells with additives still show capacity fading at elevated temperature.

Impedance analysis on the electrodes recovered from HT failed cells placed most of the blame on cathode side, as confirmed by the re-assembled half cells. XRD did not find any substantial structural change in cathode bulk. The origin of fading is apparently electrolyte or interphase breakdown at HT. More work is need to passivate the oxidizing surfaces of LMNO.

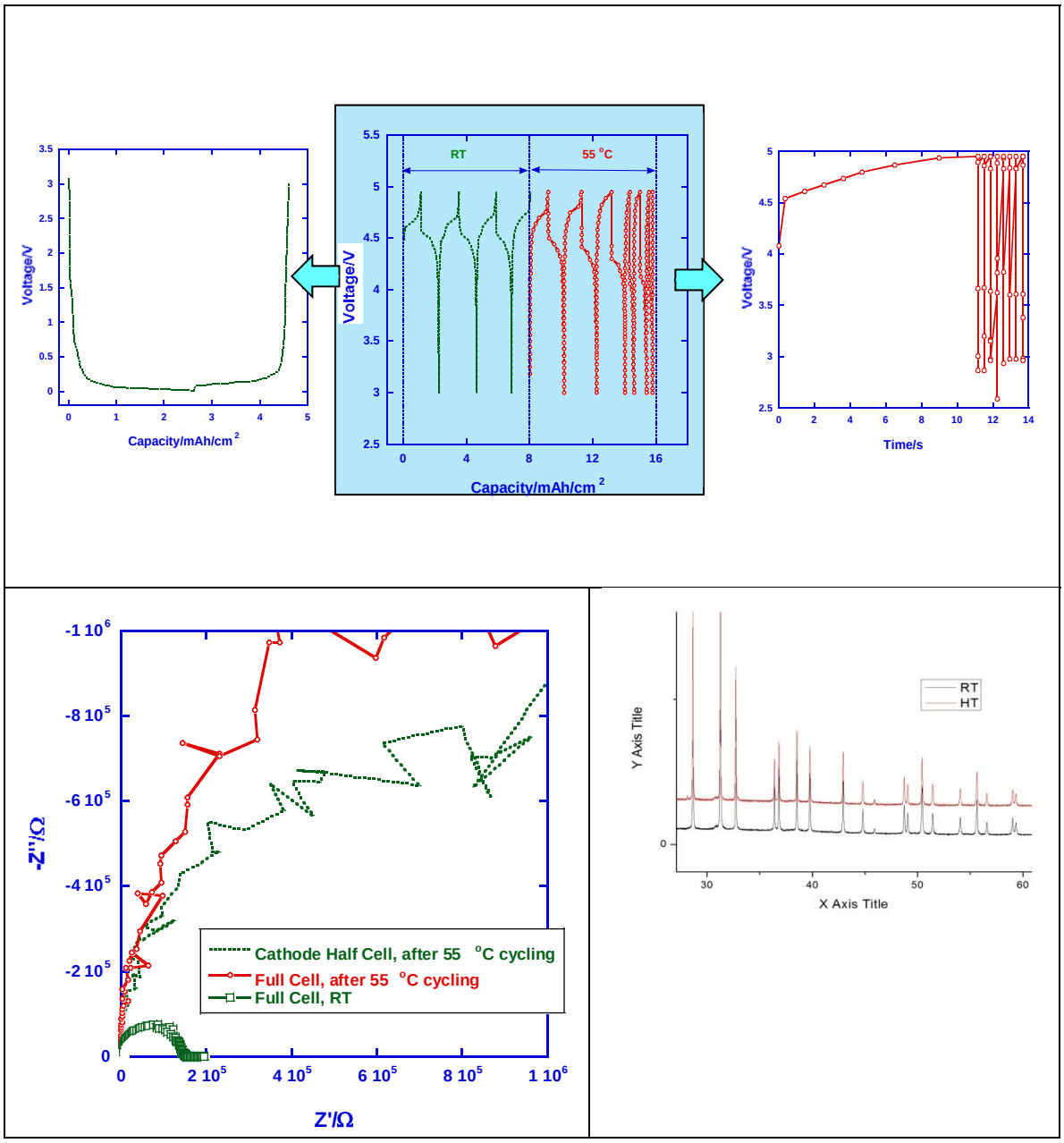

(c) Erratum and Re-characterization (Arthur Cresce, Kang Xu)

Previously-reported PFBP with the belived structure was found to be an intermediate compound during the synthesis of the target phosphate. Apparently the bulky size of perfluorinated alkyl groups prevented the full esterification of phosphorus center. Currently re-characterization on all additives is being carried out, and an alternative route to PFBP is being explored, and the syntheses of several new additives have been inspired by this error.

Meanwhile, since the intermediate compound also showed certain electrochemical benefits, ANL facility is scaling up it.

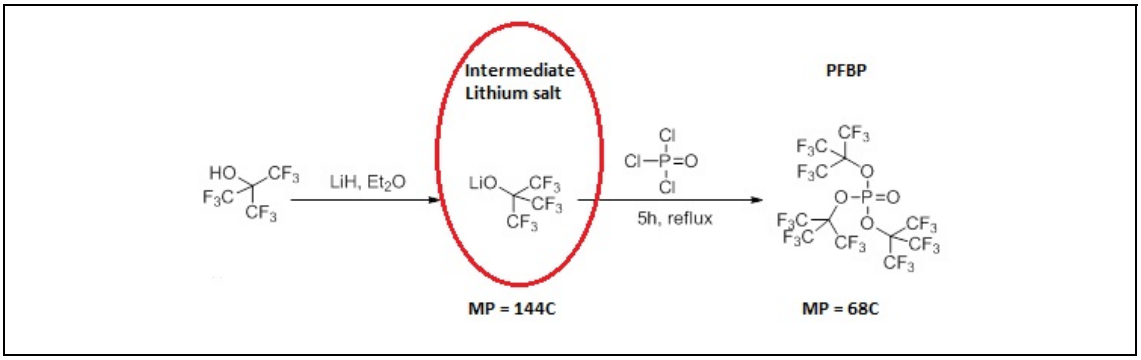

(d) Impact of Additives on Cycling of LNMO/A12 at 55 ^{o}C (Samuel Delp, Jan Allen, Richard Jow)

The LNMO/A12 full cells, in which both LNMO ($LiNi_{0.5}Mn_{1.5}O_4$) and A12 (graphite) were supplied by ANL, cycled well between 4.9 and 3.5 V at a rate of 1 C with a Couombic Efficiency (CE) around 99% in the baseline (or standard) electrolyte [1.2 M $LiPF_6$ in EC:EMC (3:7)] and the baseline electrolyte containing additives such as HFiP and P1 (supplied by 3M) at room temperature. However, the cycling of LNMO/A12 at 55 ^{o}C that showed fast capacity fading is a challenge. We found several additives including HFiP and P1 could improve the cycling at 55 ^{o}C with a reasonable capacity fading and a CE of about 98.5% as shown in the figure below. The capacity of the full cells in the baseline electrolyte cycled at a rate of C/5 as a function of cycle number at room temperature is also shown in the figure for comparison.

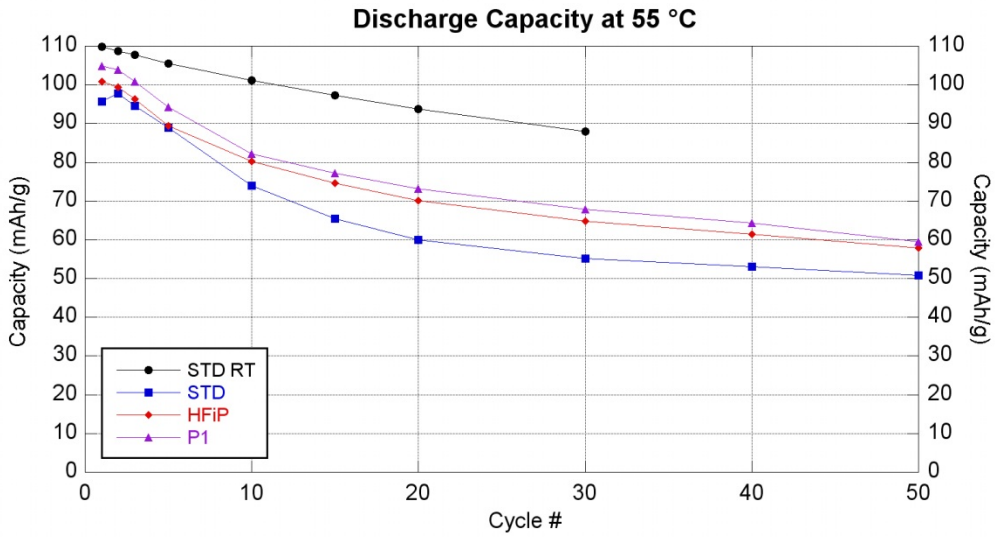

(e) High Temperature Cycling of Doped Lithium Cobalt Phosphate High Voltage Cathode (Jan Allen, Samuel Delp, Richard Jow)

A new batch of iron doped lithium cobalt phosphate (Fe-LCP) was synthesized. The manually coated electrodes were fabricated and tested in Fe-LCP/Li half cells in the baseline electrolyte. The cells were cycled at C/3 rate between 3.5 and 4.95 V. Steady capacity retention at room temperature at room temperature and a faster capacity fading at 55 ^{o}C were observed as shown in the figure below. These results indicate thermally promoted reactions existed between the high voltage Fe-LCP electrodes and the baseline electrolyte. Machine coated electrodes will be fabricated and tested in the baseline and baseline containing additives electrolytes in full cell configurations in the coming months.

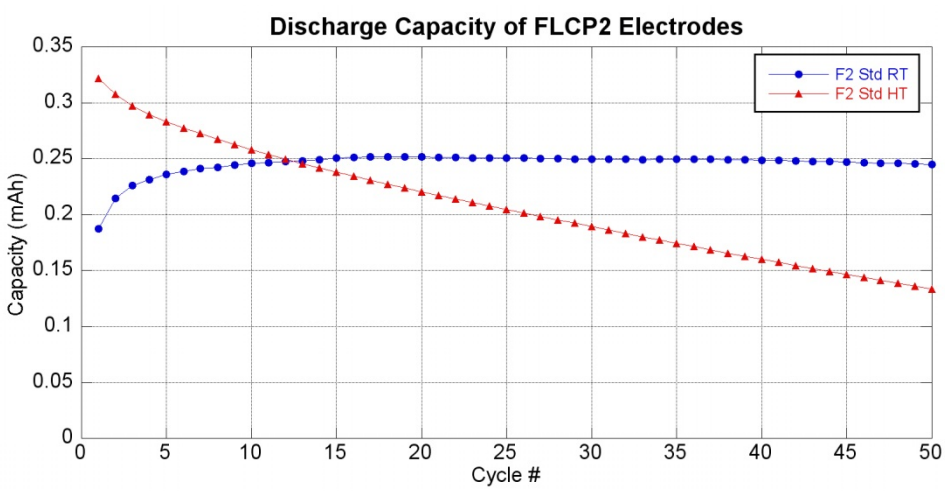

(f) Quantum Chemistry Studies of Representative Electrolyte Complexes (Oleg Borodin, Richard Jow)

Quantum Chemistry Studies of Representative Electrolyte Complexes

Previous quantum chemistry QC studies of electrolyte additives reported in FY2012 were complemented by extensive exploration of the initial stages of oxidation induced decomposition and oxidation stability of the solvent/anion complexes[6] and additives reported in Section **a**. Calculations were performed in the gas-phase using the PCM model to implicitly account for the surrounding solvent, as in the case of isolated solvents and anions. Table 1 summarizes oxidation potentials for the solvent-anion complexes from DFT calculations. Benchmark calculations using more accurate levels were performed but not included in Table 1 for clarity.

It has been found that the oxidation of complexes containing carbonate solvents such as EC, PC, DMC, EMC, FEC and anions with high oxidation stability such as PF_6^-, BF_4^-, ClO_4^-, $B(CN)_4^-$ resulted in a spontaneous H-abstraction from the solvent, F-abstraction from the anions and HF-formation. This spontaneous oxidation-induced reaction resulted in a significant decrease of the complex oxidation stability compared to the intrinsic oxidation stability for the isolated solvent and anions. The difference between solvent complexes with BF_4^- and PF_6^- anions was also examined. DFT calculations predict that EC/BF_4^- and PC/BF_4^-complexes are less oxidatively stable than corresponding complexes containing the PF_6^- anion (EC/PF_6^- and PC/PF_6^-) by 0.2-0.4 V with the largest difference observed in the gas-phase and the smallest difference at high dielectric constant.

Table 1. Oxidation potential (adiabatic energy) of solvent/anion complexes from DFT calculations from the M05-2X/cc-pvTz and M05-2X/6-31+G** calculations denoted in parentheses. Free energy is shown in bold. LC-wPBE/6-31+G** energies are in green and in brackets.

	H or F transfer	e=1	e=4.2	e=20.5	e=78.4
DMC/BF_4^-	yes	4.14	5.79	6.21, 5.92[a]	6.29
EC/BF_4^-	yes	4.55	5.95	6.28, **6.07** (6.39, **6.21**) [6.36, 6.15]	6.34
EC_2/BF_4^-	yes	5.17		6.38 (6.46, **6.30**)	
EC_3/BF_4^-	yes			6.55, **6.37** (6.51,**6.43**)	
EC/$LiBF_4$ (v1)	yes	8.74		6.64	
EC/$LiBF_4$ (v2)	yes	8.46		6.82	
EC_2/$LiBF_4$	no			(7.51, **7.31**)	
EC_2/$LiBF_4$	yes			(6.72, **6.60**)	
EC_4/$LiBF_4$	yes				(6.53, **6.24**) (e=90)
FEC/BF_4^-	yes	4.93	6.31	6.62	6.68
VC/BF_4^-	no	4.17	5.16	5.46	5.49
DMC/PF_6^-	yes	4.56	6.12	6.51, 6.29[a]	6.58
EMC/PF_6^-	yes	(4.55, **4.44**)	(6.10,**5.91**)	(6.50,**6.31**) [6.66,**6.62**]	
EC/PF_6^-	yes	4.94, **4.71,** 4.64[a]	6.27	6.57, **6.37** [6.70] (6.71, **6.50**)	6.63 6.36[a]
EC_3/PF_6^-	yes				6.47, **6.44**
EC_4/PF_6^-	yes			(6.47, **6.53**)	

$EC_3/LiPF_6$	yes			6.94 (**6.78**)	
PC/BF_4^-	yes	4.57		6.25	
PC/PF_6-	yes	4.84, **4.63**		6.46,**6.29**	
FEC/PF_6^-	yes	5.16		6.78, 6.48[a]	
EMS/BF_4^-	no	5.31	6.41	6.62	6.66
TMS/PF_6^- (a)	no	5.44	6.36	6.54	6.57
TMS/PF_6^- (b)	no	5.48	6.35	6.49	6.52
EMS/PF_6^-	no	5.46	6.47	6.66	6.69
TMP/BF_4^- (a)	no			(6.47,**6.45**)	
TMP/BF_4^- (b)	no			(6.68)	
TMP/PF_6^-	no	5.07		6.62	
PMS/PF_6^- (a)	yes	4.56		6.57	
PMS/PF_6^- (b)	yes	4.42,4.38[a]	5.78	6.10, 6.09[a]	6.17
PMS/PF_6^- (c)	yes	4.29	5.55	5.84	5.89
EC/ClO_4^-	yes	5.01		6.65	
$EC/B(CN)_4^-$	yes	4.70, 4.58[a]	5.46	6.05,**5.96** (6.13,**6.04**)	
$EC/DCTA^-$	No	4.66		5.83	
$EC/DFOB^-$ (a)	No			6.03, **5.92,** [6.22, **6.10**]	
$EC/DFOB^-$ (b)	No			6.08, **5.94,** [6.25, **6.18**]	

It is also important to understand the predicted trends of oxidation stability as a function of the surrounding solvent dielectric constant. The increase of the dielectric constant results in the decrease of the solvent oxidation stability, while anions and solvent-anion complexes show the opposite trend of increasing oxidation stability with increasing surrounding solvent dielectric constant. Experimental data for EMC:EC/$LiPF_6$ shown show an increased oxidation stability with increasing dielectric constant of the mixture as a low dielectric constant EMC (e=3) is replaced with a high dielectric constant EC (e=90). At PCM(e=4), the EMC/PF_6^- calculated oxidation stability was 5.9 V (M05-2X/6-31+G**), which is in good agreement with the measured value of 5.7 V for EMC-1M $LiPF_6$ on GC but it is significantly lower than the previously reported value of 6.7 (GC 0.65 M Bu_4NBF_4). An increase of the dielectric constant from e=4 to 20 resulted in a 0.4 V increase of the EMC/PF_6^- oxidation stability, which is in good agreement with a 0.4 higher oxidation stability experimentally found for EMC:EC(1:1)-1M $LiPF_6$ on GC compared to EMC-1M $LiPF_6$ on GC. The comparison of DFT and G4MP2 results indicates that DFT methods (M05-2X/6-31+G**) overestimated EMC/PF_6^- and EC/PF_6^- oxidation potential by ~0.4 eV indicating that results for carbonate-anions presented in Table 1 likely systematically overestimate oxidation stability of complexes by 0.4 eV. A detailed discussion of the initial oxidation-induced decomposition of carbonate, alkyl phosphate and sulfone-based electrolytes is presented in ref.[6].

Publications

(1) "Correlating Li+-solvation sheath structure with interphasial chemistry", A. v. Cresce, O. Borodin, and K. Xu, *J. Phys. Chem. C*, **2012**, *116*, 26111

(2) "Architecturing Hierarchical Function Layers on Self-Assembled Viral Templates as 3D Nano-Electrode Arrays for Integrated Li ion Microbatteries", Y. Liu, W. Zhang, Y. Zhu, Y. Luo, A. Brown, J. N. Culver, K. Xu, C. A. Lundgren, Y. Wang, and C. S. Wang, *Nano Lett.,***2013,** *13,* 293

(3) "3D Sn nanoforest template on viral scaffolds as high capacity anodes for Na ion chemistry", Yihang Liu, Yunhua Xu, Yujie Zhu, Adam Brown, James N. Culver, Cynthia A. Lundgren, Kang Xu, and Chunsheng Wang, in press at *ACS Nano*

(4) "Understanding Li+-carbonate interaction with 17O-NMR", X. Bogle, S. Greenbaum, and K. Xu, to be submitted

(5) "Direct Observation of SEI Formation on Graphitic Electrodes", D. Baker, S. Russell, A. v. Cresce, and K. Xu, to be submitted

(6) Borodin*, O.; Behl, W.; Jow. T. R. "Oxidative Stability and Initial Decomposition Reactions of Carbonate, Sulfone and Alkyl Phospate-Based Electrolytes" *J. Phys. Chem. C.* (submitted)

Presentations

(1) "High Voltage Electrolytes and Their Interphases", K. Xu, **invited speech** at the 2013 Advanced Automotive Battery Conference, Pasadena, Ca (Feb 4~8, 2013)

(2) "Interfacing Electrolytes with Electrodes in Li Ion Batteries", K. Xu, Seminar at Department of Materials Sciences, University of Washington (Feb 11, 2013)

(3) **(invited)** O. Borodin, T. R. Jow, L. Xing, "Insight into Electrolyte Stability, Decomposition and Transport Properties from DFT and MD Simulations" PRiME 2012, 222nd Meeting of Electrochem. Soc. Honolulu, Hawaii, October 7-12, **2012.**

(4) Borodin, O.; Vatamanu, J.; Xing, L.; Smith, G.; Bedrov. D.; "Bulk and Interfacial Properties of Ionic Liquids and Their Mixtures with Lithium Salts" Honolulu PRiME 2012 - Honolulu, Hawaii. October 7 - October 12, 2012

TASK 1
Battery Cell Materials Development

Project Number: ES026

Project Title: Electrolytes for Use in High Energy Li-Ion Batteries with Wide Operating Temperature Range

Project PI, Institution: Marshall Smart, Jet Propulsion Laboratory, California Institute of Technology

Collaborators (include industry): (1) University of Rhode Island (Prof. Brett Lucht) (Analysis of harvested electrodes, on-going collaborator), (2) Argonne Nat. Lab (Khalil Amine) (Source of electrodes, on-going collaborator), (3) LBNL (John Kerr, Li Yang) (Evaluation of novel salts), (4) Loker Hydrocarbon Institute, USC (Prof. Surya Prakash) (Fluorinated Solvents and novel salts), (5) A123 Systems, Inc. (Electrolyte development, on-going collaborator), (6) Quallion, LCC. (Electrolyte development, on-going collaborator), (7) Yardney Technical Products (Electrolyte development, on-going collaborator), (8) Saft America, Inc. (Collaborator, industrial partner under NASA program), (9) NREL (Smith/Pesaran)(Supporting NREL in model development by supplying data), (10) Sandia National Laboratory (Safety testing of low flammability electrolyte and supplier of electrode materials), (11) Hunter College (Prof. Greenbaum) (Ex-situ NMR measurements), and (12) North Carolina State University (Prof. Wesley Henderson) (Evaluation of novel salts).

Project Start/End Dates: Start Date: Oct 1, 2009, Projected End Date: September 30, 2014

Objectives:

- Develop a number of advanced Li-ion battery electrolytes with improved performance over a wide range of temperatures (-30 to +60°C) and demonstrate long-life characteristics (5,000 cycles over 10-yr life span).
- Improve the high voltage stability of these candidate electrolyte systems to enable operation up to 5V with high specific energy cathode materials.
- Define the performance limitations at low and high temperature extremes, as well as, identify life limiting processes.
- Demonstrate the performance of advanced electrolytes in large capacity prototype cells.

Approach: The development of electrolytes that enable operation over a wide temperature range, while still providing the desired life characteristics and resilience to high temperature (and voltage) remains a technical challenge. To meet the proposed objectives, the electrolyte development will include the following general approaches: (1) optimization of carbonate solvent blends, (2) use of low viscosity, low melting ester-based co-solvents, (3) use of fluorinated esters and fluorinated carbonates as co-solvents, (4) use of novel "SEI promoting"

and thermal stabilizing additives, (5) use of alternate lithium based salts (with USC, LBNL, and NCSU). Many of these approaches will be used in conjunction in multi-component electrolyte formulations (i.e., such as the use of low viscosity solvents and novel additives and salts), which will be targeted at improved operating temperature ranges while still providing good life characteristics.

The candidate electrolytes are characterized using a number of approaches, including performing ionic conductivity and cyclic voltammetry measurements, and evaluating the performance characteristics in experimental ~ 200-400 mAh three-electrode cells. In addition to evaluating candidate electrolytes in spirally-wound experimental cells, studies will be performed in coin cells, most notably in conjunction with high voltage cathode materials. Cells will be fabricated using a number of electrode couples: (a) MCMB/$LiNi_{0.8}Co_{0.2}O_2$, (b) graphite/$LiNi_{0.8}Co_{0.15}Al_{0.05}O_2$, (c) graphite/$LiNi_{1/3}Co_{1/3}Mn_{1/3}O_2$, (d) $Li_4Ti_5O_{12}$ (LTO)/$LiNi_{0.5}Mn_{1.5}O_2$ (LMNO), and (e) graphite/$LiNiCoMnO_2$ (lithium excess, layered-layered composite). Other chemistries can be evaluated depending upon availability from collaborators. In addition to performing charge/discharge characterization over a wide range of temperatures and rates on these cells, a number of electrochemical characterization techniques will be employed, including: (1) Electrochemical Impedance Spectroscopy (EIS), (2) DC linear (micro) polarization, and (3) Tafel polarization measurements. The electrochemical evaluation in proven three-electrode test cells enables electrochemical characterization of each electrode (and interface) individually and the identification of performance limiting mechanisms for each electrode and for the cell. Electrodes are easily harvested from these test cells and samples will be delivered to collaborators (i.e., URI and Hunter College).

Performance testing of prototype cells containing candidate advanced electrolytes will be performed and evaluated under a number of conditions, i.e., assessment of wide operating temperature capability and life characteristics. JPL has on-going collaborations with several battery vendors and also has the capabilities to perform extensive testing. Typical prototype cell designs that will be considered include (i) Yardney 7 Ah prismatic cells, (ii) Quallion prismatic cells (0.250Ah size and 12 Ah size), and (iii) A123 2.2 Ah cylindrical cells. Cells will be procured and/or obtained through on-going collaborations

Milestones:

Month/Year	**Milestone**
Sept. 2013	Milestone A: Prepare and characterize experimental laboratory cells containing advanced electrolytes, designed to operate over a wide temperature range in high-voltage systems (i.e., $LiNiMnCoO_2$), and identify performance-limiting characteristics. (Sept. 13)
Sept. 2013	Milestone B: Demonstrate improved performance of experimental and prototype cells with next generation electrolytes over a wide temperature range (-30° to $+60^oC$) compared with baseline electrolytes. (Sept. 13)

Financial data:

Total project funding:

- 875K total (~ 175K/year)
- Contractor share = 0K

Funding received:

FY'10 = 175K (Start Date = Oct 1, 2009)
FY'11 = 175K
FY'12 = 170K
FY'13 = 170K

Accomplishments and Progress toward Milestones:

In the recent quarter, we have continued the performance testing of number of large capacity 12 Ah cells (MCMB Carbon/$LiNiCoAlO_2$) manufactured by Quallion, LCC that contain JPL wide operating temperature range electrolytes. The cells are being tested to determine their life characteristics, and to evaluate the degree to which the low temperature capability degrades with time. The cells contain electrolytes that have been reported and demonstrated to have excellent low temperature capabilities, namely (i) 1.20M $LiPF_6$ in EC+EMC+MP (20:20:60 v/v %) and (ii) 1.20M $LiPF_6$ in EC+EMC+MP (20:20:60 v/v %) + 4% FEC. In addition to JPL developed electrolytes, the group of cells contain a Quallion developed wide operating temperature range electrolyte and the DOE baseline electrolyte (i.e., 1.2M $LiPF_6$ in EC+EMC (30:70 v/v %). After performing initial low temperature discharge rate testing, the cells were subjected to partial depth of discharge cycling (approximately 50% DOD) consisting of one cycle performed each day using a variable load profile with low to moderate rates. The cells have been re-characterized after completing increments of 100 cycles to determine the capacity, impedance, and low temperature discharge rate capability. As shown in Table 1, good capacity retention was observed with all of cells after completing initial characterization, low temperature testing, and the life testing described (>100 cycles), representing approximately 1.5 years of testing. The best capacity retention observed was with the cell containing the methyl propionate-based electrolyte that contains FEC as an additive (4%), slightly outperforming the baseline electrolytes, suggesting that the additive has produced a desirable, protective SEI layer. In addition to performing 100% DOD capacity and impedance determination, the cells were subjected to discharge rate testing at low temperature (-20° to -50°C) over a range of rates (C/10 to 2C) to determine the extent to which the low temperature capability has degraded. As shown in Table 2, good retention of low temperature capability was observed at -20° when evaluated at C/5 and 2C rates after competing 200 cycles, with the cells containing the methyl propionate-based cells delivering the highest capacity. It should be noted that the cell containing the electrolyte with the 1.20M $LiPF_6$ in EC+EMC+MP (20:20:60 v/v %) + 4% FEC electrolyte displayed the best retention of the initial low temperature capability, suggesting that the additive does function to minimize impedance growth. However, it should be mentioned that under certain conditions higher capacity at low temperatures was observed after life

testing, which is attributed to the increased impedance leading to enhanced internal cell heating during discharge.

				Cell QP-49				Cell QP-65				Cell QP-66				Cell QP-46			
				1.20 M $LiPF_6$ in EC+EMC (30:70 v/v %)				Quallion Electrolyte A1				1.20 M $LiPF_6$ in EC+EMC+MP (20:20:60 v/v %)				1.20 M $LiPF_6$ in EC+EMC+MP (20:20:60 v/v %) + 4% FEC			
	Temperature	Discharge Rate	Discharge Current (A)	Discharge Capacity (Ah)	Percent C/5 Capacity at 20°C	Discharge Watt-Hr (Wh)	Discharge Energy (Wh/Kg)	Discharge Capacity (Ah)	Percent C/5 Capacity at 20°C	Discharge Watt-Hr (Wh)	Discharge Energy (Wh/Kg)	Discharge Capacity (Ah)	Percent C/5 Capacity at 20°C	Discharge Watt-Hr (Wh)	Discharge Energy (Wh/Kg)	Discharge Capacity (Ah)	Percent C/5 Capacity at 20°C	Discharge Watt-Hr (Wh)	Discharge Energy (Wh/Kg)
Initial Capacity	20°C	C/5	2.400	13.6031	100.00	49.5323	93.74	12.5561	100.00	45.6779	88.83	14.1289	100.00	51.3849	97.25	13.2675	100.00	48.3083	91.42
After Low Temperature Testing	20°C	C/5	2.400	13.4195	98.65	48.7900	92.34	12.3607	98.44	44.9340	87.39	13.4466	95.17	48.9430	92.62	13.2637	99.97	48.1530	91.13
After Completing 100 Cycles	20°C	C/5	2.400	13.1084	96.36	47.6936	90.26	11.9451	95.13	43.4942	84.59	13.0794	92.57	47.6478	90.17	12.8422	96.79	46.6732	88.33
After Completing 200 Cycles	20°C	C/5	2.400	13.0209	95.72	47.3834	89.67	11.8335	94.25	43.0957	83.81	12.9007	91.31	46.9969	88.94	12.7123	95.82	46.1975	87.43

Table 1: Capacity determination of 12Ah MCMB-$LiNiCoAlO_2$ cells (Quallion, LCC) containing various electrolytes after low temperature characterization and partial DOD cycle life testing , using C/5 rates over a voltage range of 2.75V to 4.10V.

				Cell QP-49				Cell QP-65				Cell QP-66				Cell QP-46			
				1.20 M $LiPF_6$ in EC+EMC (30:70 v/v %)				Quallion Electrolyte A1				1.20 M $LiPF_6$ in EC+EMC+MP (20:20:60 v/v %)				1.20 M $LiPF_6$ in EC+EMC+MP (20:20:60 v/v %) + 4% FEC			
	Temperature	Discharge Rate	Discharge Current (A)	Discharge Capacity (Ah)	Percent C/5 Capacity at 20°C	Discharge Watt-Hr (Wh)	Discharge Energy (Wh/Kg)	Discharge Capacity (Ah)	Percent C/5 Capacity at 20°C	Discharge Watt-Hr (Wh)	Discharge Energy (Wh/Kg)	Discharge Capacity (Ah)	Percent C/5 Capacity at 20°C	Discharge Watt-Hr (Wh)	Discharge Energy (Wh/Kg)	Discharge Capacity (Ah)	Percent C/5 Capacity at 20°C	Discharge Watt-Hr (Wh)	Discharge Energy (Wh/Kg)
Initial Capacity	-20°C	C/5	2.400	11.5647	85.02	40.0224	75.74	11.1605	88.88	38.5397	74.95	11.9173	84.35	41.1668	77.91	11.4780	86.51	39.4647	74.69
		2.0C	24.00	11.2530	82.72	35.2471	66.71	11.1740	88.99	35.9119	69.84	11.9768	84.77	38.2553	72.40	11.3029	85.19	35.2538	66.72
After Completing 100 Cycles (100 Days)	-20°C	C/5	2.400	11.2645	82.81	38.7449	73.32	10.7659	85.74	36.6501	71.28	11.3759	80.52	38.8384	73.50	11.3547	85.58	39.1845	74.16
		2.0C	24.00	11.2025	82.35	34.8236	65.90	10.8843	86.69	34.4055	66.91	11.5607	81.82	36.3958	68.88	11.4050	85.96	34.8383	65.93
After Completing 200 Cycles (200 Days)	-20°C	C/5	2.400	11.2046	82.37	38.4657	72.80	10.6943	85.17	36.3392	70.67	11.2470	79.60	38.2072	72.31	11.2553	84.83	38.6714	73.19
		2.0C	24.00	11.1193	81.74	34.5188	65.33	10.8156	86.14	34.1029	66.32	11.4543	81.07	35.9009	67.94	11.3529	85.57	34.4195	65.14

Table 2: Discharge rate testing at -20°C of 12Ah MCMB-$LiNiCoAlO_2$ cells (Quallion, LCC) containing various electrolytes after low temperature characterization and partial DOD cycle life testing (cells were charged at 20°C prior to low temperature discharging).

When the cells were evaluated at -40°C, as shown in Table 3, similar trends were observed with respect to electrolyte type, with the cells containing the MP-based electrolyte delivering the highest capacity at -40°C. For example, the cell containing MP+FEC delivered over 80% of the room temperature capacity when discharged at 2.0C rate at -40°C, providing more capacity than when initially characterized. Again, this increase in capacity delivered at low temperature as the cell ages has been attributed to

the thermal characteristics of the cell (i.e., as the impedance increases cycling it leads to increased heat generation upon low temperature discharge).

				Cell QP-49				Cell QP-65				Cell QP-66				Cell QP-46			
				1.20 M $LiPF_6$ in EC+EMC (30:70 v/v %)				Quallion Electrolyte A1				1.20 M $LiPF_6$ in EC+EMC+MP (20:20:60 v/v %)				1.20 M $LiPF_6$ in EC+EMC+MP (20:20:60 v/v %) + 4% FEC			
	Temperature	Discharge Rate	Discharge Current (A)	Discharge Capacity (Ah)	Percent C/5 Capacity at 20°C	Discharge Watt-Hr (Wh)	Discharge Energy (Wh/Kg)	Discharge Capacity (Ah)	Percent C/5 Capacity at 20°C	Discharge Watt-Hr (Wh)	Discharge Energy (Wh/Kg)	Discharge Capacity (Ah)	Percent C/5 Capacity at 20°C	Discharge Watt-Hr (Wh)	Discharge Energy (Wh/Kg)	Discharge Capacity (Ah)	Percent C/5 Capacity at 20°C	Discharge Watt-Hr (Wh)	Discharge Energy (Wh/Kg)
Initial Capacity	-40°C	C/5	2.400	9.4562	69.52	27.9256	52.85	10.1802	81.08	31.3574	60.98	10.8938	77.10	33.5327	63.46	10.1753	76.69	31.3902	59.41
		2.0C	24.00	9.7003	71.31	26.3924	49.95	10.7160	85.35	31.6800	61.61	11.4353	80.94	33.5327	63.46	10.4989	79.13	30.3517	57.44
After Completing 100 Cycles (100 Days)	-40°C	C/10	1.20	10.0118	73.60	30.8227	58.33	9.7335	77.52	30.1521	58.64	10.2400	72.48	32.0023	60.56	10.2327	77.13	32.2940	61.12
		C/5	2.40	9.6569	70.99	28.2589	53.48	9.6088	76.53	28.7043	55.82	10.1014	71.49	30.4018	57.54	10.0273	75.58	30.3270	57.39
		C/2	6.00	9.5562	70.25	26.7520	50.63	9.7484	77.64	28.3068	55.05	10.2337	72.43	29.8563	56.50	10.0529	75.77	29.1979	55.26
		2.0C	24.00	10.0405	73.81	27.3641	51.79	10.4198	82.99	30.0234	58.39	11.0347	78.10	31.7327	60.05	10.7799	81.25	29.9095	56.60
After Completing 200 Cycles (200 Days)	-40°C	C/10	1.20	9.9514	73.16	30.5927	57.90	9.6474	76.83	29.7944	57.94	10.0995	71.48	31.3569	59.34	10.1334	76.38	31.8464	60.27
		C/5	2.40	9.6191	70.71	28.1142	53.21	9.5292	75.89	28.3840	55.20	9.9639	70.52	29.7991	56.40	9.9285	74.83	29.8674	56.52
		C/2	6.00	9.4853	69.73	26.5200	50.19	9.6429	76.80	27.9001	54.26	10.1105	71.56	29.3918	55.62	9.9540	75.03	28.8185	54.54
		2.0C	24.00	10.0045	73.55	27.2027	51.48	10.3516	82.44	29.7156	57.79	10.9376	77.41	31.2356	59.11	10.7450	80.99	29.5237	55.87

Table 3: Discharge rate testing at low temperature of 12Ah MCMB-$LiNiCoAlO_2$ cells (Quallion, LCC) containing various electrolytes after low temperature characterization and partial DOD cycle life testing (cells were charged at 20°C prior to low temperature discharging).

We have also continued our investigation of electrolytes that are permutations of this approach described above, and consists of methyl propionate with varying amount of mono-fluoroethylene carbonate (4, 10, and 20%), with the intent of improving the high temperature resilience. In the last case, we have entirely replaced ethylene carbonate (EC) with FEC. We have also continued the study of using LiBOB as an additive to methyl propionate-based electrolytes, based upon previous findings from three electrode cell results that it improves the cathode kinetics significantly. Our performance evaluation of these electrolytes in prototype cells (0.25Ah MCMB/$LiNiCoAlO_2$ cells manufactured by Quallion, LCC) is on-going. As illustrated in Fig. 1, all of electrolyte lead to improved performance when evaluated at high discharge rates (5.0C) at low temperature (-40°C) compared with the DoE baseline all carbonate electrolyte, with the cells containing 1.20M $LiPF_6$ + 0.10M LiBOB in EC+EMC+MP (20:20:60 v/v %) delivering the best performance (i.e., delivering 49 Wh/kg with a 5C discharge rate at -40°C).

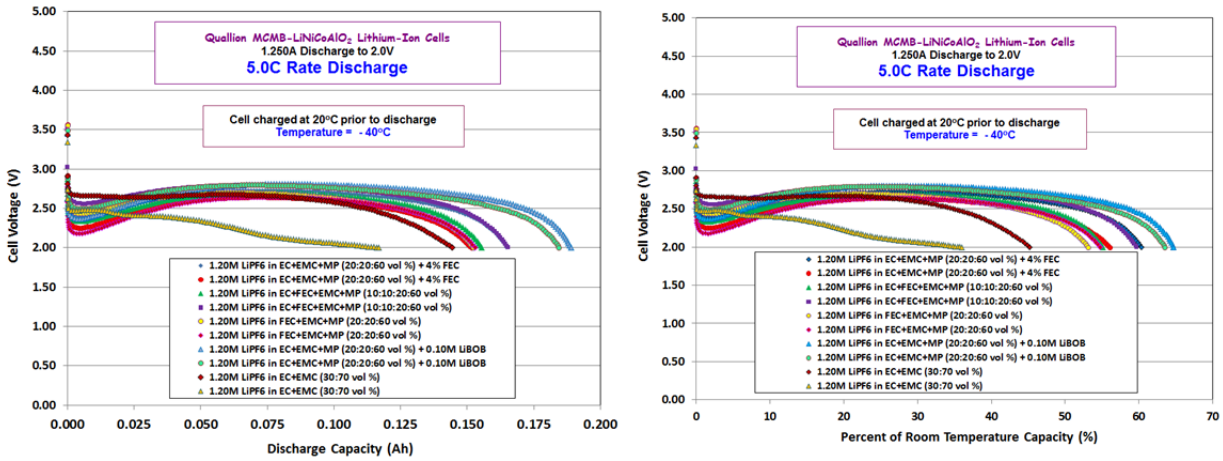

Figure 1: Discharge performance of 0.25Ah MCMB-$LiNiCoAlO_2$ cells (Quallion, LCC) containing a methyl propionate-based electrolytes at -40°C using 5C discharge rates. (Cells were charged at room temperature prior to low temperature discharging).

As part of the evaluation of these cells, we are performing cycle life testing under a number of conditions, including 100% DOD cycling at 20°C, 40°C, and 50°C, as well as variable temperature cycling between temperature extremes (i.e., -20° and +50°C). As illustrated in Fig. 2, excellent performance has been obtained with many of the formulations when subjected to 100% DOD cycle life testing at 20°C, with over 1,100 cycles completed to-date. An interesting trend is that lower capacity fade is observed with increasing FEC content in the electrolyte, although high FEC content led to somewhat lower initial capacity. For example, the cell containing 1.20M $LiPF_6$ in FEC+EMC+MP (20:20:60 v/v %) displays excellent cycle life characteristics and is actually delivering more capacity after 1,200 cycles (i.e., 245 mAh) compared to the initial performance (i.e., 241 mAh). Although the cell containing the baseline all carbonate electrolyte is delivering more capacity after 1,200 cycles (i.e., 258 mAh) compared to the cell containing methyl propionate and high FEC content, it is exhibiting much greater capacity fade (i.e., 86% of the initial capacity) and the MP+FEC-based cell is projected to have improved long term life.

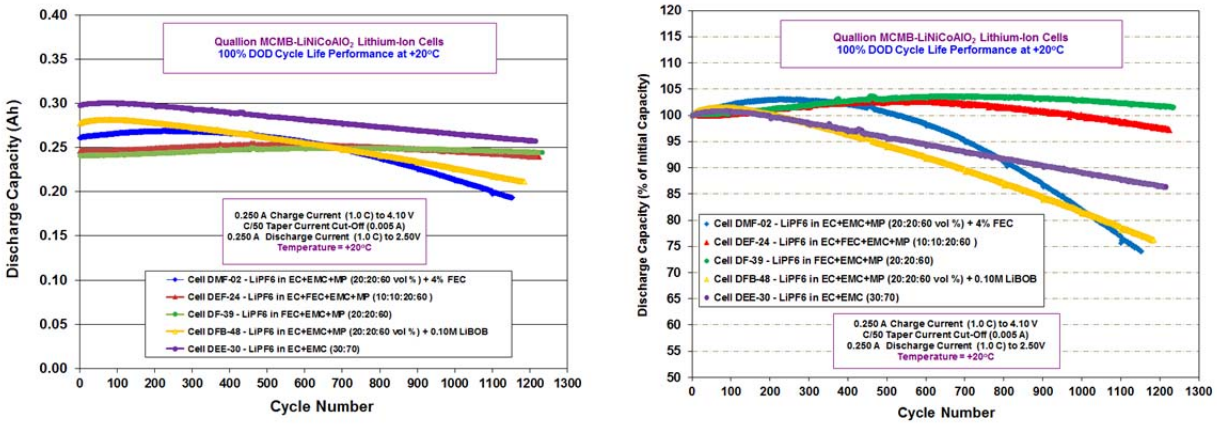

Figure 2: Cycle life performance 0.25Ah MCMB-$LiNiCoAlO_2$ cells (Quallion, LCC) containing a methyl propionate-based electrolytes at 20°C using C rate charge and discharge.

We also continue to evaluate the life characteristics of a number of A123 cells that possess methyl butyrate-based electrolytes previously investigated under this program (i.e., specifically 1.20M $LiPF_6$ in EC+EMC+MB (20:20:60 vol %) + 4% FEC and 1.20M $LiPF_6$ in EC+EMC+MB (20:20:60 vol %) + 2% VC). As previously noted in the program, these cells have exhibited excellent rate capability over a wide temperature range (down to -60 ^oC), and have been shown to have good cycle life performance up to +60^oC. As illustrated in Fig. 3, excellent cycle life has been obtained with the cells exhibiting over 7,500 cycles to-date (on test for over 2.5 years) and displaying comparable performance to the baseline electrolyte (over 82% of the initial capacity). We also continue to determine the impact of electrolyte type upon the high temperature resilience of these systems by implementing variable temperature cycling tests, in which the cells are continuously cycled between temperature extremes (i.e., at - 20° and +50^oC) with charging and discharging at the respective temperature, as shown in Fig 3B. Although the electrolyte variant with FEC was observed previously to be less resilient to high temperature exposure compared to the VC-containing electrolyte, good performance was observed over the temperature range with only modest loss in capacity. We are in the process of determining the relative impedance growth of these cells observed during the on-going cycling life testing, by analyzing the results of DC current interrupt measurements that have been performed periodically throughout the testing.

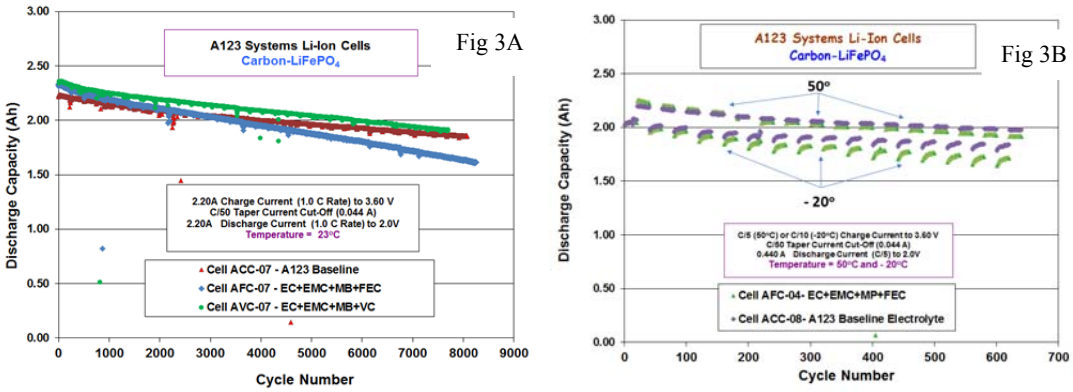

Figure 3: Cycle life performance of $LiFePO_4$-based A123 cells containing various electrolytes at +23^oC (Fig. 3A) and variable temperature cycling between +50^oC and -20^oC (Fig. 3B).

We are currently evaluating various methyl butyrate-based formulations in cells consisting of Conoco graphite anodes and NMC cathodes (HE5050) supplied by Argonne National Labs, in an extension of our previous studies with this system. This study is being performed in both coin cells as well as larger experimental three electrode cells equipped with lithium reference electrodes. We plan to subject these cells to a number of electrochemical measurements, including Electrochemical Impedance Spectroscopy (EIS), Tafel polarization, and linear micro-polarization measurements, over a range of temperatures. Future work will involve continuing the investigation of the use of additives in conjunction with ester-based, wide operating temperature range electrolytes evaluated

with different electrode chemistries, with a focus upon (i) assessing other candidate electrolyte additives, including new lithium-based salts provided by Prof. Wesley Henderson's group (ii) studying the high temperature and cycle life degradation modes, (iii) correlating electrochemical trends with performance, and (iv) identifying performance limiting aspects at extreme temperatures. Future work will also focus upon demonstrating these systems in prototype cells.

Publications:

1. M. C. Smart, et. al., "Development of Low Temperature Electrolytes for Lithium-Ion Batteries", Advanced Automotive Batteries Conference, Pasadena, CA, February 5, 2013.
2. M. C. Smart, C. Hwang, F. C. Krause, J. Soler, W. C. West, B. V. Ratnakumar, and K. Amine, "Wide Operating Temperature Range Electrolytes for High Voltage and High Specific Energy Li-Ion Cells", ECS Transactions, submitted.
3. M. Jun, K. Smith, E. Wood, and M. C. Smart, "Battery Capacity Estimation of Low-Earth Orbit Satellite Application", *International Journal of Prognostics and Health Management*, submitted.
4. M. C. Smart, C. Hwang, F. C. Krause, J. Soler, W. C. West, B. V. Ratnakumar, and K. Amine, "Wide Operating Temperature Range Electrolytes for High Voltage and High Specific Energy Li-Ion Cells", 222nd Meeting of the Electrochemical Society, Honolulu, HI, October 7-12, 2012. (Abstract #1235).
5. M. C. Smart, B. L. Lucht, S. Dalavi, F. C. Krause, and B. V. Ratnakumar, "The Effect of Additives upon the Performance of MCMB/$LiNiCoO_2$ Li-Ion Cells Containing Methyl Butyrate-Based Wide Operating Temperature Range Electrolytes", J. Electrochem. Soc., **159 (6)**, A739-A751 (2012).

The work described here was carried out at the Jet Propulsion Laboratory, California Institute of Technology, under contract with the National Aeronautics and Space Administration (NASA).

TASK 1
Battery Cell Materials Development

Project Number: ES027 **Reporting Period:** FY 2013 Q1

Project Title: Novel Phosphazene Compounds for Enhancing Electrolyte Stability and Safety of Lithium-ion Cells

Project PI, Institution: Kevin L. Gering, INL

Collaborators (include industry): Michael T. Benson (INL), Mason K. Harrup (INL), Harry W. Rollins (INL), Sergiy V. Sazhin (INL), Khalil Amine (ANL), Chris Orendorff (SNL), Princess Energy Systems, Dow Chemical

Project Start/End Dates: Jan. 2009/Ongoing

Objectives: Our focus is to understand stability of our new classes of phosphazene materials and to establish viability for their use in lithium-ion cell electrolytes, considering both conventional voltage ranges (4.2V) and higher voltage electrode couples (4.5-5V). Comprising this overall work are the following focus areas:

- Synthesize novel solvents for Li-ion cells that are safer alternatives to volatile organics.
- Gain understanding of molecular-scale interactions between phosphazenes and other electrolyte components.
- Determine what phosphazene structures are more tolerant to high and low voltage, and to high temperatures.
- Determine the effect of phosphazenes on SEI films, cell performance, and cell aging in general, using ABR-relevant electrode couples.
- Synthesize and engineer novel phosphazene polymers that would serve as safe and robust alternatives to carbon-based anodes. Linked with our electrolyte research, this enhances overall compatibility of cell chemistry.

This collective effort will enable us to engineer advanced materials for more robust lithium-ion cells and move us closer to the overall goal of a carbon-reduced cell chemistry.

Approach: The INL is leveraging this work based on interdepartmental synergy between a well-established battery testing program and its foremost experts in phosphazene chemistry that are producing new classes of novel compounds for use in lithium-ion batteries. As such, the INL is strongly positioned to approach primary targets for ABR electrolyte development while maintaining historical knowledge of phosphazene chemistry and related applications.

This work is split under four primary tasks: solvent synthesis, characterization, DFT modeling, and lithium-ion cell testing. Upfront issues are

- ♦ voltage stability (CV)
- ♦ temperature stability
- ♦ flammability (flash point)
- ♦ lithium salt solubility
- ♦ transport properties (viscosity, conductivity)
- ♦ chemical compatibility with the cell environment
- ♦ molecular interactions (solvent-ion)

Coin cell testing covers issues of formation, interfacial impedance, polarization testing, and aging, using our compounds as electrolyte additives (1-10%). In previous quarters we investigated our electrolytes with ABR electrode couples LNMO/LTO, NMC(3M)/Carbon, and HE5050/Carbon. We test our novel polymeric anodes against ABR-relevant cathodes such as NMC. For most coin cell testing the general protocol is: formation cycling (C/10 @ 3), EIS, followed by a matrix of C/10, C/3, C/1, and 3C, all at 30 °C. Testing concludes with 3C cycling at 45-55 °C to determine electrolyte effect on high temperature tolerance. Final EIS is optional.

Milestones (cumulative over FY 2011-2012):

	= Activity completed in reporting period

Milestone	Status	Date
a. Synthesis of Fluorinated Phosphazene series (FM1,2,3)	completed	March 2011
b. Synthesis of Gen1 Ionic Liquid Phosphazene (PhIL-1)	completed	Feb. 2011
c. Synthesis of newer SM series (SM 5,6,7)	completed	October 2010
d. Development of improved voltammetry techniques for SEI characterization.	completed	December 2010
e. DFT simulations of selected phosphazenes regarding interaction with lithium ions	completed	Feb./March 2011
f. Thermal stability testing of blends with SM6 and SM7	completed	March 2011
g. Cell testing using LNMO/LTO and NMC/Carbon* couples: characterization of capacity and impedance attributes	completed	March 2011
h. Cell testing using LNMO/LTO and NMC/Carbon* couples: aging studies	completed	October 2011
i. Phase 1 concept validation for alternative anode materials	completed	October 2011
j. Cell testing using HE5050/Carbon couple: characterization of capacity and impedance attributes	completed	December 2011
k. DFT study on complete FM Series (fluorinated cyclics)	completed	February 2012
l. Cell testing using HE5050/Carbon couple: aging studies	completed	March 2012

m. Phase 2 concept validation for alternative anode materials	completed	March 2012
n. Initial PALS measurements of alternative anode materials	completed	March 2012
o. Synthesis of newer FM series and second-generation Ionic Liquid Phosphazenes	In Progress	
p. Abuse testing of INL electrolyte additives at SNL, Phase 1	Completed	November 2012
q. Collaboration with ANL regarding scale-up of INL electrolyte compounds	In Progress	
r. Cell testing using NCA (Toda)/Carbon couple: characterization of capacity and impedance attributes	In Progress	
s. Phase 3 Alternative Anode materials with improved electronic conductivity and capacity	In Progress	
t. NMR evaluation of electrolyte fate at elevated temperatures (Washington State Univ.)	In Progress	
u. Abuse testing of INL electrolyte additives at SNL, Phase 2 (10-20% additives in electrolyte)	In Progress	

Financial data: Funding Received: FY 10: $ 400K; FY 11: $ 400K ; FY 12: $500K (under subcontract, a small portion of this might go to Washington State University for specialized NMR measurements).

PROGRESS TOWARD MILESTONES

(a, b) Completed 2011 Q2.

(c) Completed 2011 Q1.

(d) Completed 2011Q1.

(e) Completed 2011 Q2.

(f) Completed 2011 Q2.

(g) Completed 2011 Q2.

(h) Completed 2012 Q1.

(i) Completed 2012 Q1.

(j) Completed 2012 Q1.

(k) Completed 2012 Q2.

(l) Completed 2012 Q2.

(m) Completed 2012 Q2.

(n) Completed 2012 Q2.

(o) *A key driver of our work is to move toward an "inorganic cell chemistry" that has a common chemical basis throughout the cell. The next step in this progression is to test phosphazene-containing electrolytes against an electrode couple comprised of a phosphazene-based anode and a high voltage cathode.* Our synthesis targets during this quarter are newer generations of FM and phosphazene-based ionic liquid (PhIL) compounds. We are reviewing synthesis routes to arrive at a streamlined, economical, and high-purity path toward production of these unique compounds. In previous quarters our voltammetry studies clearly showed that our phosphazene compounds can triple the voltage window of the baseline electrolyte while at moderate levels (20%), and small amounts of phosphazenes (1%) can dramatically improved the temperature stability of the electrolyte. These compounds will be tested against ABR-relevant higher-voltage cathode materials and our novel electrode materials in (m) and (s) to further enhance cell voltage stability at 5V. Work for Q1 2013 centered around synthesis and characterization of FM6 and FM7, each having different arrangement of fluorinated pendant groups, while small amounts of FM2 were added to electrolytes used for Task (s).

(p) Phase 1 abuse testing of INL Phosphazene compounds at SNL concluded November 2012, using 18650 cells containing the NMC (3M)/carbon (A10) couple. INL additives included FM-2, SM-6, and PhIL-2 at one and three percent levels. The focus of this work was to determine how INL additives help mitigate (delay) the onset of thermal runaway. Initial results from this work indicate overall benefit of INL phosphazene additives in terms of thermal stability, in the order of {SM-6 > PhIL-2 > FM-2}. For example, at 3% levels SM-6 decreases the peak heating rate by over 100 degrees C per minute, while PhIL-2 cuts the gas evolution to one-third that of the baseline system. Flammability testing at SNL established that the PhIL-2 additive provides significant benefit. The baseline, SM-6, and FM-2 cells all exhibited similar burn times (100-300s) and relatively short ignition times. However, the PhIL-2 electrolyte showed a significantly shorter burn time (<20 s) and longer ignition times. This suggests reduced flammability for the PhIL-2 electrolyte relative to the baseline and other electrolytes. Phase 2 work will perform abuse testing for electrolytes having selected INL additives up to 20% by mass.

(q) We have continued our efforts to collaborate with ANL regarding the synthesis of INL phosphazene electrolyte compounds in the ANL materials scale-up facilities. The top candidate for scale-up will be the best compound(s) is emerging from the results of the SNL abuse testing, as mentioned in Tasks (p) and (u).

(r) Cell testing using NCA (Toda)/Carbon couple continued, covering a large matrix of INL additives from the FM series. Characterization of capacity and impedance attributes is ongoing for coin cells made with phosphazene-doped electrolytes and the NCA (Toda)/Carbon couple provided by ANL. Discharge capacity over cycling rate is shown (**Fig. 1**), wherein electrolyte formulations contained about 3-4 percent phosphazene

additives FM-1, FM-2, FM-3, or FM-4 in a baseline of EC-EMC (2:8) with 1.2M $LiPF_6$. Electrolyte performance is on par with that seen for earlier testing with LNMO/LTO, HE5050/Carbon, and NMC/Carbon couples. In some cases the electrolytes with FM-1 and FM-2 performed better than the baseline system. These results clearly suggest that the INL additives are compatible with the NCA (Toda)/Carbon couple. **Figure 2** shows results for electrolytes having 3.7 to 24.7 percent FM-2 in the baseline electrolyte. With the chosen electrode couple, acceptable performance is seen up to a C/1 rate for FM-2 levels up to 12.4 percent. Polarization effects diminish transport performance at the 24.7 percent level at cycling rates C/1 and greater. Optional follow-on testing for cells in Figs. 1 and 2 include thermal stability testing at 45 °C while cells undergo cycle-life protocols.

(s) Our work on Phase 3 alternative anode materials seeks improved electronic conductivity, as well as energy storage and safety beyond the carbon anode baseline. We are performing a third phase matrix of our alternative anode materials investigation, using a polymeric approach toward engineering new carbon-reduced anode materials. Phase 1 and 2 studies showed cycling to 5V (full cell) was achieved, yet we determined that the observed capacity was being impacted by low electronic conductivity of the 3D polymer framework. Capacities of Phase 1 and 2 materials approached that of conventional carbon systems, and we concluded that enhancing the electronic conductivity of these materials will allow us to improve capacity to achieve competitive levels. Efforts to enhance the conductivity of INL cyclophosphazene-based anode materials have pursued two different routes. New cyclophosphazene molecules with substituents that when cross-linked either electrochemically or using a chemical oxidant can become conducting have been synthesized. Second, copolymer systems have been prepared which include high performing tert-butyl hydroquinone cyclophosphazene (tbu-HQCP) materials and a second conducting polymer. To facilitate more rapid evaluation of the anode films a four point probe has been purchased and is being employed to monitor the thin film resistivity of prepared samples. The resistivities are also being correlated with electrochemical performance. We are also seeing correlations between polymer type and lithium uptake, indicating further information regarding the 3D framework of these materials. Lastly, the presence of the phosphazenes in the electrode composition adds to the overall flame resistance and safety of the cell chemistry.

In Q1 2013 *our materials achieved high gravimetric capacities* in several formulations having improved electronic conductivity through cross-linking schemes. **Figure 3** (a,b) show SEM images of the anode materials as deposited onto copper (uncalandared). **Figure 4** shows test results for one such batch of formulations, wherein gravimetric discharge capacities for some cells **exceeded 800 mAh/g**, far above that of conventional carbons. In these cells the counter electrode (cathode) was LNMO, where full cells were cycled to 4.9V. **Figure 5** shows test results toward determining self-discharge behavior where cells were charged to 4.8V, followed by OCV conditions for 300 hours. Results indicate good stability under charge conditions, where cell voltage declined by only one percent. We are currently investigating extended cycle-life testing of these novel systems to understand aging mechanisms and to determine appropriate conditions that would minimize capacity losses over time. Optimization of polymer properties in terms of cross-linking, porosity, conductivity, etc. will further enhance stability and performance

of these novel anode materials. In Q2 2013 we will also investigate the use of other cathodes vs. our polymeric anodes, such as HE5050.

(t) NMR evaluation of electrolyte fate at elevated temperatures (Washington State Univ.). Sub-contracted work with WSU (contact: Prof. Bill Hiscox) performs advanced NMR studies in two areas of our new materials development. The first area employs high resolution multi-dimensional solution NMR. The thrust here is to identify early degradation fragments from conventional electrolytes and determine the primary mechanisms of thermal degradation. Then electrolyte formulations containing INL phosphazene additives are being studied using the same techniques in an attempt to elucidate the mechanisms by which the phosphazene additives prevent the organic carbonate degradation. The value added in using WSU instead of INL facilities is their NMR center has more NMRs at various field strengths and a greater instrumental capability than currently possessed at INL. Further, their resident NMR experts have greater concentrated expertise in these types of complex multi-dimensional analyses.

From initial WSU findings, the baseline sample, having no protection from the phosphazene, formed a gel at the bottom of the tube as time progressed at 60˚C. The sample has become much more viscous overall than Sample 1 (having the protective cyclic phosphazene), which has not undergone a perceptible viscosity increase. The evidence of phosphorus-proton coupling in the reaction products of the baseline sample suggest that phosphorus is reacting with the solvent, which is a mixture of ethyl and methyl carbonates. These NMR-observable product species may be intermediates in polymerization of the carbonates, leading to a polycarbonate formation. This would account for the viscosity change in the baseline sample. However, formation of dimers, trimers, etc. of solvent molecules containing PF2 linking units, may explain why the new PF2 signals have continued to increase in intensity with respect to PF_6^- signals, and why they appear to be stable products in the mixture. However, the final fate of these species is not known from the present preliminary aging study. Continued monitoring of the two samples, and further studies of starting materials and products will be necessary to sort this out. The complexity of this system (5+ observable nuclei with spin-spin coupling interactions among at least 4 of them) will require a number of approaches to fully elucidate the mechanisms of degradation in the unprotected system, and the mode of protection of the cyclic phosphazenes. The second area employs solid-state 1- and 2-dimensional analyses of the phosphazene anode materials under development.

(u) Phase 2 of abuse testing of INL electrolyte additives at SNL will investigate the impact of having 10-20 percent INL additives in the baseline electrolyte, using 18650 cells containing the NMC (3M)/carbon (A10) couple. We leverage the knowledge gained in Phase 1 (Task p) to target best candidates that would promote significant benefit in thermal resilience and safety while allowing cells to achieve satisfactory cycling performance for the intended application. This will also allow a fair assessment of TRL values of INL materials for commercial battery applications.

Publications, Reports, Intellectual property

- "Lithium binding in fluorinated cyclic triphosphazenes" M. T. Benson, M. K. Harrup, K. L. Gering, *Computational and Theoretical Chemistry*, 1005 (2013) 25–34.
- Intellectual Property relating to novel materials is being documented case-by-case as needed.

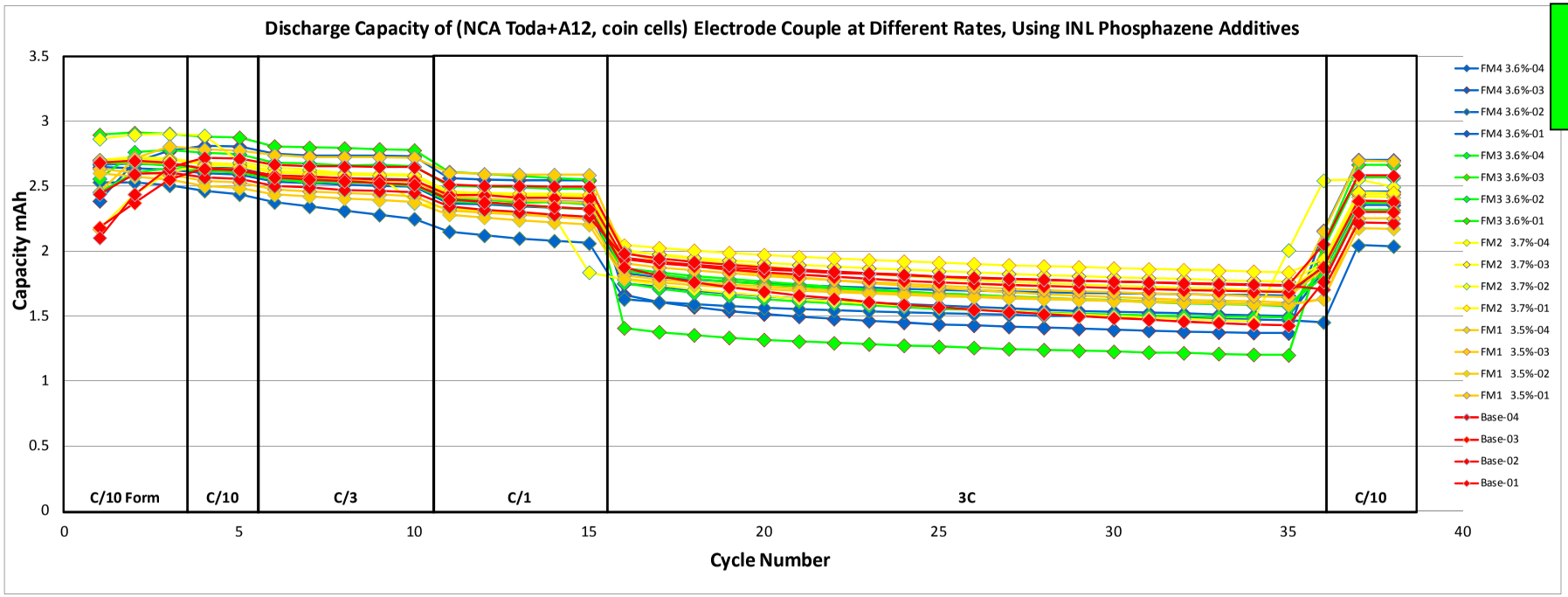
Discharge Capacity of (NCA Toda+A12, coin cells) Electrode Couple at Different Rates, Using INL Phosphazene Additives
Capacity mAh
Cycle Number
C/10 Form
C/10
C/3
C/1
3C
C/10
FM4 3.6%-04
FM4 3.6%-03
FM4 3.6%-02
FM4 3.6%-01
FM3 3.6%-04
FM3 3.6%-03
FM3 3.6%-02
FM3 3.6%-01
FM2 3.7%-04
FM2 3.7%-03
FM2 3.7%-02
FM2 3.7%-01
FM1 3.5%-04
FM1 3.5%-03
FM1 3.5%-02
FM1 3.5%-01
Base-04
Base-03
Base-02
Base-01

Fig. 1

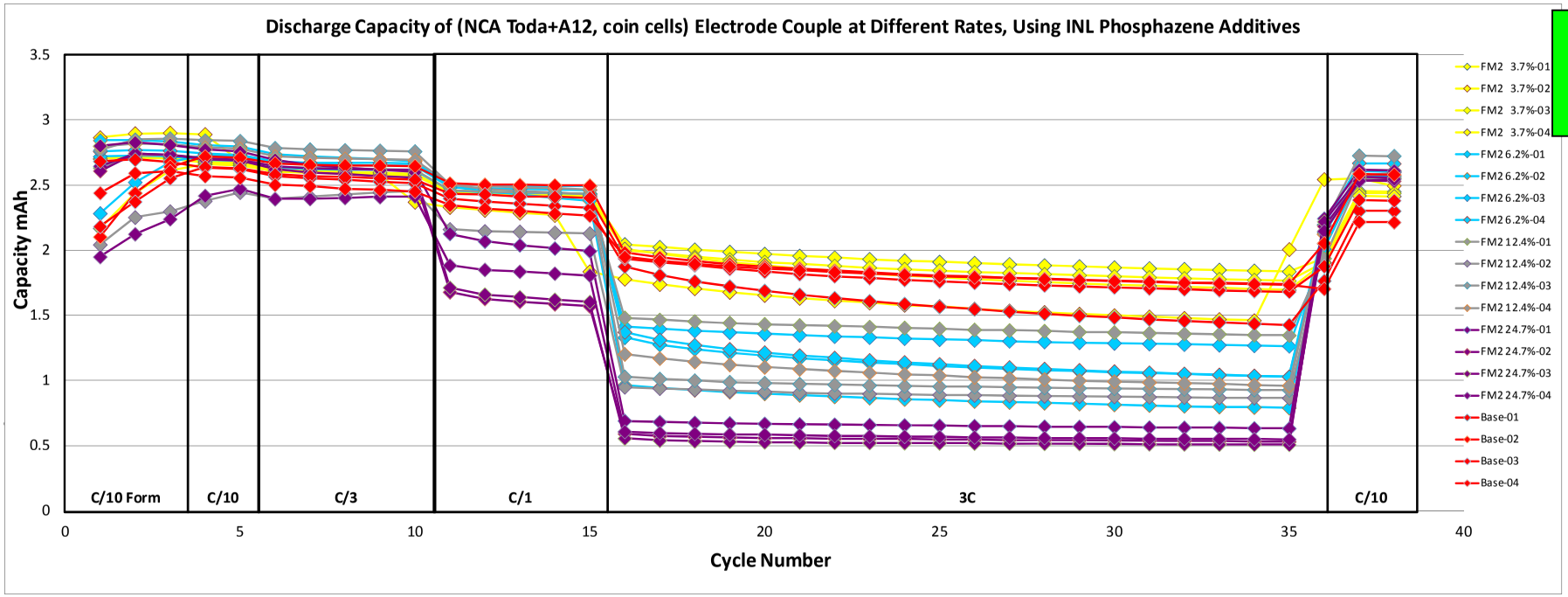
Discharge Capacity of (NCA Toda+A12, coin cells) Electrode Couple at Different Rates, Using INL Phosphazene Additives
Capacity mAh
Cycle Number
C/10 Form
C/10
C/3
C/1
3C
C/10
FM2 3.7%-01
FM2 3.7%-02
FM2 3.7%-03
FM2 3.7%-04
FM2 6.2%-01
FM2 6.2%-02
FM2 6.2%-03
FM2 6.2%-04
FM2 12.4%-01
FM2 12.4%-02
FM2 12.4%-03
FM2 12.4%-04
FM2 24.7%-01
FM2 24.7%-02
FM2 24.7%-03
FM2 24.7%-04
Base-01
Base-02
Base-03
Base-04

Fig. 2

Fig. 3 (a,b)

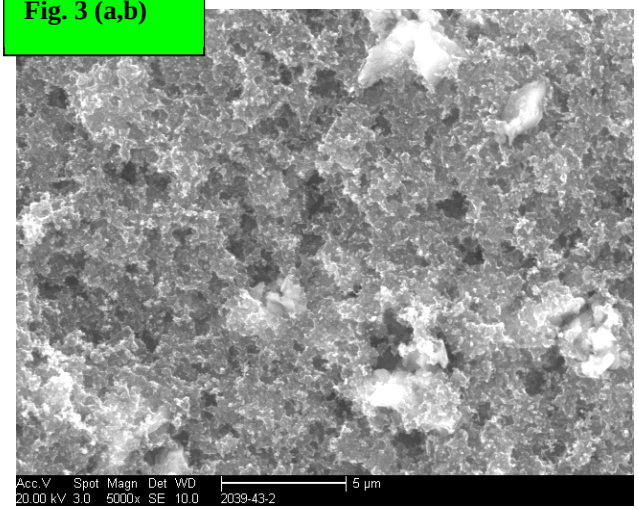

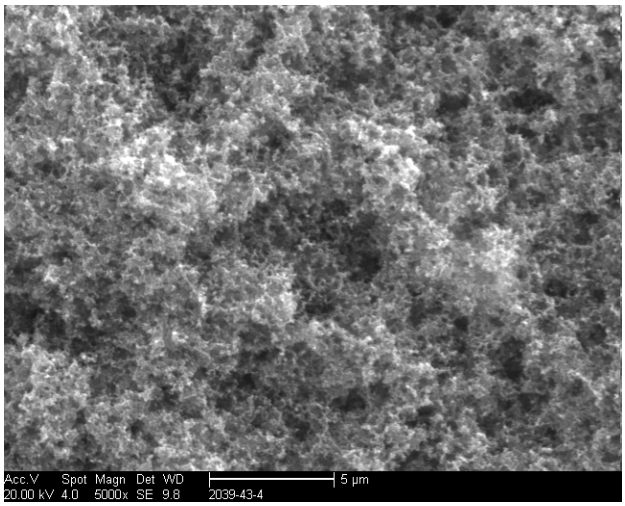

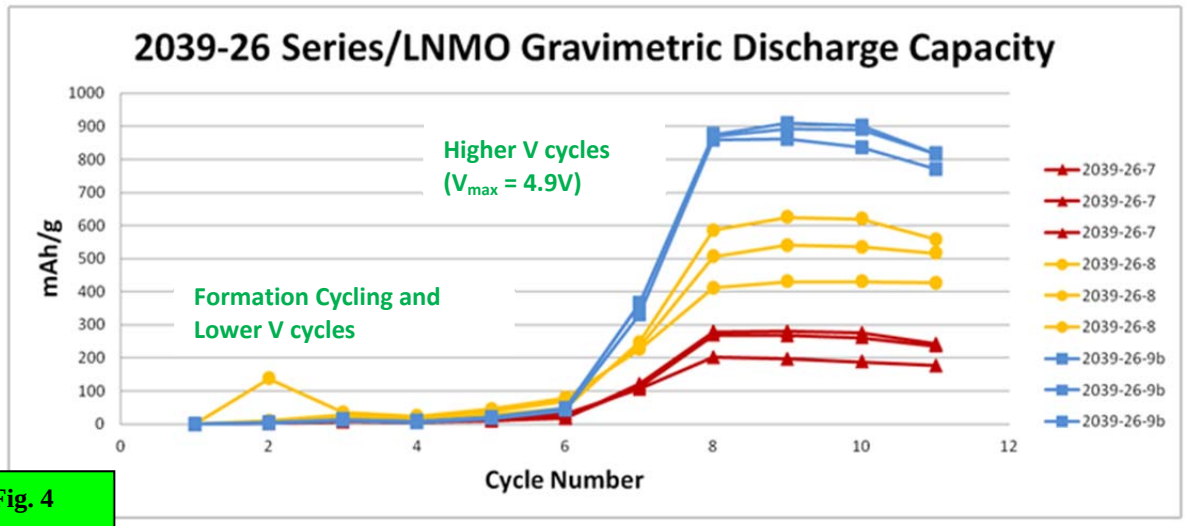

Fig. 4

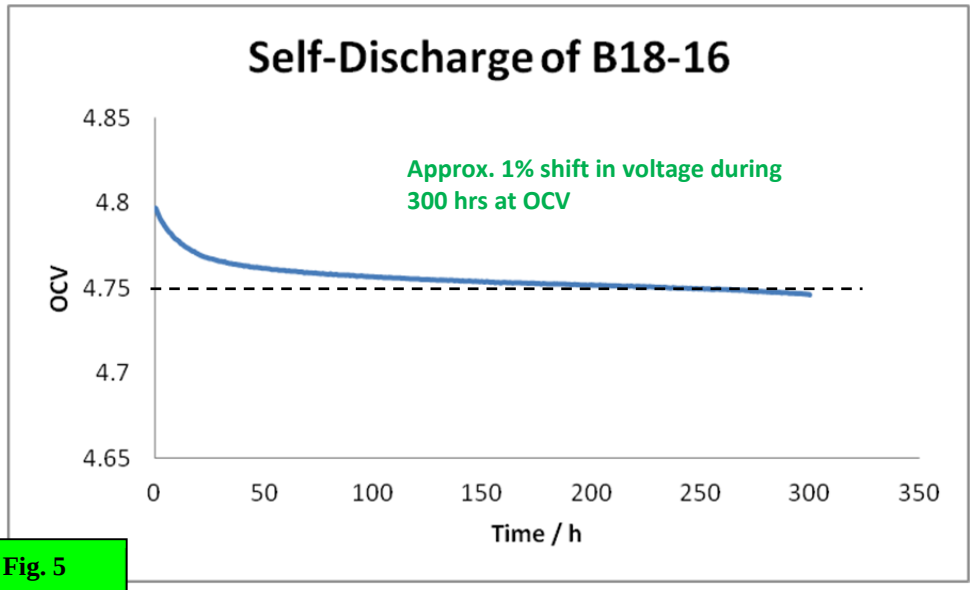

Fig. 5

TASK 1
Battery Cell Materials Development

Project Number: 1.2.2 (ES029)

Project Title: Scale-up and Testing of Advanced Materials from the BATT Program

Lead PI and Institution: Vince Battaglia, Lawrence Berkeley National Laboratory

Barrier: Cost is too high (energy density needs to be increased); life is short of 15 year target.

Specific Objectives: (*i*) Identify materials in the BATT Program that are ready for enhanced screening diagnostics, (*ii*) provide feedback on cell performance attributes to BATT researchers so that they may improve their materials, and (*iii*) provide information to the ABR Program about materials that provide significant improvements over the baseline chemistry, ABR_1.

General Approach: Work with BATT PIs in deciding what materials are ready for scale-up and enhanced testing and diagnostic evaluation in full cells. Once materials are identified, decide on the best approach for increasing the quantity of the material to approximately 10 g (1 ml if it is electrolyte). Prepare laminates of the material and test in coin cells against Li. Based on initial test results, decide on best vehicle application for the material, design the electrodes for that application, and perform long-term cycling tests. Provide comparisons to ABR Program baseline materials and cells.

Current Status as of October 1, 2012: Five Ni-spinel materials, including three from MIT and UT, were tested for rate capability to the same cut-off voltages in half- and full-cells. All but one of the materials consisted of cations in a disordered state. The one ordered material showed the lowest rate capability when tested against Li metal. When the materials were tested against graphite, the cells displayed worse rate performance than against Li. Four electrolytes were tested in graphite/Ni-spinel cells. The electrolyte with FEC showed the best rate capability. Electrolytes from CWRU and URI were tested in graphite/NCM cells. All of the electrolytes showed improved cycling performance when compared with 1 M $LiPF_6$ in EC:DEC 1:2.

Expected Improvement by September 30, 2013: Will have identified at least five more BATT Program materials that should or should not undergo further testing. There will be an emphasis on electrolytes and anodes as these projects have been running for four and three years, respectively. Results of this analysis will help guide BATT PIs and BATT management with regard to their approach to future RFPs

Schedule and Deliverables: Attend review meetings and present interim results on the scale-up of BATT Program materials (November 2011, February 2012, August 2012) and in Quarterly Reports.

Milestone:
Battery design, performance, and cycling characteristics of multiple materials from the BATT Program and for the $LiNi_{1/2}Mn_{3/2}O_4$ system will be reported on at the DOE Annual Merit Review (May 2012).

PLAN TO ACHIEVE DELIVERABLES

Beyond testing materials developed in the BATT Program, it is our group's responsibility to test supplier materials for a $LiNi_{1/2}Mn_{3/2}O_4$ baseline for both the ABR and BATT Programs. Through this effort, the active material from NEC was identified. This quarter, three carbons from Timcal: Super C65, Super C45, and Super P-Li; and VCGF were tested and compared to the present baseline material Denka black (ATD Gen 2 baseline conductive additive).

Half-cells were fabricated with a fairly low active material loading of approximately 0.6 mAh/cm^2 with roughly 4% binder and 3% conductive carbon. It has been shown by our lab that for *half-cells* with Denka black there is an extended amount of side reaction during the C/10 charge when a 4.95 V upper cut-off voltage is employed. Independent of the carbon used, the results shown below were indicative except the Super P-Li.

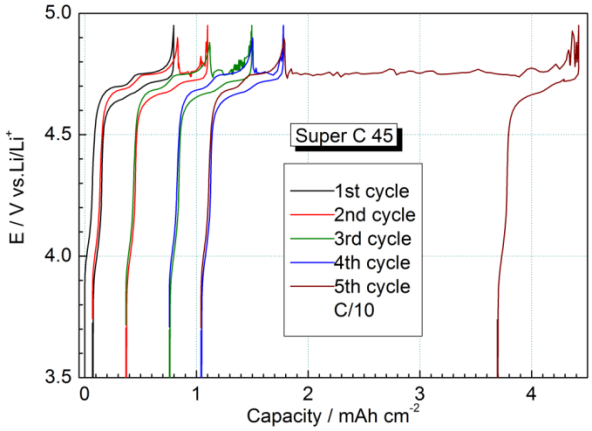

Close inspection of the data shows a highly variable voltage response during the constant-current charge and an extended charge time during the 5th charge cycle. Such an irregular voltage response is not only an indication of a side reaction but also of a side reaction that involves the production of a gas. And, not only is this a gas, but a gas that is reversibly oxidized or reduced to generate a benign shuttle between the two electrodes.

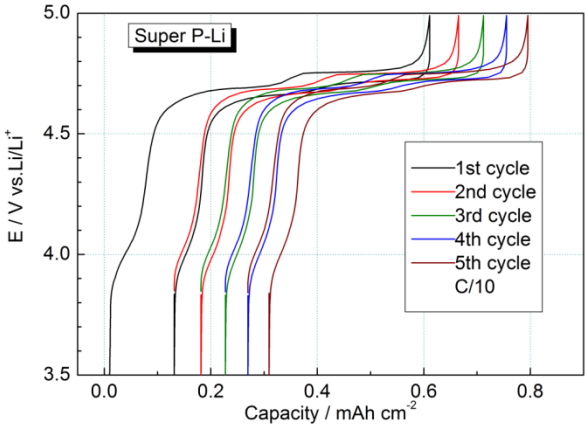

For a cell with a comparable loading but containing Super P-Li, the response is much more favorable, as seen in the second figure.
Consistent with this result, is that the Super P-Li consists of larger particles and a lower surface area. Also consistent with this result, is that at double the loading the half-cell response appears similar to that of the cells with the other carbons at half the loading.

Product	Thickness	JIS Gurley	Porosity
2400	25 µm	620 seconds	Medium
2500	25 µm	200 seconds	High
3501	25 µm	200 seconds	High

Separators from Celgard were also tested: 2400, 2500, and 3501. They were all polypropylene based, however, the 2500 and 3501 are high-power separators with high porosity, and the 3500 also contains a wetting agent. Charging results, not provided here, indicated erratic voltage dependence for the more porous separators and favorable performance for the low-porosity separator. Based on these results, Super P-Li is recommended as the conductive additive and Celgard 2400 the separator for cells with high-voltage $LiNi_{1/2}Mn_{3/2}O_4$ cathodes.

TASK 1
Battery Cell Materials Development

Project Number: CPS Project 18502, CPS Agreement 23060, ORNL FWP CEVT110 (ES164)

Project Title: Overcoming Processing Cost Barriers of High Performance Lithium Ion Battery Electrodes

Project PI, Institution: David Wood, Oak Ridge National Laboratory

Collaborators: Argonne National Laboratory, Sandia National Laboratories

Project Start/End Dates: 10/1/11 to 9/30/14

Objectives: Electrode suspensions for lithium ion batteries are currently formulated using expensive polyvinylidine fluoride (PVDF) binder and toxic, flammable n-methylpyrrolidone (NMP) solvent. It is desirable to replace these components with water and water-soluble binders, but methods of mass production of these suspensions are currently underdeveloped. The major problems with aqueous electrode dispersions are: 1) agglomeration of active phase particles and conductive carbon additive; 2) poor wetting of the dispersion to the current collector substrate; and 3) cracking of the electrode coating during drying. NMP based processing also has the inherent disadvantages of high solvent cost and the requirement that the solvent be recovered or recycled. Initial projections of the minimum cost savings associated with changing to water and water-soluble binder are 70-75%, or a reduction from $0.210/Ah to $0.055/Ah. The objective of this project is to transform lithium ion battery electrode manufacturing with the reduction or elimination of costly, toxic organic-solvents.

Approach: Fabrication of composite electrodes via organic (baseline) and aqueous suspensions will be completed. A focus will be placed on the effect of processing parameters and agglomerate size on the aqueous route cell performance and microstructure of the composite electrode. Several active anode graphite and cathode (NMC, $LiFePO_4$, etc.) materials will be selected with various water-soluble binders. The conductive carbon additive will be held constant. Rheological (viscosity) and colloidal (zeta potential) properties of the suspensions with and without dispersant will be measured with a focus on minimization of agglomerate size. These measurements will show the effects of agglomerate size and mixing methodology on suspension rheology and help determine the stability (i.e. ion exchange processes across the surfaces of various crystal structures) of active materials in the presence of water. Composite electrodes will be made by tape casting and slot-die coating, and the drying kinetics of the electrodes will be measured by monitoring the weight loss as a function of time and temperature. Solvent transport during drying will also be monitored as a method to control electrode morphology, porosity, and tortuosity. Electrode microstructure and surface chemistry will be characterized and correlated with cell performance. Electrochemical performance of electrode coatings made from the various suspensions

will be supplied to ORNL's strategic industrial partners for external validation in large cell formats.

Improved cell performance with reduced processing and raw material cost will be demonstrated using pilot-scale coatings. At ORNL coin cells will be tested and evaluated for irreversible capacity loss, AC impedance, capacity vs. charge and discharge rates, and long-term behavior through at least 500 charge-discharge cycles. Half cells, coin cells, and pouch cells will be constructed and evaluated. The coin cells will be used for screening and coarse evaluation of different suspension chemistries and coating methodologies. A fine tuning of these research areas will be completed using ORNL pouch cells and large format cells with ORNL's industrial partners. Electrode coatings will be produced on the ORNL slot-die coater and supplied in roll form to the industrial partners for assembly into large format cells.

Electrode morphology will be characterized by scanning electron microscopy (SEM) and TEM. The bulk structure and surface of the active materials will be characterized using XRD and XPS, respectively.

FY13 Milestones:

1) Complete half-cell, full coin cell, and pouch cell round robin testing with ANL and SNL with CP A10/A12 and Toda NCM 523 electrochemical couple for NMP/PVDF based dispersion chemistry (January 2013 – delayed to March 2013).
2) Match full coin cell performance through 100 cycles (0.2C/-0.2C) of aqueous suspension and water-soluble binder to NMP/PVDF based suspensions for CP A10/A12 and Toda NCM 523 electrochemical couple (June 2013).
3) Match pouch cell (≥3 Ah capacity) performance through 100 cycles (0.2C/-0.2C) of aqueous suspension and water-soluble binder to NMP/PVDF based suspensions for CP A10/A12 and Toda NCM 523 electrochemical couple (September 2013).

Financial data: $300k/year (FY12-FY13)

PROGRESS TOWARD MILESTONES

Summary of work in the past quarter related to milestones (1)-(3)

A TODA NCM 523 dispersion (NCM 523/Denka carbon black/Solvay 5130 PVDF=90/5/5 wt.) and a ConocoPhillips A12 graphite dispersion (A12/super P Li carbon/Kureha 9300 PVDF=92/2/6 wt.) were prepared with solid contents of 55 wt% and 40 wt%, respectively. Figure 1 shows the flow chart of dispersion preparation. In both dispersions, active materials (NCM523 and graphite A12) were dispersed in PVDF solution first followed by dispersion of carbon black. The dispersions were mixed with a planetary mixer (Charles Ross, PDM-1/2) and coated using the ORNL slot-die coater. Wet electrodes were pre-dried using seven hot-air convection zones with temperatures ranging from 150°F to 270°F.

An in-line laser caliper setup is currently in use on the slot-die coater to monitor the thickness of wet coatings. For detailed information regarding this in line laser caliper system, refer to the quarterly report for CPS Project 18502, CPS Agreement 23060, ORNL FWP CEVT110. Figure 2 shows the wet coating thickness of the NCM523 and graphite A12 electrodes. The average thickness of the NCM523 cathode (coating plus foil) was 134.34 ± 2.35 µm, which includes a contribution of 119 µm for the cathode coating and 15 µm for the Al foil. The wet coating had excellent uniformity with less than 2% variation. Its dry thickness without calendaring was 86 µm, including a 15 µm contribution from the Al foil, indicating 40% volume shrinkage during drying. For the graphite A12 anode, the thickness of the wet coating was 109.00 ± 1.27 µm, which includes a 9 µm contribution from the Cu foil (only 1% thickness variation). The dried graphite thickness was 71 µm, indicating 29% volume shrinkage during drying.

The areal loadings were 12.92 mg/cm^2 and 6.93 mg/cm^2 for the NCM523 cathode and graphite A12 anode, respectively, corresponding to an electrode balance of 1.1. The electrode balance was in the middle of the range of 1.0 to 1.2 specified for round robin testing between Argonne

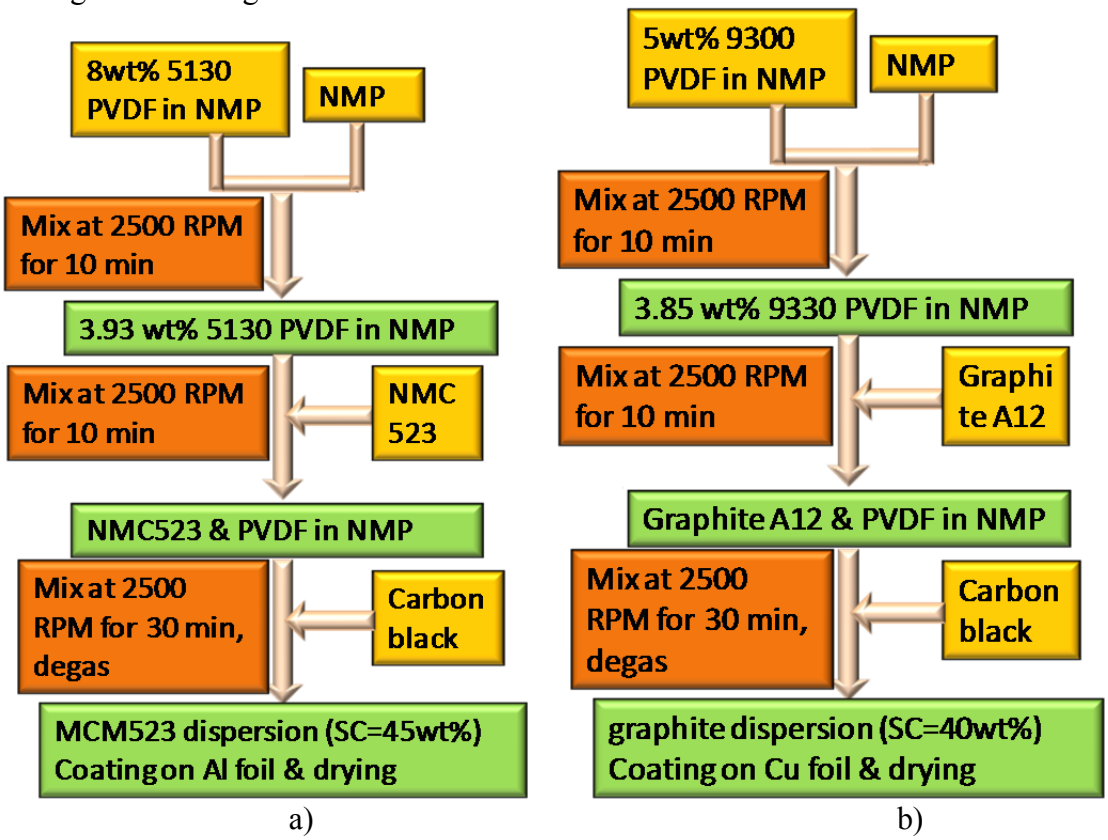

Figure 1. Flow chart for preparing (a) TODA NCM 523 cathode and (b) ConocoPhillips A12 graphite anode dispersions.

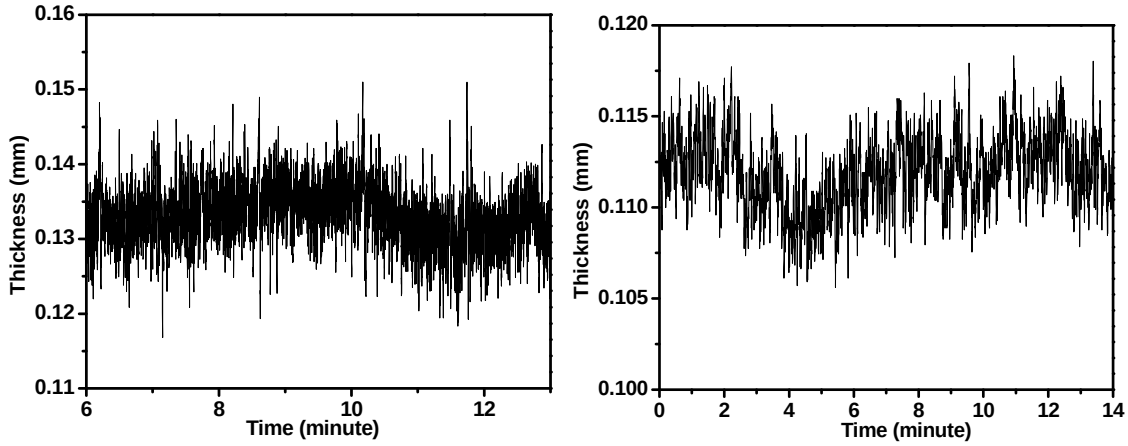

a) b)

Figure 2. Thickness of wet (a) NCM 523 cathode and (b) A12 graphite anode coatings including current collector foils as measured by in-line laser thickness; excellent thickness uniformity was observed for both coatings.

National Laboratory (ANL), Oak Ridge National Laboratory (ORNL), and Sandia National Laboratories (SNL). One roll each of the NCM523 cathode and A12 graphite anode was sent to ANL and SNL last November for round robin testing. Both half cells and full coin cells were assembled and tested at ORNL. Half cells were assembled inside an Ar-filled glove box with Li metal as the counter electrode and Celgard 2325 as the separator. Full coin cells were also assembled inside the glove box with NCM523 and A12 as the cathode and anode, respectively. The electrolyte was 1.2 M $LiPF_6$ in ethylene carbonate (EC):dimethyl carbonate (DMC) (3/7 wt. ratio, Novolyte). The NCM523 half cells and full cells were cycled using a VSP potentiostat (BioLogic) between 2.5 and 4.2 V, while the A12 half cells were cycled between 10 mV and 1.5 V. For the rate capability testing, the cells were charged at 0.2C to the cut-off voltage and then charged at constant voltage until the current dropped to 0.05C before being discharged at various rates. Five cycles were recorded for each rate step. For long term cycling, the charging protocol was the same as that for the rate capability test, but the cells were discharged at 0.2C until the cut-off voltage for each cycle.

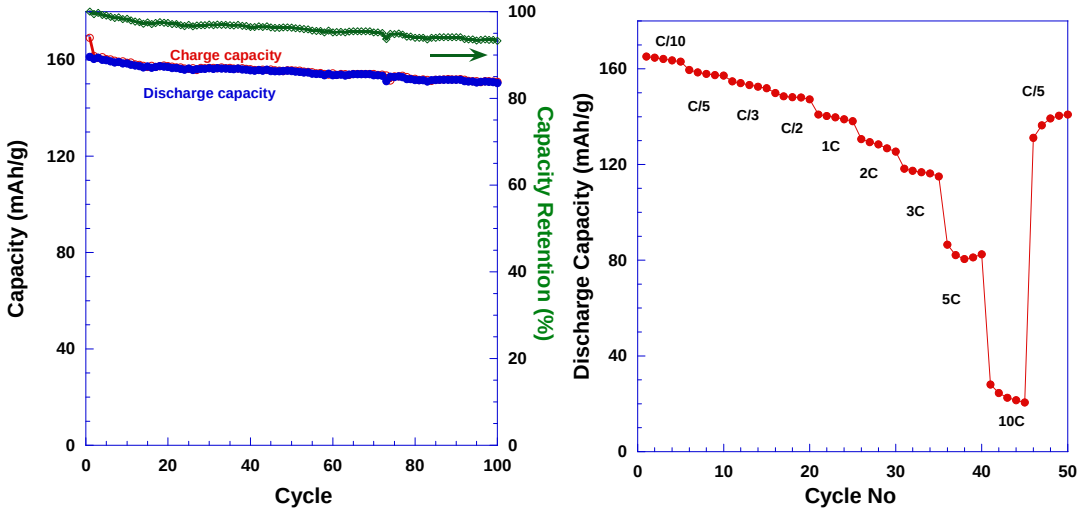

a) b)

Figure 3. Performance of full coin cells with NCM 523 cathode and A12 graphite anode couple; a) long term cycling and b) rate performance. Full cells demonstrate outstanding long term cycling and rate performance.

Figure 3 shows the performance of full coin cells with the NCM 523 cathode and A12 graphite anode couple. The electrode balance was 1.1 and the specific capacity is normalized by the weight of NCM 523. Excellent long-term stability (Figure 3a) and coulombic efficiency (>99%) was observed through 100 cycles with the exception of the first cycle. The coulombic efficiency of the first cycle was 95%, which could be attributed to formation of solid electrolyte interface (SEI) layer. The SEI layer formation also led to 8.0 mAh/g irreversible capacity loss for the first cycle, and discharge capacity retention was 93% after 100 cycles. These cells also exhibited good rate capability of ~120 mAh/g and higher capacity when discharged at ≤3C, and recovered to near the original 0.2C discharge capacity after higher rate cycling. It should be mentioned that no sophisticated formation cycle protocols were applied to these full cells. Only two 0.1C/-0.1C charge-discharge cycles were implemented before the long-term cycling and rate capability tests. It is expected that the capacity retention would be greater if an adequate formation cycle protocol was applied.

Figure 4 shows the performance of the A12 graphite half cells, which demonstrate 320 mAh/g discharge capacity at 0.1C and maintain good performance until 0.5C. The capacity was relatively low at high C rates and is due to kinetic limitations of graphite anodes. The capacity recovered to greater than its original value at 0.2C after the high rate testing, however, which could also be due to the SEI formation. It may have took significant time to form the SEI layer on the entire graphite surface, and the SEI layer may not have been completely formed when the cells were first cycled at 0.2C. After 45 cycles of rate capability testing, a stable SEI layer was likely formed and more graphite was available for the redox reaction leading to the higher observed capacity.

Half-cell rate capability and cycling performance of five different NCM 523 cells was also investigated and is shown in Figure 5a. Observed rate performance was similar to

that of the full cells with the A12 graphite anode (Figure 2b). Performance of the five half cells was consistent at or below 2C, as evidenced by their average capacity and standard deviation in Figure 5b. However, variation between cells became pronounced when the cell were discharged at 2C and above.

These NCM 523 cells showed significant degradation in capacity during long-term cycling after 20 cycles or less. To further investigate this high observed capacity fade, another long term test was carried out with a fresh half-cell, and the results are shown in Figure 5c. This cell maintained excellent capacity retention until 60 cycles, but significant capacity fade took place afterword, which is in agreement with the results in Figure 5a. This trend is likely due to lithium plating at the NCM 523 electrode or formation of dendrites.

Future work:
Rheological properties of aqueous NCM 523 with carbon black at various solid loading will be investigated to optimize electrode formulation. Subsequently NCM 523 electrodes will be fabricated through aqueous processing and performance will be investigated. Similar formulation optimization and coating trials will be performed for the ConocoPhillips A10/A12 anode.

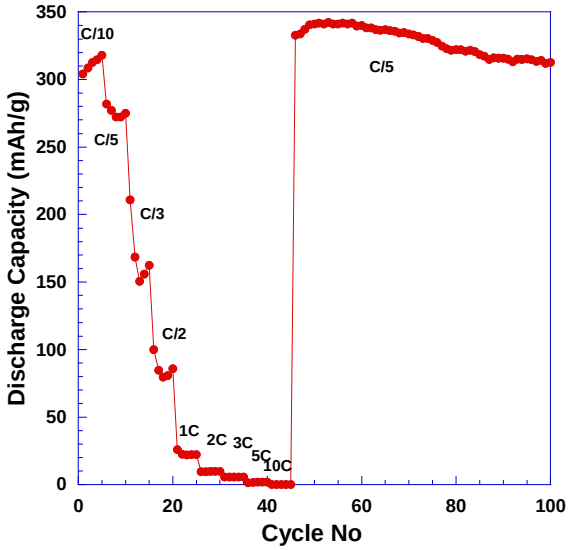

Figure 4. Performance of A12 graphite half cells showing high capacity at lower C rates.

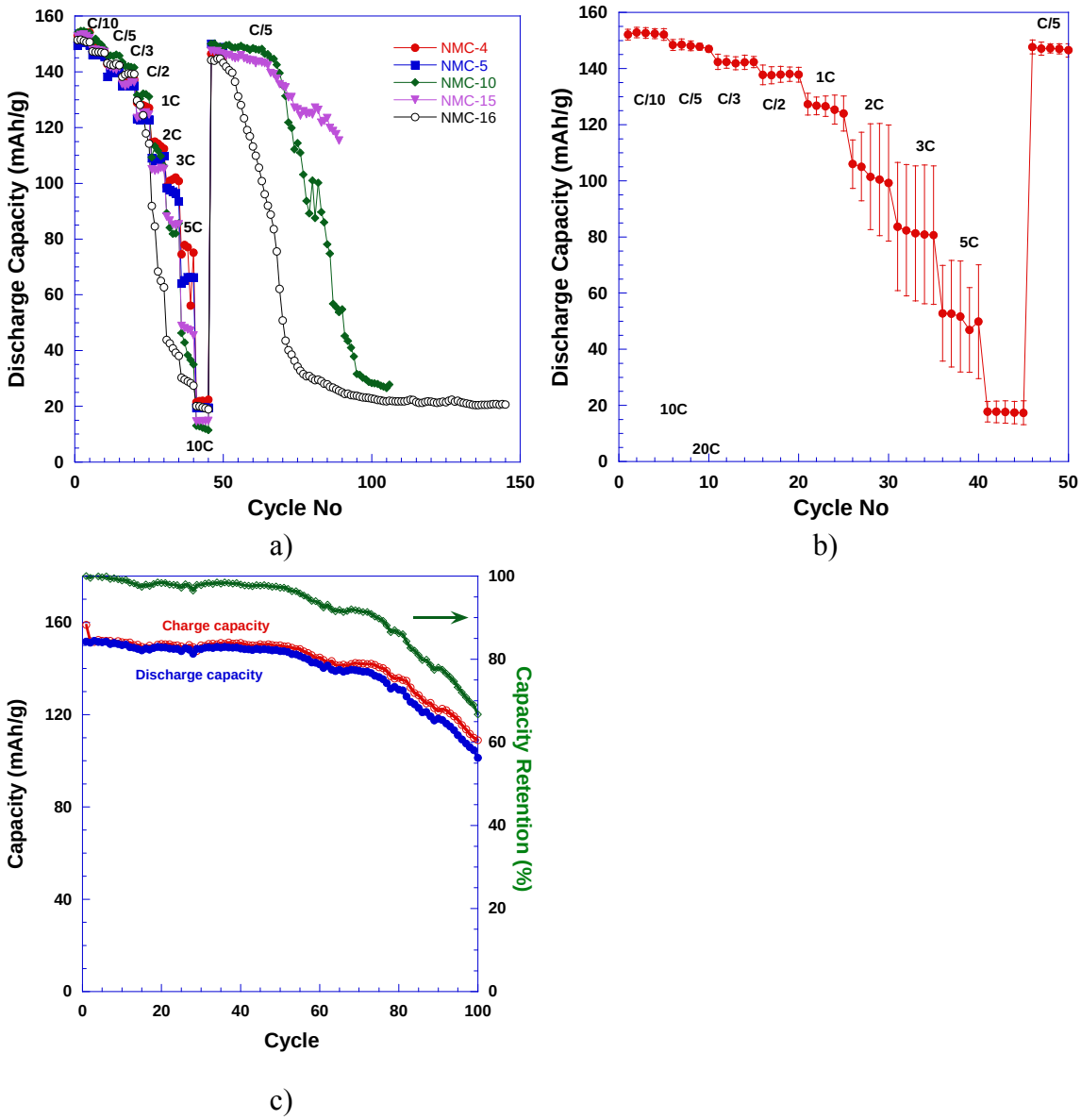

Figure 5. Performance of NCM 523 half cells; a) rate performance and long term cycling from five different coin cells; b) average rate performance from five coin cells; c) 100 cycles at 0.2C/-0.2C from one half-cell. The cells show significant capacity degradation during long term cycling likely due to lithium plating or dendrite formation.

Publications, Reports, Intellectual Property or Patent Application filed this quarter.

1. J. Li, B. Armstrong, J. Kiggans, C. Daniel, and D.L. Wood, "Lithium Ion Cell Performance Enhancement Using Aqueous $LiFePO_4$ Cathode Dispersions and Polyethyleneimine Dispersant", *Journal of The Electrochemical Society*, **160(2)**, A201–A206 (2013).
2. J. Li, B. Armstrong, J. Kiggans, C. Daniel, and D. Wood, "Optimal Polyethyleneimine Concentration and Mixing Sequence for $LiFePO_4$ Aqueous

Nanoparticle Dispersions", *Particles and Particles System Characterization*, Under Review (2013).

3. D. Wood, J. Li, M. Debasish, C. Daniel, B. Armstrong, R. Dinwiddie, H. Wang, R. Trejo, N. Gallego, C. Contescu, J. Howe, R. Meisner, J. Kiggans, B. Brown, "Advanced Materials Processing and Novel Characterization Method for Low-Cost, High Energy-Density Lithium-Ion Batteries", Conference Proceedings of the Advanced Automotive Battery Conference 2013, Pasadena, California, February 4-8, 2013.
4. D. Wood, J. Li, D. Mohanty, S. Kalnaus, B. Armstrong, and C. Daniel, "Advanced Materials Processing for Lithium-Ion Battery Applications", 222nd Meeting of the Electrochemical Society, Honolulu, HI, October 7-12, 2012.

TASK 1
Battery Cell Materials Development

Project Number: ES162

Project Title: Development of Industrially Viable Battery Electrode Coatings

Project PI, Institution: Robert Tenent, NREL

Collaborators (include industry): Chunmei Ban (NREL), Steven George (University of Colorado, Boulder), Chris Orendorff (Sandia National Laboratory), Bryant Polzin (Argonne National Laboratory), Anthony Burrell (Argonne National Laboratory)

Project Start/End Dates: December 2012 – September 2016

Objectives: (1) To develop a deposition method for thin protective battery coatings using a modified "in-line" atomic layer deposition (ALD) reactor design that can be integrated into a battery manufacturing line to improve rate capability, life, and abuse tolerance of electrodes in a cost effective manner. (2) To perform an assessment of the effect of ALD coatings on the voltage fade phenomenon observed with the HE5050 cathode materials as provided by Argonne.

Approach: Recent work conducted at NREL has demonstrated improved performance for both anode and cathode materials following deposition of a thin protective Al2O3 coating using ALD. ALD is not likely compatible with present battery manufacturing processes as it is performed under a moderate vacuum (100 mTorr) as well as by sequential, *and separate*, exposures of two (or more) reacting species to a stationary substrate surface with extensive purging required between precursor exposure steps. NREL is developing a new in-line reactor design that will enable ALD depositions to be performed not only at increased pressures, but also on a moving substrate, as is required for battery manufacturing. Early phase work has focused on providing ABR partners with alumina ALD coated samples in an attempt to determine a suitable electrode material/coating combination for initial scaling evaluation. A variety of materials have been coated including the Toda HE5050, NMC111 and NMC 523 cathode materials as well as the Conoco Philips A10 graphite anode material in both formed electrode and powder format. These various materials have been formed into both coin and 18650 format cells for further testing. Accelerated rate calorimetry analysis of 18650 cells showed that anode coatings led to an improvement in high temperature thermal runaway. The electrode coating work was conducted in conjunction with the initial design and construction of new in-line ALD equipment. It was determined that the coating of a highly porous electrode surface presents unique issues related to rapid penetration and removal of ALD precursors required to achieve conformal coatings in a rapid process. NREL, in conjunction with partners at the University of Colorado at Boulder are proposing an improved in-line ALD design that will enable rapid precursor penetration and removal from a porous substrate using an in-line format.

Milestones: (a) Design and construction of prototype in-line ALD coater for deposition on porous substrates (b) Continued supply of ABR collaborators with alumina ALD coated electrodes and materials.

Financial data: $300K/year

PROGRESS TOWARD MILESTONES (1 page)

(a) Summary of work in the past quarter related to milestone (a)

An improved design for a so called "push-pull" in-line ALD reactor scheme was completed through work with our collaborators at the University of Colorado at Boulder. The earlier in-line ALD demonstration device was originally designed for atmospheric pressure in-line ALD deposition of aluminum oxide onto silicon wafer samples. While this system was useful for feasibility demonstration of atmospheric pressure ALD in a controlled fashion, the system does not take into account the specific needs of deposition onto a highly porous moving substrate. The ability to obtain conformal coating of a highly porous substrate requires complete penetration of the porous film by precursor materials. This is particularly problematic for a moving substrate in that excessive amounts of time may be required to achieve both precursor penetration and reaction product removal from the porous substrate. The "push-pull" reactor design concept is based on moving the coated electrode foil between alternating regions of high and low pressure of precursor gases as well as purge or exhaust gas regions in the reactor. A high pressure of precursor gas leads to rapid penetration within the porous substrate and subsequent exposure to low pressure regimes allows rapid removal of reaction products prior to exposure of a second high pressure precursor exposure zone to complete the ALD cycle. We have proposed and are beginning to construct our improved design based on this concept. Design has predominantly taken place over the last quarter and we have also recently added the assistance of a post doctoral researcher who is in the process of identifying and ordering the necessary parts as well as coordinating custom fabrication work for the new designed reactor.

(b) Summary of work in the past quarter related to milestone (b)

In support of the voltage fade project current occurring at Argonne National Laboratory, NREL has performed alumina ALD coatings on multiple samples of the HE5050 cathode material. NREL has performed ALD alumina coatings on both formed electrodes of HE5050 and powder samples as supplied by the Argonne team. Following detailed discussions with the Argonne team, NREL has recently modified its testing protocol to fit the new standard testing protocol for voltage fade analysis as proposed by the Argonne team. This represents a change from our earlier testing procedure, so previous work is currently being replicated with the new testing process.

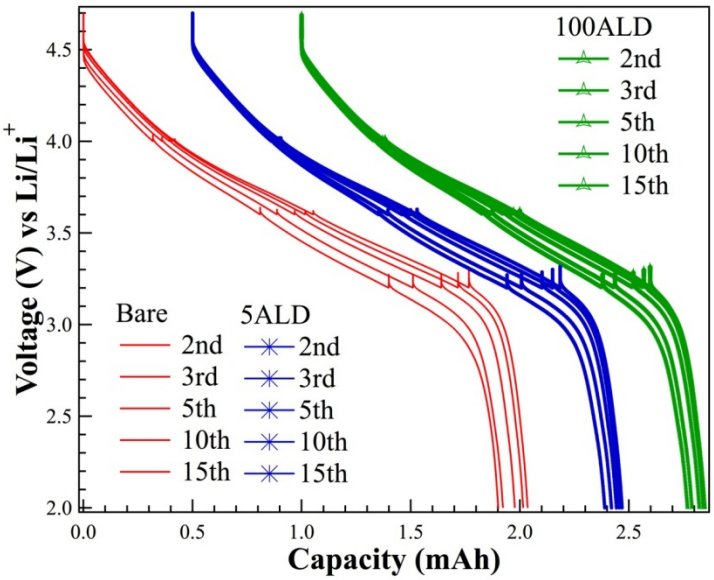

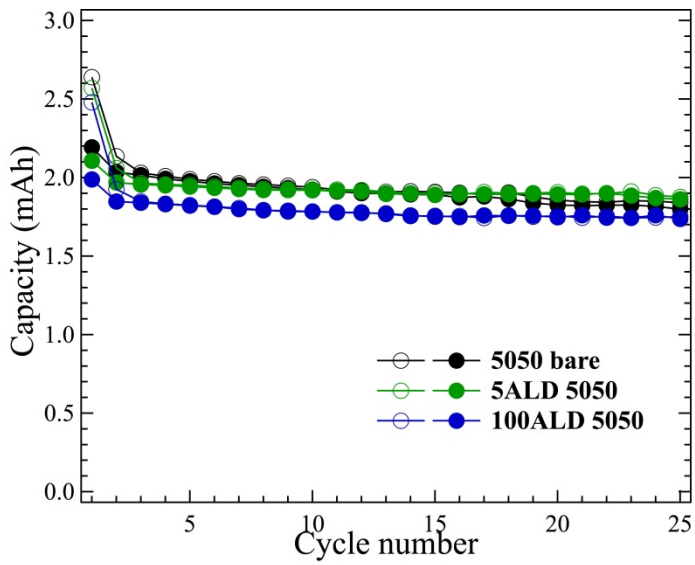

Preliminary results for coated electrode foils appear to show some possible mitigation of capacity loss, but possible effects on the voltage fade phenomenon are not immediately clear. Results for coatings on electrode powders appeared to lead to a high overpotential which is likely induced by the presence of an electrically insulating layer on the active material powders. All NREL data collected with respect to the HE5050 cathode material is currently being prepared for transfer to the Argonne group for analysis and comparison with internal data as well as that provided by other coatings work.

In addition to the HE5050 coatings, the NREL team had more detailed discussions with Chris Orendorff from Sandia NL related to earlier work conducted to determine safety improvements that may be provided through ALD coatings. In earlier experiments, NREL provided coated electrode foils to the Sandia team who fabricated 18650 cells and performed safety analysis. Multiple cell failures were observed in this analysis and initially damage caused to the electrode foils during the coating process was suspected as the cause. Sandia has recently been able to assign cause for these device failures to other mechanisms and the coating experiments are being repeated. We anticipate providing Sandia with ALD coated samples of NMC523 in the near future, likely both in coated electrode and coated powder forms.

Publications, Reports, Intellectual property or patent application filed this quarter. (Please be rigorous, include internal reports--invention records, etc.)

Our new “push-pull” reactor design is currently being evaluated internally for potential intellectual property. If suitable IP is identified patent applications will be sent in shortly.

The NREL team also presented their work and capabilities at the recent USDrive meeting at Argonne National Laboratory related to the possible effects of ALD coatings on the voltage fade phenomenon observed for the HE5050 cathode.

TASK 1
Battery Cell Materials Development

Project Number: 25194 (IV.B.2.5) (ES196)

Project Title: Evaluate ALD Coatings of LGCPI Cathode Materials and Electrodes

Project PI, Institution:
Shriram Santhanagopalan, National Renewable Energy Laboratory, Golden CO 80401

Collaborators (include industry):

Mohamed Alamgir, LG Chem Power Inc., Troy MI
Karen Buechler, David King, ALD Nanosolutions, Broomfield CO

Project Start/End Dates: June 2012 – June 2013

Objectives:

The objectives of this work are two-fold: i) to evaluate the scalability of the process to coat LG Chem Power Inc. (LGCPI) cathodes with alumina, using the Atomic Layer Deposition (ALD) technique, and ii) to demonstrate improvements in rate capability and life of ALDcoated LGCPI electrodes.

Approach:

LGCPI and NREL have collaborated to demonstrate the scalability of the ALD coating process over the last 6 months, and the benefits of ALD coatings for long term cycling and calendar life are being quantified.

- NREL received samples of baseline material to be coated from LGCPI.
- NREL carried out ALD coating of the samples with help from a subcontractor - ALD Nanosolutions.
- NREL fabricated cells from those samples for quick screening and feedback to ALD Nanosolutions.
- LGCPI is currently fabricating larger format cells for further evaluation.

Milestones: Project deliverables and decision points. Milestones should clearly show progress towards your project objectives, including overcoming issues, and should clearly support achieving a significant improvement in cell energy density, safety, and/or cost. If your material or couple has known issues, please address some or all of them in your milestones.

(a) Receipt and characterization of baseline material and electrodes, July 2012, Complete
(b) ALD coating and characterization of baseline cathode powder, Sept. 2012, Complete

(c) ALD coating of baseline electrodes, Dec. 2012, Complete
(d) Pouch cell fabrication and long term evaluation, June 2013, On Schedule

Financial data: 110k (2012), 50k Sub-contract to ALD Nanosolutions

Progress Towards Milestones:

Our results from the previous quarter demonstrated that the Atomic Layer Deposition technique is quite scalable with the cathode powders. The sub-contractor (ALD Nanosolutions) has also developed a semi-continuous production option that has validated for large-scale manufacturing and will facilitate industry adoption.

The work in this quarter focused on coating electrodes directly using the Atomic Layer Deposition technique. The sub-contractor, ALD Nanosolutions, already had in place small volume traditional flat ALD reactors and roll to roll ALD coating capabilities. Under the current effort, these were extended to coat large size (6" x 6") sheet electrodes by installing a holder into the large volume ALD particle reactor. The modified reactor can accommodate the new electrode holder for up-to 25 electrodes per batch. Initial evaluation of the reactor performance included analysis of coating uniformity across the web and through the depth of the reaction chamber.

The process steps for coating the sheet electrode samples are essentially the same as those for the fluidized bed reactors:

1) Load Reactor with Electrodes
2) Bring reactor to coating temperature and pressure
3) Sequentially introduce ALD precursors
4) Repeat 3 for desired number of cycles

Static dosing on the electrodes until after breakthrough in the residual gas analysis signals ensured the uniformity of the coating across the chamber dimensions.

The coated samples were shipped back to LGCPI for fabrication of pouch format cells that will be characterized for improvements to the cycling capability from the ALD coating process. Future work will include optimizing the coating process for the electrodes based on the initial run carried out in this quarter, and improvements to the recipe to build the cathodes from the ALD coated powders.

Publications, Reports, Intellectual Property or Patent Application filed this quarter:

1. Robert Tenent, USDRIVE Electrochemical Tech Team Meeting at ANL - 24 January 2013.
2. Shriram Santhanagopalan, Mohamed Alamgir, Karen Buechler and David King, Milestone Report titled *Evaluate ALD Coatings of LGCPI Cathode Materials and Electrodes*, Submitted October 2012.

TASK 2
Calendar & Cycle Life Studies

Project Number: 1.1 (ES030)

Project Title: Cell Fabrication Facility Team Production and Research Activities

Project PI, Institution: Andrew N. Jansen, Argonne National Laboratory

Collaborators (include industry): Dennis W. Dees, Daniel P. Abraham, Kevin G. Gallagher, Wenquan Lu, Bryant J. Polzin, Stephen E. Trask, Nancy L. Dietz-Rago, Javier Bareno, Qingliu Wu, Martin Bettge, Ye Zhu, Joseph J. Kubal, and Paul A. Nelson (Argonne National Laboratory)
Prof. Jai Prakash (Illinois Institute of Technology)
Prof. Ivan Petrov (University of Illinois)
Prof. Alex Wei (Purdue University)
Yan Li (University of Rochester)

Toda Kogyo
Phillips 66
JSR Micro
Zeon Chemicals
Materials Engineering Research Facility (MERF)
Post-Test Facility (PTF)
Electrochemical Analysis and Diagnostic Laboratory (EADL)

Project Start/End Dates: October 2008 / September 2014

Objectives: The overarching objective of this core-funded effort is to design, fabricate, and characterize high-quality prototype cells of at least 200-mAh capacity to enable a realistic and consistent evaluation of candidate chemistries in a time-effective manner. In order to achieve this main objective, it was necessary to divide this effort into interlinked sections designed to support the activities of the Cell Fabrication Facility (CFF). As with the CFF, each of these support sections (Materials Validation, Modeling, and Diagnostics) are designated specific goals and responsibilities. It is not the aim of this task to become a small battery manufacturer, but instead to become a laboratory research facility with cell production capabilities that adequately evaluate the merits and limitations of mid-to-long term lithium-ion chemistries in a close-to-realistic industrial format.

Approach: As new cell chemistries and systems progress, they may reach the point where they are considered for further development in larger prototype cells. When this happens, a limited quantity of these materials, along with their preliminary data, are transferred from the inventor or originator to the Materials Validation support section, where they will be evaluated to determine if they warrant production in prototype cells by

the CFF. The source of these materials (anodes, cathodes, electrolytes, additives, separators, and binders) may originate from the ABR and BATT Programs, as well as from other domestic and foreign organizations such as universities, national labs, and industrial vendors. Electrochemical couples with high power and energy density will be given extra priority.

Coin cells (2032 size) will be used for materials validation purposes with initial studies performed at room temperature or 30°C. After formation cycles, the coin cells will go through hybrid pulse power characterization (HPPC) testing, rate capability testing, and limited cycle life testing. Accelerated aging studies will also be performed at 45°C to 55°C for promising materials to give a preliminary indication of life. Where appropriate, the thermal abuse response will be studied using a differential scanning calorimeter. The key areas to monitor are the materials' influence on capacity, energy, power, and cycle/calendar life. The Materials Validation results will be used by the other support efforts, and if needed, by the Materials Engineering Research Facility (MERF) and the Post-Test Facility (PTF).

Once the materials' performance has been validated, promising cell chemistries will be recommended for further development by the CFF. Using the recommendations and results obtained by the Materials Validation, the CFF will initiate a prototype cell build that will include the generation of single-sided electrodes for the Diagnostics support effort. Diagnostics examines the new cell chemistries in detail using advanced electrochemical and analytical techniques, including the employment of micro-reference electrode cells. This information lays the foundation for the electrochemical Modeling support effort focused on correlating the electrochemical and analytical studies, in order to identify performance limitations and aging mechanisms. The Modeling effort supports the CFF through the development and utilization of efficient simulation and design tools for advanced lithium-ion battery technologies. These modeling tools cover a broad range of applications, from correlating analytical diagnostic results with electrochemical performance in small test cells to predicting the performance and cost of full size PHEV battery packs based on limited results.

If the results from Diagnostics still look promising, the CFF will begin fabrication of full cell builds using double-sided electrodes. The CFF at Argonne has the capability to make two prototype cell formats in their 45 m^2 dry room: pouch cells (xx3450 format, with capacity around 0.4 Ah) and 18650 cells. Pouch cells are anticipated to be easier to assemble, but they may suffer from bulging if gases are evolved during cell aging and cycling. 18650s, which are rigid containers, may be used if the pouch cell format is deemed unreliable due to gassing, or if higher capacity cells are needed (greater than 1 Ah). Central to this effort is a pilot-scale coating machine that operates with slurry sizes that range from 20 grams to a few kilograms. This is a key feature of the CFF that enables a professional evaluation of small quantities of novel materials. If needed, the MERF is available for scaling up materials for these prototype cell builds.

The main emphasis of the CFF will be to fabricate electrodes and prototype cells for calendar and cycle life studies. These cells will undergo rigorous electrochemical

evaluation and aging studies under the combined effort of the CFF and Argonne's Electrochemical Analysis and Diagnostic Laboratory (EADL). The Diagnostics effort will use advanced electrochemical and physicochemical diagnostic tools and techniques to identify factors that determine cell performance and performance degradation (capacity fade, impedance rise) on storage and on extensive deep-discharge cycling. The results of these tests are used to formulate data-driven recommendations to improve the electrochemical performance/life of materials and electrodes that will be incorporated in pouch– and 18650– type PHEV cells assembled in the CFF. After testing, the cells will be destructively examined by the Post-Test Facility that will interface with the Diagnostics effort to elucidate failure mechanisms in end-of-life cycled cells from CFF – the information generated will enable the design of cell chemistries that meet the performance, life and safety targets of PHEV cells. The CFF & Support effort will collect and share all results with other members of the ABR Program and to the materials origin. This information is then used to further improve the new chemistry, as well as future electrode and cell builds. The CFF may also provide this information and prototype cells to battery developers for their evaluation.

The general approach taken in the Modeling effort is twofold. First, spreadsheet based simulations are employed that determine the impedance behavior, available capacity, and thermal effects for general and specific cell, battery module, and battery pack designs. The design model calculates power and energy, weight and volume of materials and components, as well as their thermal performance. The model is also capable of performing simulations on multiple battery designs for comparison and optimization. The battery design model also includes a module that calculates battery costs by combining materials and components costs with manufacturing expenses based on a plant design.

The second part of the Modeling effort utilizes an electrochemical model that accurately describes all the pertinent physicochemical phenomena in the cell under study. Continuum based transport equations using concentrated solution theory describe the movement of salt in the electrolyte. Volume-averaging of the transport equations accounts for the composite electrode geometry. Electrode kinetics, thermodynamics, electronic migration, and diffusion of lithium in the active material particles are also included. Phase change in the active materials and detailed transport through the solid electrolyte interphase or SEI can also be included. Two versions of the electrochemical model have been developed (i.e. AC and DC) to describe the full range of electrochemical tests conducted on the advanced lithium-ion battery technologies.

Milestones:

(a.) Obtain viable supplier of battery grade silicon powder, March, 2013 (On schedule)

(b.) Assess influence of LiDFOB, LiBOB, and HFiP electrolyte additives for HE5050 cathode, May, 2013 (On schedule)

(c.) Evaluate MERF cathodes ($Li_{1.25}Ni_{0.3}Mn_{0.62}O_2$) based on hydroxide and carbonate precursors, July, 2013 (On schedule)

(d.) Add silicon-graphite, LiFePO4, LiCoO2, and hard carbon to electrode library, July, 2013 (On schedule)
(e.) Fabricate pouch cells based on silicon-graphite anodes and LMR-NMC cathodes, August, 2013 (On schedule)
(f.) Validate performance of advanced battery materials, September, 2013 (On schedule)
(g.) Determine sources of impedance rise and capacity fade during extensive cycling of cells containing various electrochemical couples, September, 2013 (On schedule)
(h.) Recommend solutions that can improve the life of high energy LMR-NCM electrodes and cells by 30% at 30°C and 15% at 55°C, September, 2013 (On schedule)
(i.) Enhance battery design and cost model concentrating on designs for advanced lithium-ion electrochemical couples, September, 2013 (On schedule)
(j.) Advance development of electrochemical models focusing on the impedance of LMR-NMC positive electrodes, September, 2013 (On schedule)

Financial data: $2500K / FY13 **(**subcontracted $30K to Purdue University, $70K to Illinois Institute of Technology, and $30K to University of Rochester)

PROGRESS TOWARD MILESTONES

(a) Summary of work in the past quarter related to milestone (a).

Two commercially available silicon materials have been obtained and are being tested by Materials Validation. The first material is a 1-5μm silicon powder from Alfa Aesar (Figure 1a); while the second is a silicon powder from Shanghai Guan Jin (particle size distribution is currently being determined). A multitude of electrodes have been made out of the Alfa Aesar silicon powder with varying amounts of silicon powder: 100% Si, 90% Graphite/10% Si, and 85% Graphite/15% Si. Since PVDF has been generally shown to be an inferior binder with uncoated silicon-based electrodes, other binders needed to be employed. Silicon undergoes major expansions and contractions during cycling, and when PVDF is used as the binder, electrical contacts between particles are difficult to be maintained. Repeated cycling of the electrode tends to fracture and isolate silicon particles from the conductive network, which diminishes the capacity. Using a stiffer binder such as CMC, Alginic Acid or PAA has been shown to increase cyclability by helping prevent the loss of contacts between particles. Binders currently being tested are CMC/SBR, alginic acid, and PAA. Lithium half cells have been made with laminates of various compositions. Currently in this study, the best electrode produced using Alfa Aesar silicon was a nearly pure silicon electrode with a lithiated PAA binder and a citric acid buffer (76 wt.% silicon, 10 wt.% C-45 carbon, and 14 wt.% LiPAA with citric acid buffer) (Figure 1b). This electrode was able to maintain high gravimetric capacities even at a 2C rate and has an average columbic efficiency of 99.4% during cycling.

(a) 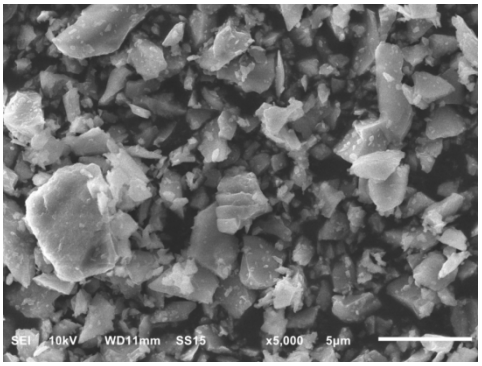

(b) 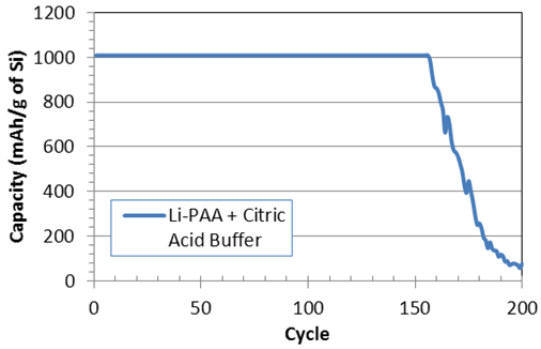

Figure 1 (a) SEM image of silicon powder from Alpha Aesar, and (b) capacity results for a silicon electrode (76 wt.% Alpha Aesar silicon, 10 wt.% C-45, and 14 wt.% LiPAA with citric acid buffer) vs. Li metal in 2032 coin cell (capacity limited cycles).

While the morphology (and lack of surface treatment) of the readily available silicon powder from Alfa Aesar is not ideal, it is at least capable of being cycled and will thus be used as a temporary baseline for further binder development. Surprisingly, the cycle life is relatively poor for initial electrode formulations that use high graphite to silicon content and is attributed to competing binder functions, i.e., binders developed for silicon may not be ideal for graphite. The SEM image of the powder (Figure 1a) showed that the silicon has sharp edges, which would likely promote particle fracturing during cycling. With this knowledge, some surface modification techniques have been performed such as acid and base washes and heat treating of the silicon. These treatments may also be able to improve adhesion and binding properties of the Si. The treated materials are now being imaged to see if any improvements were made to the morphology of the silicon.

Other sources of battery grade silicon are actively being pursued and a few promising sources have been identified. One of which is Dow Corning, which has committed to provide silicon powder to ANL for evaluation purpose. This initial study will investigate three silicon/graphite blends with three different binders once the silicon powder is received. The silicon/graphite blends consist of 0%, 10%, and 20% silicon, and the three binder systems will be PVDF, CMC/SBR, and PAA (with and without SBR).

(b) Summary of work in the past quarter related to milestone (b)

Effort by the Diagnostics team has shown improved capacity retention over time and cycles using LiDFOB and/or LiBOB additives in the standard 1.2 M $LiPF_6$ in EC:EMC 3:7 by wt (Gen2) in coin cells. The additive validations for LiDFOB and HFiP from MERF have been completed. The improved electrochemical performance (rate and cycle life) were obtained when 2 wt.% LiDFOB was used in graphite/LMR-NMC cells. Based on these promising results, two combinations of the additives were chosen to be tested in the xx3450 pouch cell configuration in the CFF, namely: 1) Gen2 + 2 wt.% LiDFOB and 2) Gen2 + 2 wt.% LiDFOB + 1 wt.% LiBOB. The electrode couple used for

the pouch cell testing was Toda HE5050 ($Li_{1.2}Ni_{0.15}Mn_{0.55}Co_{0.1}O_2$) and A12 Graphite from Phillips 66.

The CFF nomenclature shown in the table below (Table 1), depicts the CFF Build 9 (Toda HE5050 vs. A12) electrode couple with varying suffixes (i.e. "A", "B", "C") for the electrolyte variables. 8 pouch cells were constructed and tested for B9A, 4 for B9B, and 4 for B9C.

Build ID	Electrode Couple	Electrolyte
CFF-B9A	HE-5050 vs. A12	Gen2
CFF-B9B	HE-5050 vs. A12	Gen2 + 2wt.% LiDFOB
CFF-B9C	HE-5050 vs. A12	Gen2 + 2wt.% LiDFOB + 1wt.% LiBOB

Table 1 CFF Pouch cell build constructed for electrolyte additive study using Gen2 electrolyte (1.2 M $LiPF_6$ in EC:EMC (3:7 by wt).

The electrolyte additives were prepared for the B9B and B9C pouch cells by the Diagnostics team on the same day the cells were filled with electrolyte and started formation procedure. Due to the nature of the pouch cell design and increased electrode area to electrolyte volume, the evacuated and sealed cells underwent a 24 h soak in the electrolyte to encourage wetting of the separator and electrodes. Immediately prior to the 24 h soak, a 5 minute C/10 tap charge was performed on each cell to drive the anode potential down to mitigate corrosion of the anode copper foil. Following the 24 hour soak, formation cycling of the cells began. The electrochemical formation data can be seen in Figure 2a.

There are slight differences in the voltage profile formation data when comparing the "Gen2 only" cells to the additive cells. These differences in the features can be seen in Figure 2a, 2b, and 2c. It appears that the additives are being partially activated during the tap charge, and then fully activated during the first charge to 4.1 V (after the 24 hour hold).

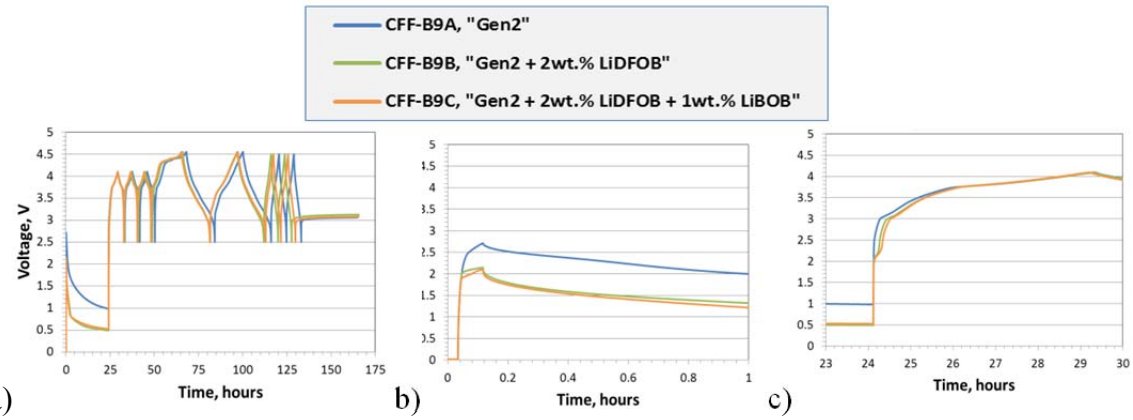

Figure 2. Formation profile for B9A, B9B, and B9C consisting of sequential cycling with voltage window of 2.5 V to 4.1 V at C/10, then 4.55 V at C/10, then 4.5 V at C/3, performed at 30°C. All three plots have the same y-axis with a) entire formation profile, including tap charge, 24 h hold, and subsequent cycling, b) expansion of tap charge and rest, and c) expansion of first charge on cells after 24 h hold (2.5 V to 4.1 V)

Following the formation procedure, the cells were taken to the dry-room, cut open, evacuated, and resealed to remove any generated gas from formation (standard for typical pouch cell testing protocol). Cycling was then continued to determine the rate capability for each set of cells, which is shown in Figure 3.

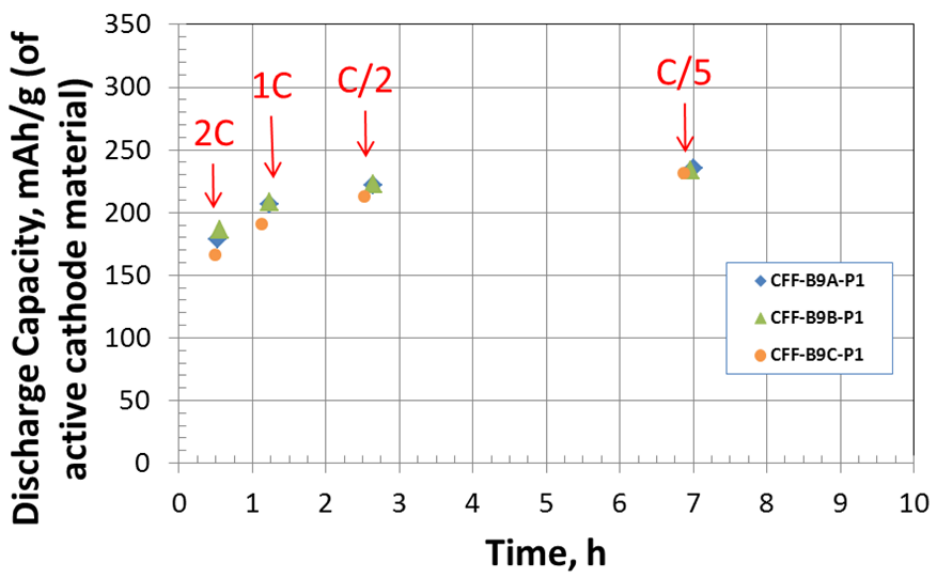

Figure 3. Rate Study of B9A, B9B, and B9C. Testing performed at 30°C. Voltage widow of 2.5 V to 4.5 V. Nominal rates of C/5, C/2, 1C and 2C at 3 cycles each were used. The 3rd cycle for each rate is plotted above.

B9A, B9B, and B9C all resulted in similar rate performance when compared with each other. The ~240 mAh/g for the C/7 rate and ~165 mAh/g for the 2C rate matched well to the half-cell coin cell data from Materials Validation effort results for HE5050 in Gen2 electrolyte. Following the rate study, Hybrid Pulse Power Characterization (HPPC)

testing was performed on these cell builds. The resulting ASI plots for both discharge and charge pulses are shown in Figure 4.

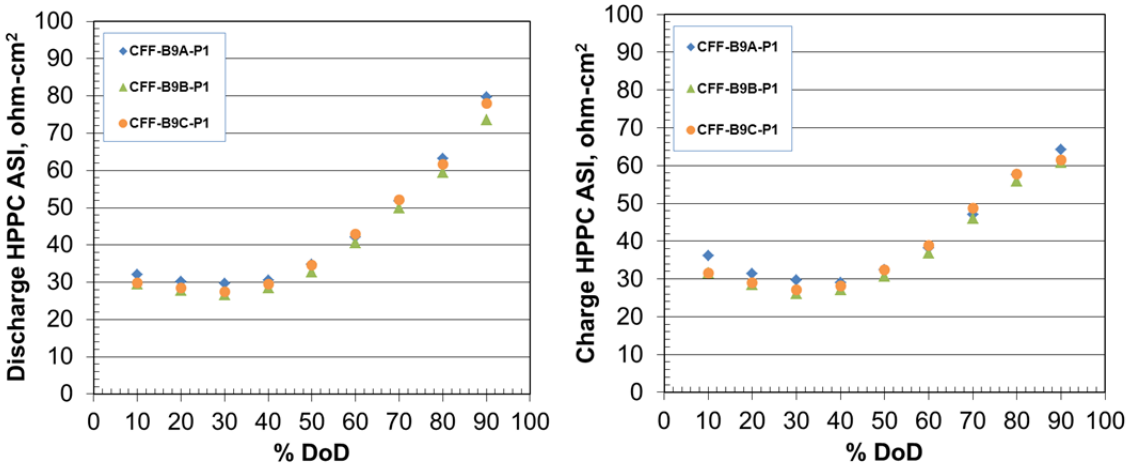

Figure 4. HPPC data for B9A, B9B, and B9C pouch cells. Testing performed at 30°C. Voltage window of 2.5 V to 4.4 V with 5C discharge pulse with 3.75 charge pulse at 10 s each. The plot on the left is the Discharge ASI pulse data at various depths of discharge (DOD). The plot on the right is the Charge ASI pulse data at various DOD.

Similar to the rate study results, the initial HPPC results between the 3 cell builds show strong similarities to one another. Overall, a slight improvement in the discharge and charge ASI can be seen for the cell builds with additives. The Diagnostics team also reported improvements in the impedance with the use of the LiDFOB/LiBOB additives. Cycle life testing began after the HPPC testing. The cells are still cycling, but general trends can be observed as summarized in the cycle life plot in Figure 5 below. Noticeable differences in cycle life performance are seen between B9A, B9B, and B9C. B9B shows a significant increase of capacity fade when compared to B9A. Whereas, B9C has similar capacity fade to B9A, but lower overall capacity in the cell. The initial cycle capacities of B9B and B9C are also lower than B9A. It would be expected that all three builds would have the same starting capacity for the cycle life because they have all experienced the same testing conditions, but this was not the case here.

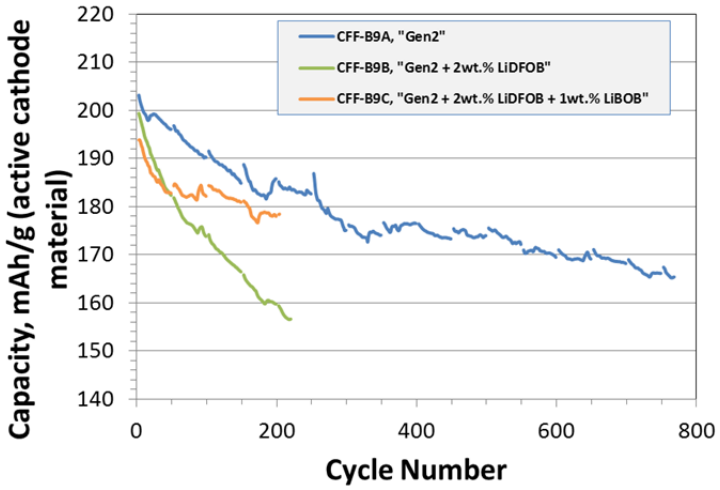

Figure 5. Cycle life study of B9A, B9B, B9C cell builds. Plot does not include cycle data from formation, rate study, or HPPC testing. All testing was performed at 30°C. Voltage window of 2.5 V to 4.4 V. Cells cycled at C/2 rate, with interruptions every 50 cycles for RPT/HPPC tests (data not shown in plot above).

In summary, the expected cycle life capacity retention improvements of the additives to the Gen2 electrolyte were not observed in the pouch cells as they were seen in the coin cell results. In these pouch cells, the additives actually poisoned the cells. Plans are underway to determine why this was the case, with efforts centered on exploring the effects of the different formation protocols used in a coin cell vs. a pouch cell. To test this, the CFF will make identical coin cells, and then use several different protocols for formation to help understand if this step has significant influence on the performance of the cells. Also, the volume of electrolyte to area of electrode ratio is significantly less in a pouch cell than a flooded coin cell, which may influence the ability of the additive to be adequately dispersed across all the electrodes. Current cells on test, with and without the additive, will be sent to PTF after the cells have died for evaluation, which may give insights as to why the additives did not improve the pouch cell performance as expected.

(c) Summary of work in the past quarter related to milestone (c)

The MERF has supplied the CFF with two separate batches of the $Li_{1.25}Ni_{0.3}Mn_{0.62}O_2$ cathode (LMR-NMC) material made via the carbonate process. The first batch (Lot# 2012-02-22) had a particle size distribution at D50 of 15µm, with a tap density of 1.36 g/cc (Figure 6). The second batch (Lot# 2012-07-09&11) has a particle size distribution at D50 of 7.8µm, with a tap density of 1.49 g/cc (Figure 7). The SEM images show the improved particle morphology from Lot# 2012-02-22 to Lot# 2012-07-09&11. The latter also has both a lower particle size distribution at D50 and higher tap density.

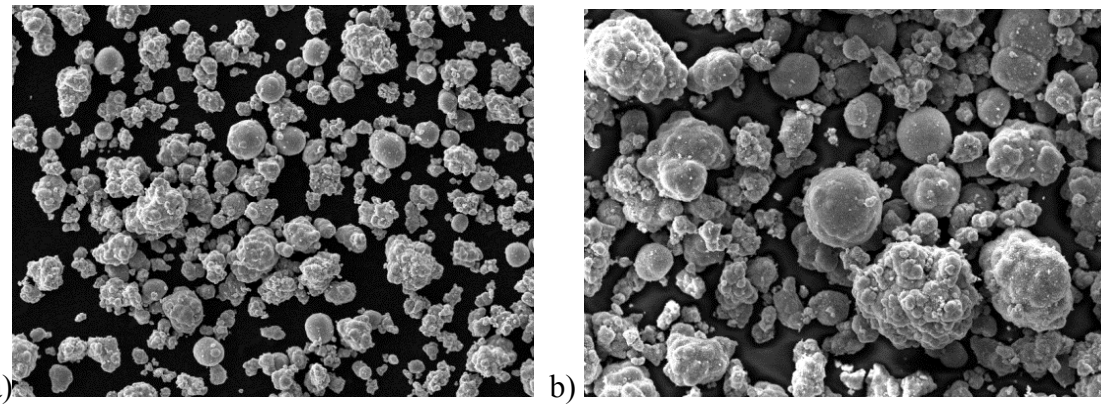

Figure 6. SEM images of MERF $Li_{1.25}Ni_{0.3}Mn_{0.62}O_2$ (Lot# 2012-02-22) powder at a) 500x and b) 1000x

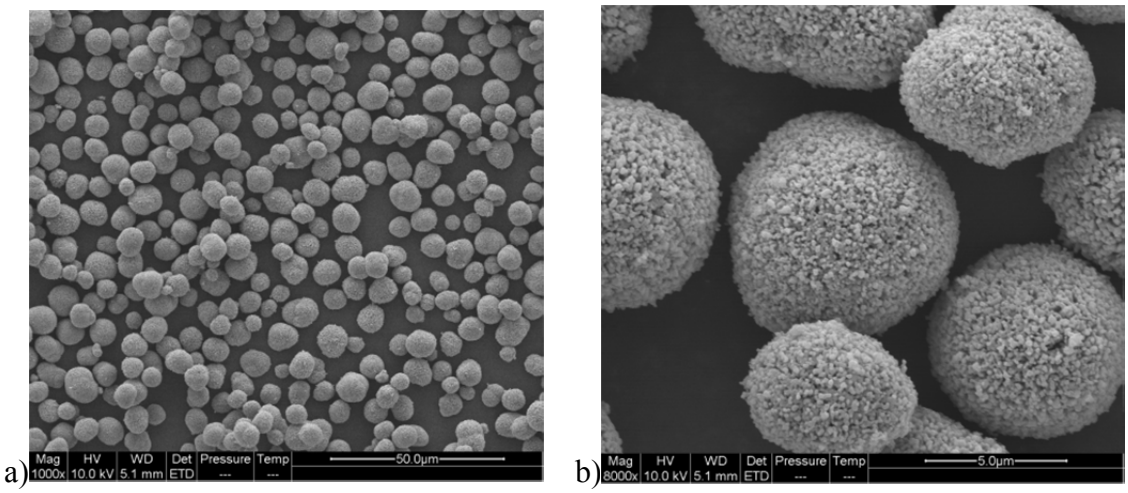

Figure 7. SEM images of MERF $Li_{1.25}Ni_{0.3}Mn_{0.62}O_2$ (Lot# 2012-07-09&11) powder at a) 1000x and b) 8000x

Each cathode powder was used to fabricate electrodes for individual pouch cells builds made at the CFF. The Lot# 2012-02-22 was given the CFF build name (CFF-B8), and the Lot# 2012-07-09&11 was given the CFF build name (CFF-B13). Both cathode electrodes were fabricated using 90 wt.% LMR-NMC, 5 wt.% Timcal C-45 carbon black, and 5 wt.% Solvay 5130 PVDF. Both anode electrodes were fabricated using 91.8 wt.% Phillips 66 A12 graphite, 2 wt.% Timcal C-45 carbon black, 6 wt.% Kureha KF-9300 PVDF, and 0.17 wt.% oxalic acid. The coated and calendered cathode SEM images may be found in Figure 8 (CFF-B8) and Figure 9 (CFF-B13). Both cathode electrodes experienced particle fracturing during the calendering process, as seen in the SEM images, but the CFF-B13 cathode had less particle fracturing than CFF-B8.

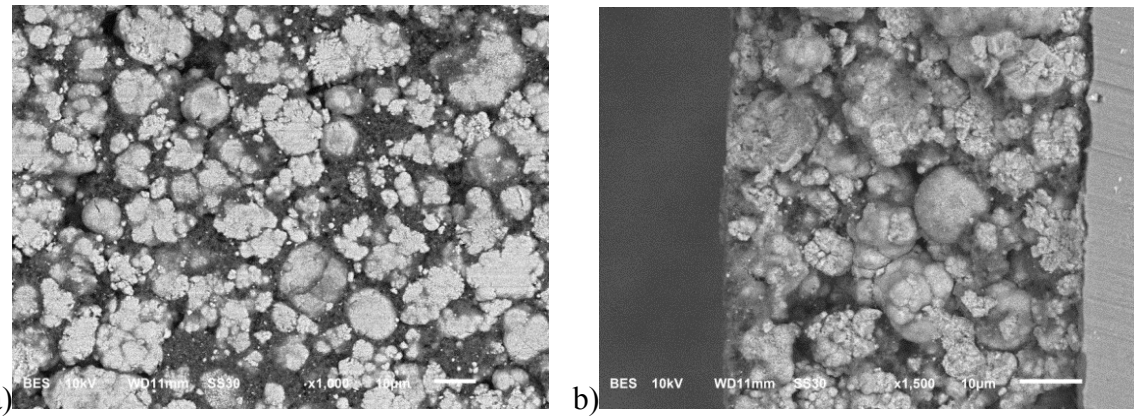

Figure 8. SEM images of CFF-B8 for a) Surface and b) Cross section

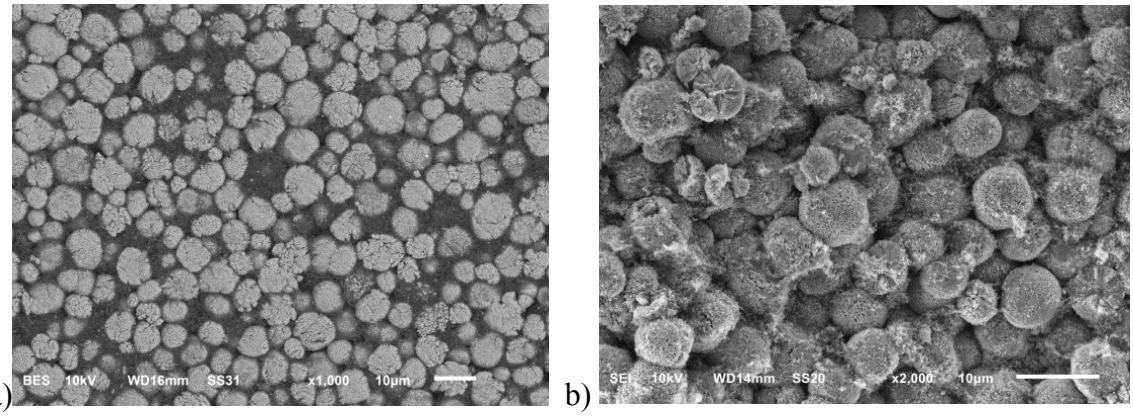

Figure 9. SEM images of CFF-B13 for a) surface and b) cross section

The rate testing results of the CFF-B8 and CFF-B13 are shown in Figures 10a and 10b, respectively. CFF-B13's rate performance surpassed that of CFF-B8's. The improved performance is likely due to the minimized particle cracking and fracturing during the calendering process, more uniform particle morphology, and lower particle size distribution. The CFF-B13 performance at lower rates (C/5) is reasonable, but the higher rates quickly degrade the rate capability of the cathode as can be observed in the data spread of the 8 cells plotted.

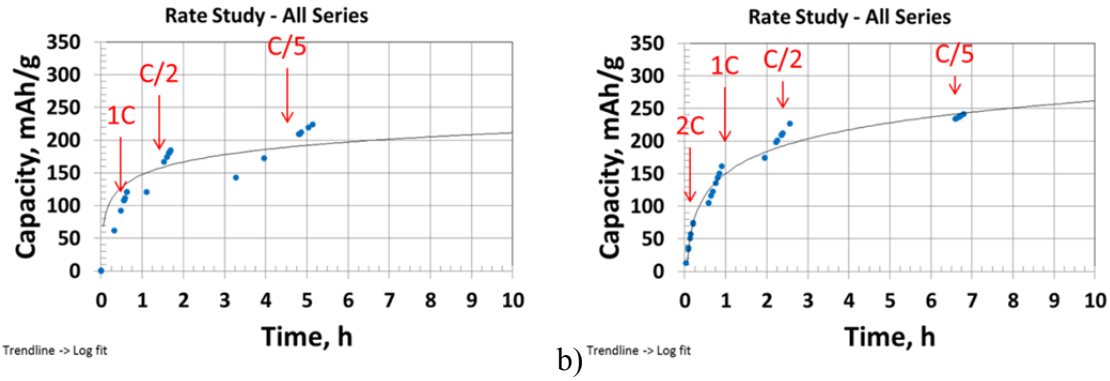

a) b)

Figure 10. a) Rate performance results of 8 identical CFF-B8 cells tested using various rates. b) Rate performance results of 8 identical CFF-B13 cells tested using various rates. Note: testing was performed at 30°C using 1.2 M $LiPF_6$ in EC:EMC (3:7 by wt.). Trend line in both plots is the average log fit for the 8 cell data series.

Similar trends were seen during the cycle life testing of CFF-B13 in Figure 11, where the cathode electrode is able to transfer charge at lower rates, but significant loss of charge transfer occurs during the C/2 rates. The pouch cell electrochemical results show improved performance of the MERF LMR-NMC Lot# 2012-07-09&11 over the MERF LMR-NMC Lot# 2012-02-22. These results coincide with the SEM and raw powder specification improvements in terms of particle size, morphology, and tap density. Continued efforts by the CFF will be performed to evaluate future MERF cathode materials using pouch cells. These include LMR-NMC powders made via the carbonate and hydroxide processes.

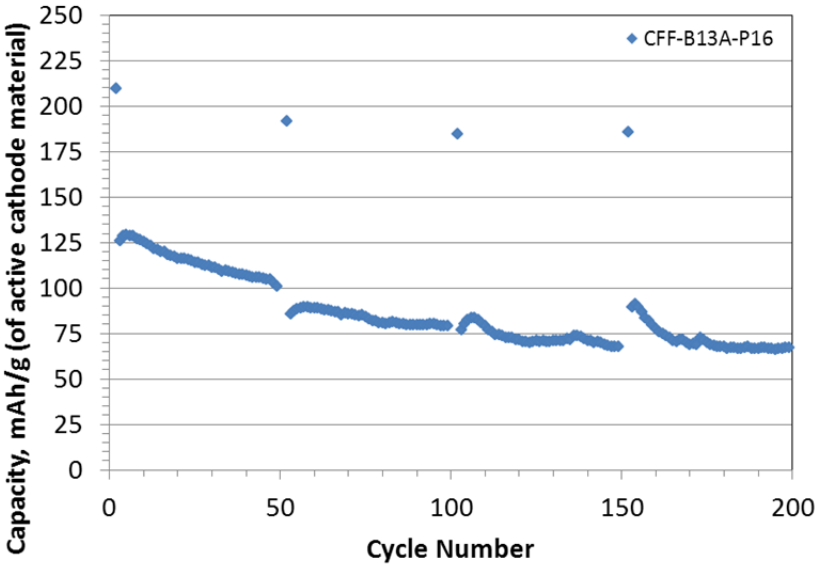

Figure 11. Cycle life plot of a CFF-B13 pouch cell with ~400 mAh C/1 capacity and 169 cm² cathode area, at 30°C, and C/2 rate. C/24 rate (data points included in plot) and HPPC (data points not reported in plot) performed every 50 cycles. 4.4 V to 2.5 V voltage window used.

(d) Summary of work in the past quarter related to milestone (d)

We received $LiFePO_4$ powder from Hanwha and $LiCoO_2$ from BTR. The electrodes for both cathode materials have been fabricated and lithium half cells are under test.

We have contacted Kureha for hard carbon material. Kureha has agreed to sample ANL two different hard carbon materials. The order process is in progress.

(e) Summary of work in the past quarter related to milestone (e)

Various materials are in the Materials Validation process to determine the best silicon/graphite/binder composition. Once a satisfactory formulation is determined and characterized, the data will be used to design a pouch cell with LMR-NMC cathode. We are on schedule for this task provided a viable source of silicon can be obtained.

(f) Summary of work in the past quarter related to milestone (f)

Anode A new graphite material from Phillips 66 was tested. This product is a surface modified synthetic graphite with high tap density (1.3g/cc). The received power was used as is to make a hand-coated electrode. In order to get the true capacity of graphite, the electrode consisted of only 8% PVDF (no carbon additive). The lithium half cell was cycled between 0V and 1.5V at C/10 rate. The reversible capacity is about 310 mAh/g with only less than 5% irreversible capacity loss during the first formation cycle (Figure 12).

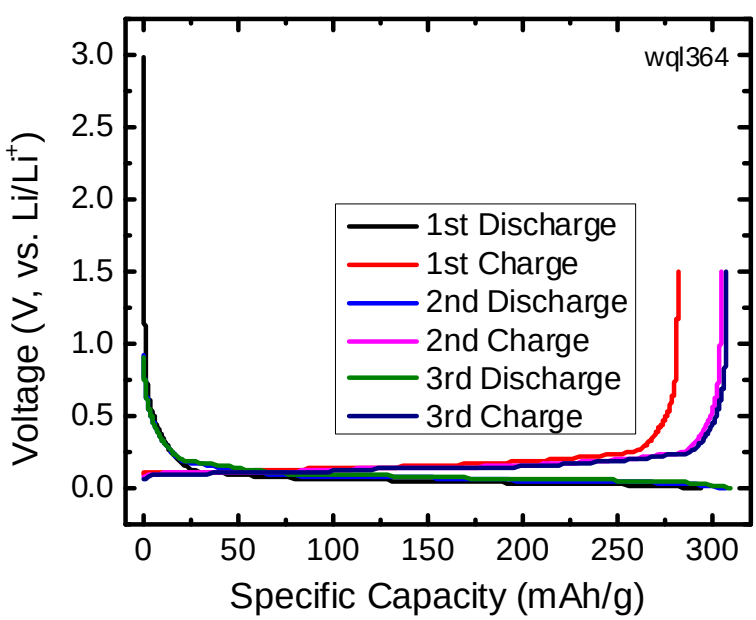

Figure 12. Voltage profile of Phillips 66 new graphite during formation cycles.

Cathode Two cathode powders were received from Jet Propulsion Lab (JPL). One powder is $Li_{1.2}Mn_{0.54}Ni_{0.13}Co_{0.13}O_2$ and the other one is a similar powder with 1 wt.% $AlPO_4$ coating (see SEM image by Post Test Facility). The brightness of the coated particle is caused by the charge during SEM measurement, which indicates the insulating feature of coating.

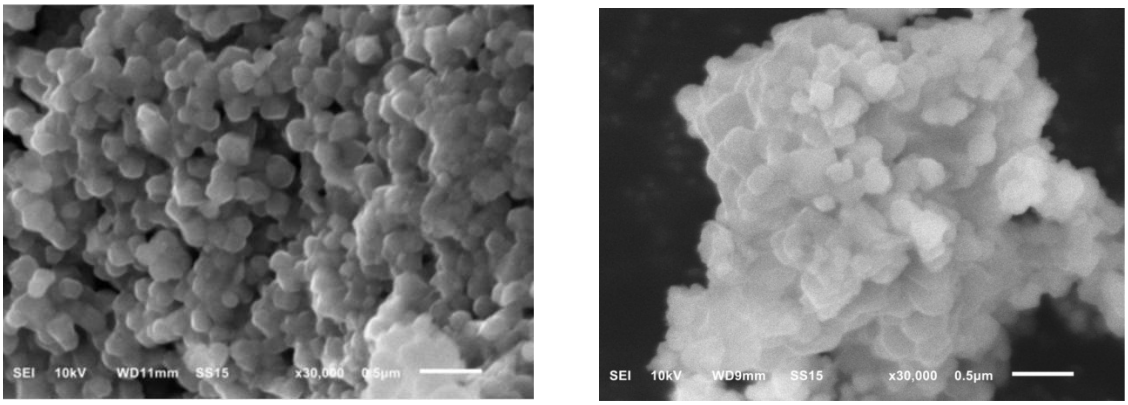

$Li_{1.2}Mn_{0.54}Ni_{0.13}Co_{0.13}O_2$ **1wt.% $AlPO_4$**

Figure 13. SEM images of $Li_{1.2}Mn_{0.54}Ni_{0.13}Co_{0.13}O_2$ (left) and similar material with 1 wt.% $AlPO_4$ coating (right)

These powders were made into electrodes using the same formulation: active materials/SFG-6/carbon black/PVDF = 86/4/2/8. Lithium half cells were used to characterize the electrochemical performance of these two active materials. The separator was Celgard 2325 and 1.2 M $LiPF_6$ in EC/EMC solvent was used as the electrolyte.

It was noticed from the formation cycle that both materials showed a typical activation voltage plateau near 4.5 V, which is similar to other lithium manganese rich transition metal oxides (LMR-NMC). However, a difference between the two active materials was observed when the differential capacity profile was compared in Figure 14. For the coated sample, the reduction peak slightly above 3.0 V shifted to lower potentials. In addition, a new reduction peak was observed near 2.5 V, which suggests that the coating process has an impact on the electrochemical performance of LMR-NMC.

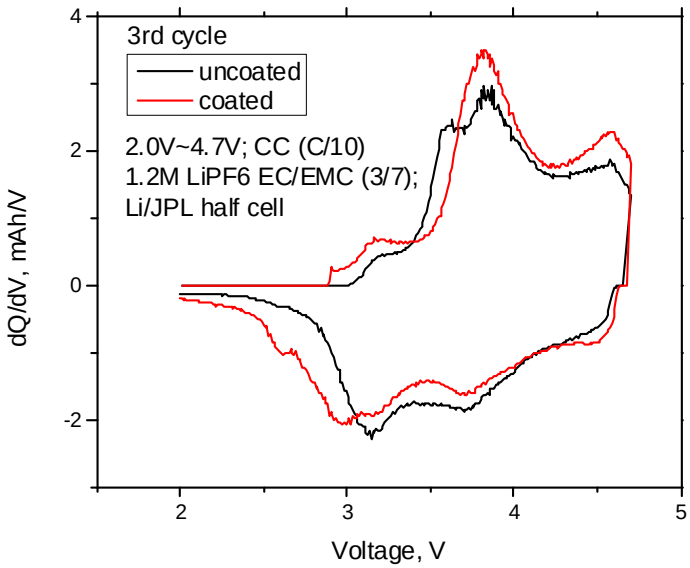

Figure 14. Different capacity plot of $Li_{1.2}Mn_{0.54}Ni_{0.13}Co_{0.13}O_2$ with and without $AlPO_4$ coating.

The voltage fade protocol was also applied to these two materials. Basically, a low current of 10 mA/g was used for the 1st formation cycle, followed by cycling at a current of 20 mA/g. The voltage profiles vs. normalized capacity are shown in Figure 15a. The black curves correspond to the uncoated sample and the red curves correspond to the coated sample. The lower operational voltage of the coated sample can be clearly seen near the end of discharge. This results in a lower average discharge voltage for the coated sample as shown in Figure 15b. We also noticed that the discharge voltage fade rate of the coated sample is comparable, if not worse, to that of the uncoated sample.

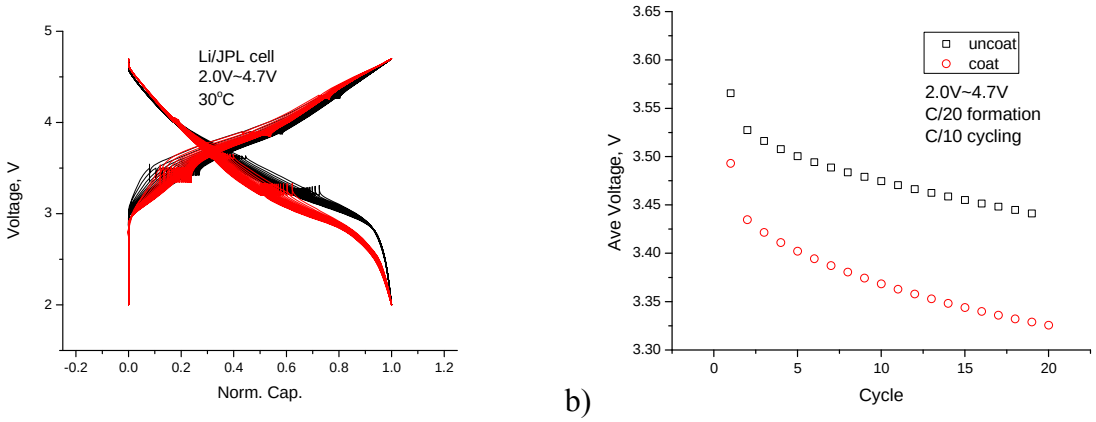

Figure 15. a) Voltage profile and b) average voltage as a function of cycling.

Aqueous Binder Due to its stronger adhesive ability and environmental friendliness, aqueous based binders have become very popular with anode materials. Recently, Argonne has investigated the SBR based aqueous binders from JSR Micro for graphite electrodes. The electrochemical performance results obtained look promising.

JSR Micro is also working on an aqueous binder for cathode electrodes. Argonne used their fluorinated acrylic hybrid latex binder for a cathode using LMR-NMC (Toda HE5050). In this study, three different binder content, 1%, 2% and 4%, were used to make slurries. The carbon content in all the slurries was 5 wt.%. Lithium half cells were used as the test vehicle to investigate the binder impact on the electrochemical performance of LMR-NMC.

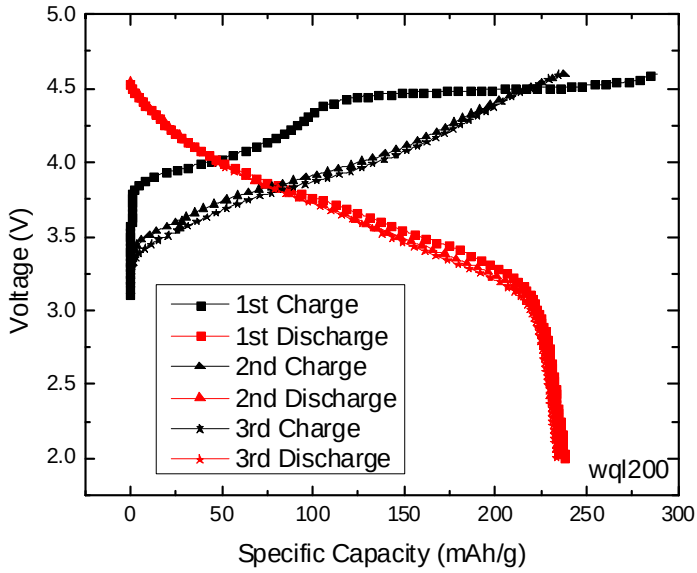

Figure 16. Formation cycles of LMR-NMC using aqueous binder.

Figure 16 shows the resulting voltage profile of these Li/LMR-NMC half cells using 1 wt.% aqueous binder during three formation cycles. Compared to our previous test results on HE5050 using PVDF-NMP binders, no difference was observed. The lithium half cells with 2% and 4% aqueous binders show similar results. Hybrid pulse power characterization (HPPC), rate performance, and cycling tests were also conducted on the half cells. They all show comparable performance to that of cells with PVDF-NMP binders. Work will continue on this aqueous binder to figure out how it behaves in full cells against anodes using SBR aqueous binder.

(g) Summary of work in the past quarter related to milestone (g)

The ABR-1 positive electrodes contain 86 wt% $Li_{1.2}Mn_{0.55}Ni_{0.15}Co_{0.1}O_2$ (HE5050), 4 wt.% SFG-6 graphite (Timcal), 2 wt.% Super P (Timcal) and 8 wt.% PVDF (Solvay 5130). The ABR-1 negative electrodes contain ~90 wt% graphite (Phillips 66 A12), 6 wt% PVDF (Kureha KF-9300) and 4 wt.% Super P (Timcal). In previous reports we have shown that cell impedance rise is mainly governed by the positive electrode; impedance rise at the negative electrode is relatively small. In AC impedance data, the positive electrode impedance rise appears as an increase in the high-frequency arc width (electronic impedance) and in the mid-frequency arc width (ionic impedance). The

following X-ray Diffraction and Raman Spectroscopy results indicate structural changes in the positive electrode carbons during cell cycling.

X-ray diffraction data from a fresh positive electrode indicate a relatively sharp graphite (002) peak at 2θ = 26.5°. This peak arises from the SFG-6 graphite, present as an electron conduction additive, in the electrode coating. The peak becomes weak and broadens significantly after only a few 2–4.6V full-cell cycles; however, it does not disappear entirely and shows a small, but measurable, intensity even in electrodes harvested from cells after 300 and 1500 cycles.

Changes in the positive-electrode graphite behavior on cycling are also evident in data from Raman spectroscopy. Figure 17 shows representative Raman spectra from a fresh positive electrode and from electrodes harvested from cycled cells.

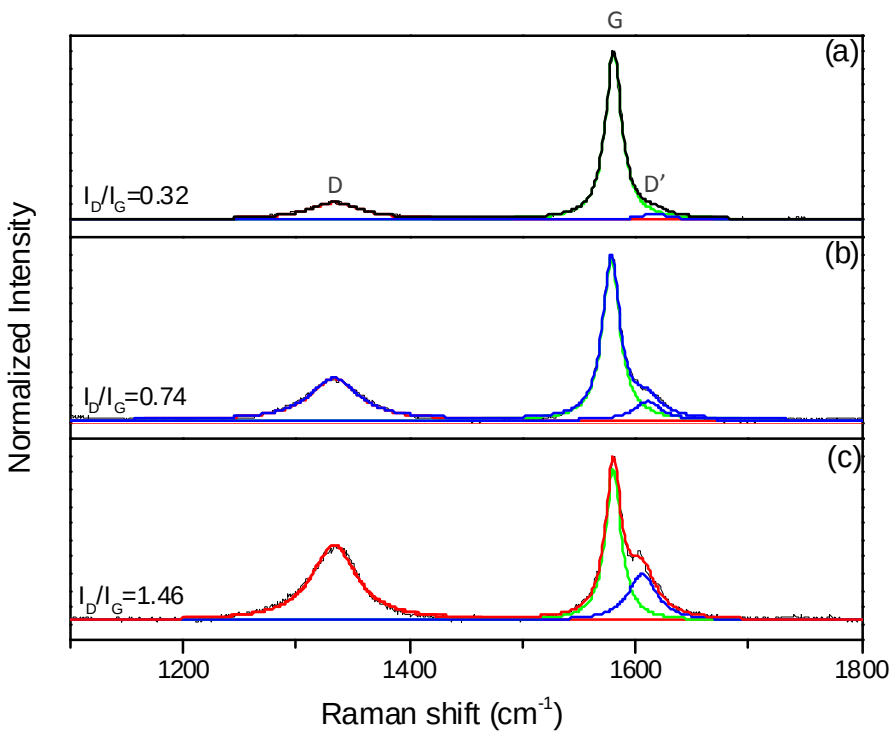

Figure 17. Raman spectra from (a) fresh positive electrode, (b), (c) positive electrodes harvested from cells after initial cycles, and after 1500 cycles, respectively. Band intensities are normalized to the G-band.

The G-band observed at ~1580 cm^{-1} corresponds to the E_{2g} vibrational mode and is commonly attributed to the in-plane stretching of all pairs of sp^2 carbon atoms in both rings and chains. The D-band observed at ~1350 cm^{-1} and the D'-band observed at ~1620 cm^{-1} are defect-induced Raman features. The D– to G– band intensity ratio (I_D/I_G) is commonly used to determine the extent of structure disorder in graphite. Figure 17 shows that the I_D/I_G ratio for the fresh electrode is 0.32. This value is higher than that expected for pure graphite because the electrode also contains Super P carbon, which is disordered and has an I_D/I_G ratio of 2.47. The I_D/I_G value increases to 0.74 for the initial–cycle

sample, and to 1.46 for the 1500–cycle sample. These data indicate that the positive electrode carbons undergo severe structural disordering upon prolonged cycling. The structural disordering is related to the intercalation of PF_6^- anions into graphitic structures. Separate experiments have shown that significant PF_6^- intercalation into SFG-6 graphite occurs at voltages >4.45 V vs. Li. Anion intercalation into the Super P carbons also occurs, albeit, in quantities that are ~2 orders of magnitude smaller than that for the graphite. These changes in the positive electrode carbons are partially responsible for degradation of the electron conduction network that appears as the high-frequency arc in the AC impedance data. Based on the electrochemistry, diffraction, and spectroscopy data, it is recommended to not use graphite-based electron conductive additives in the preparation of LMR-NMC electrodes that are cycled at voltages >4.4 V vs. Li.

(h) Summary of work in the past quarter related to milestone (h)

It has been reported that addition of alumina powder to the positive electrode coating can improve cell capacity retention. To test this claim, positive electrodes were prepared by blending 5 wt% Al_2O_3 nanosized powder with the other electrode constituents: $Li_{1.2}Mn_{0.55}Ni_{0.15}Co_{0.1}O_2$ (HE5050), SFG-6 graphite, Super P carbon and PVDF (Solvay 5130) binder. The Al_2O_3 powder had a particle size of ~50 nm and a high surface area (32–40 m^2/g). To ensure adequate dispersion, the Al_2O_3 powder was mixed into the NMP (N-Methyl-2-pyrrolidone) at the beginning of the slurry making process.

Figure 18 shows cycling data and impedance spectra from full–cells containing the alumina-powder modified positive electrode and the ABR-1 negative electrode described earlier. The capacity fade after 50 cycles (~C/3 rate) is ~0.12 % per cycle, significantly better than the ~0.48 % per cycle for the baseline ABR-1 cell. The improved cell capacity retention probably results from HF- and water- scavenging by the alumina. On the other hand, the impedance rise of the alumina-powder modified cells is similar to that of baseline ABR-1 cells. The data suggest that cell capacity fade is largely independent from impedance rise for the ABR-1 type couples.

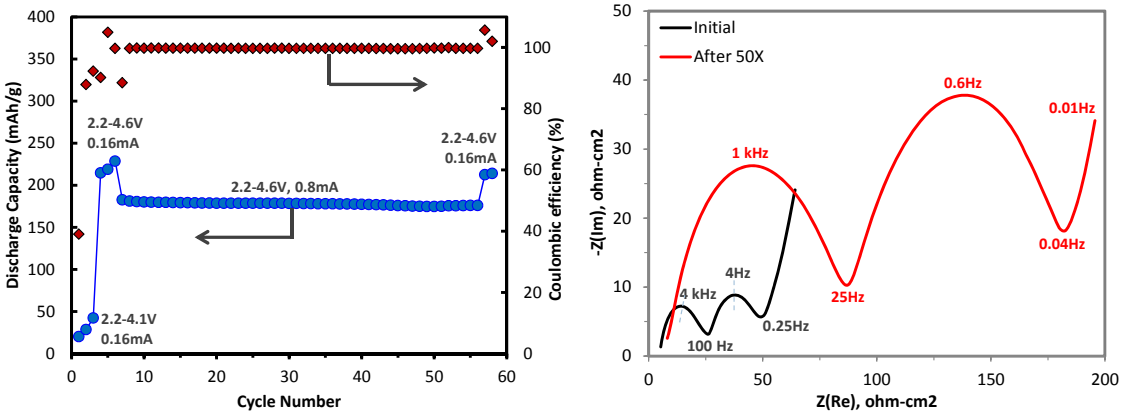

Figure 18. Plots for full cells containing the alumina-powder modified positive electrode showing (left) discharge capacity and columbic efficiency changes with cycle number, voltage range, and current, and (right) EIS data after initial cycles (black) and after fifty 2-4.6 V cycles (red).

(i) Summary of work in the past quarter related to milestone (i)

The public release of BatPaC v2.1 was completed with a revised and updated report that is available from www.cse.anl.gov/batpac. The BatPaC model and report were first openly distributed to the public, free of charge, in November 2011. During the first year of release, over 450 independent downloads have occurred from leading universities, laboratories and companies around the world. Users of the model include PhD students, policy makers, high-profile startups, and Fortune 500 corporations. Some have modified the model for their own use, while others use it as is.

The major updates included in BatPaC v2.1 include the following:

- Air-based thermal management option
- Automatic calculation of uncertainty in point cost estimate
- Updated transition metal based cathode material costs
- Parallel pack and module option
- Improved heat generation estimation
- Multiple cost-breakdown formats

A trade-off between electrode specific-capacity and cell voltage may be necessary when evaluating moving to an advanced Li-ion cell chemistry. In other words, the highest voltage couple does not necessarily lead to the lowest cost battery. These situations are readily examined using BatPaC. For example, significant research efforts are ongoing to improve the volumetric capacity of the positive electrode, but often concurrently lower the average cell potential. Examining Figure 19 (left), the trade-off between capacity and voltage may be quantitatively approximated by holding the negative electrode properties constant (i.e. graphite). For positive volumetric capacities less than 300 mAh cm^{-3} (~120 mAh g^{-1}), a 50 % increase in capacity is roughly equivalent to an 800 mV increase in cell voltage. Whereas, an increase in capacity from 400 to 600 mAh cm^{-3} is only equivalent to a 300 mV increase. The allowable tradeoff becomes even less at higher capacities.

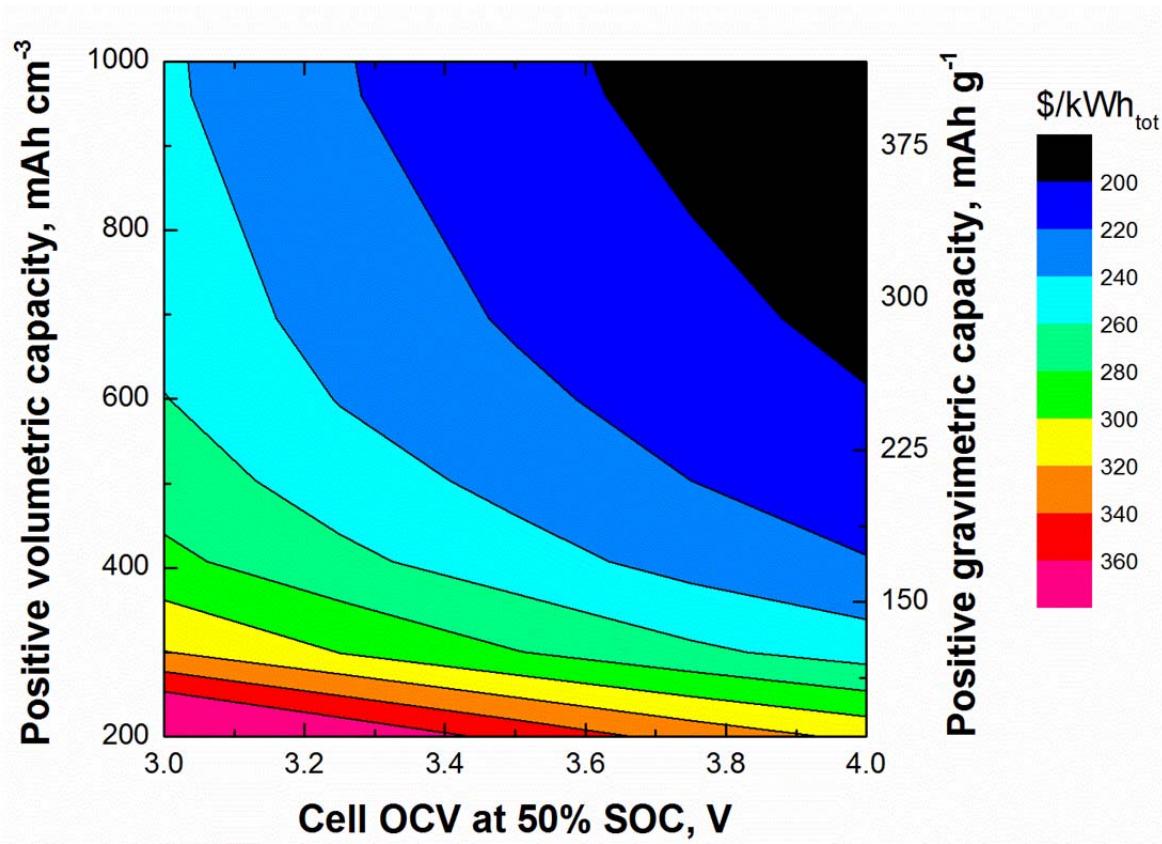

Figure 19. Trade-off between cell voltage and positive electrode volumetric capacity on the price per unit energy for a PHEV40 60 kW and 17 kWh battery. Negative electrode is treated as a graphite electrode.

(j) Summary of work in the past quarter related to milestone (j)

The evaluation of hysteresis in the open-circuit voltage vs. SOC function in lithium and manganese rich transition metal layered oxide materials has been linked to the voltage fade phenomenon being studied at Argonne. Future work on modeling the hysteresis behavior will be undertaken in the voltage fade effort to better align the resources with outcomes.

Modeling efforts continue to evaluate interfacial and bulk transport properties of LMR-NMC cathodes as a function of SOC and the path dependence that results from the hysteresis. Efforts will examine how these parameters change with lithium content and if a greater understanding of the increase in impedance at low SOC can be reached.

Publications, Reports, Intellectual property or patent application filed this quarter. (Please be rigorous, include internal reports--invention records, etc.)

"A Volume Averaged Approach to the Numerical Modeling of Phase-Transition Intercalation Electrodes Presented for LixC6", by Kevin G. Gallagher, Dennis W. Dees, Andrew Jansen, Daniel Abraham, and Sun-Ho Kang, accepted by *Journal of The Electrochemical Society*.

"Electrochemical Modeling the Impedance of a Lithium-Ion Positive Electrode Single Particle", by Dennis W. Dees, Kevin G. Gallagher, Daniel P. Abraham, and Andrew N. Jansen, *Journal of The Electrochemical Society* **160**(3), A478-A486 (2013).

"Positive Electrode Passivation by LiDFOB Electrolyte Additive in High-capacity Lithium-ion Cells", by Ye Zhu, Yan Li, Martin Bettge, and Daniel P. Abraham, *Journal of The Electrochemical Society* **159,** A2109-2117 (2012).

"Overcharge Effect on Morphology and Structure of Carbon Electrodes for Lithium-ion Batteries", Wenquan Lu, Carmen M. Lopez, Nathan Liu, John T. Vaughey, Andrew Jansen, and Dennis W. Dees, *Journal of The Electrochemical Society* **159**, A1-A5 (2012).

TASK 2
Calendar & Cycle Life Studies

Project Numbers: 1.1.1 and 2.4 (ES033)

Project Title: Strategies to Enable the Use of High-Voltage Cathodes (1.1.1) and Diagnostic Evaluation of ABRT Program Lithium Battery Chemistries (2.4)

Project PI, Institution: Robert Kostecki, Lawrence Berkeley National Laboratory

Collaborators (include industry): None

Project Start/End Dates: LBNL carried out diagnostics in the ATD Program since its 1999 inception, and the ABRT Program began October 2008

Objectives: Task 1.1.1: To enable increased energy density by addressing the impact of high-voltage cathodes on the conducting carbon matrix. Task 2.4: (i) Determine the key factors that contribute to the degradation mechanism in the PHEV test cells and individual cell components. (ii) Characterize SEI formation on model electrode surfaces to improve understanding of key interfacial phenomena in PHEV cells.

Approach: Task 1.1.1**:** (i) determine the mechanisms for carbon damage and retreat at high potentials. (ii) Investigate mitigating treatments, additives, and procedures. Task 2.4: Use in situ and ex situ advanced spectroscopic and microscopic techniques in conjunction with standard electrochemical methods to characterize components harvested from fresh and tested PHEV cells, model thin-film cells, and special cells used to evaluate SEI formation processes.

Milestones: (i) Determine degradation mechanism in high-voltage cathodes (August 2013), (ii) synthesize a new type of CB with improved interfacial properties (September 2013), (iii) attend review meetings and present diagnostic results obtained in collaboration with ABRT Program participants.

Financial data: FY 2013 funding $600K

PROGRESS TOWARD MILESTONES

The focus of our work in the first quarter of FY13 included comprehensive analysis of the irreversible capacity losses in high-energy composite positive electrodes, examination of the positive effect of the oxidative heat treatment of carbon black conductive additives, and fundamental investigations of the mechanism of chemical cross-talk in lithium-ion battery cells using fluorescence spectroscopy and imaging.

A new experimental approach has ben designed and created to quantify the extent of the electrolyte oxidation at positive Li-ion composite electrodes at potentials exceeding 4.2 V vs. Li/Li^+. The potential response of the 10th galvanostatic charge-discharge cycle of the Toda He5050/Super-P/PVdF electrode (see Figure 1 in 4Q FY 2012 report) was used as a

model to produce a similar potential profile program that consists of 1980 short (3-12 s) potentiostatic steps. This model potential profile was used to carry out a voltage profile simulation (VPS) measurements on pure carbon black/PVdF electrodes with no active material present. These measurements provided direct quantitative information about the charge consumed by electrolyte decomposition at the carbon black additive alone during a typical charge-discharge process. Figure 1 depicts the model potential profile and the corresponding current responses of the pristine and CO_2 heat-treated carbon black electrodes.

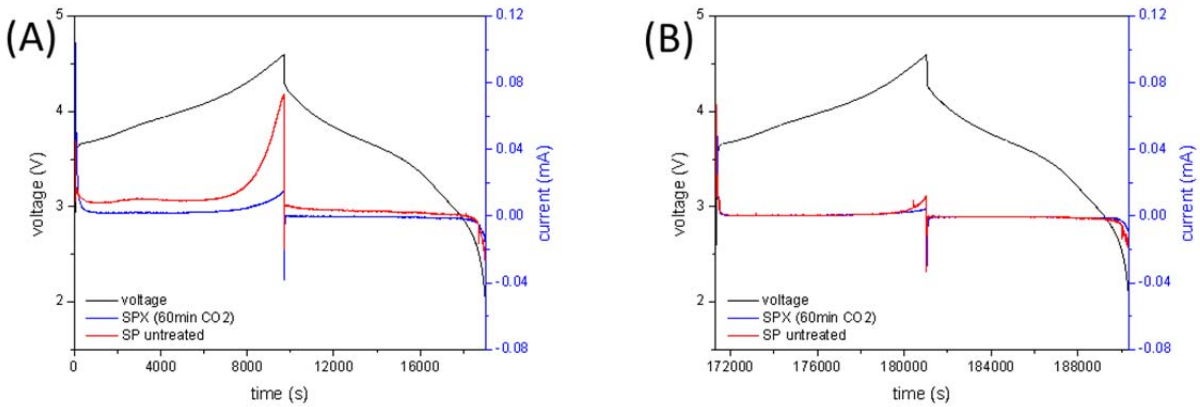

Figure 1. Simulated voltage profile (black) and current response of untreated (red) and heat treated (blue) Super-P/PVdF/ Toda He5050 electrodes: 1st cycle (A) 10th cycle (B)

The electrolyte oxidation current at the pristine carbon black/PVdF electrode is substantially higher than for the CO_2 heat-treated carbon black/PVdF electrode for both the anodic and cathodic scans during the first cycle (A). The magnitude of the anodic current tends to decrease significantly in the following scans. However, the current density for untreated CB electrode still remains three time times higher at 4.7 V that the CO_2 heat-treated electrode. The calculated charge (mAh/g of carbon) consumed during the model "charge-discharge" cycles of the CB electrodes is shown in Figure 2.

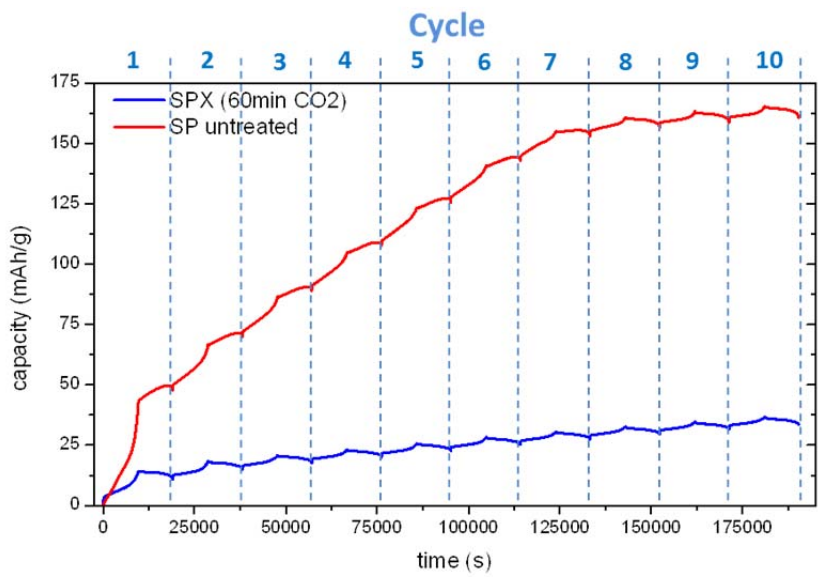

Figure 2. Charge consumed in the electrolyte oxidation side-reactions during model "charge-discharge" scans of untreated (red), and CO_2 heat-treated Super-P/PVdF electrodes (blue) during first ten cycles

This charge profile represents the faradaic component of the current and ignores any capacitive contribution from the double layer. The significant charge consumed by the electrolyte oxidation processes at the unmodified carbon black electrode during the first anodic scan indicates that the irreversible processes must have led to a partial passivation of carbon black. The following scans kept adding to the total charge used in these irreversible processes to reach an equivalent of 163 mAh/g of carbon. This is ~5 time higher than the charge consumed during similar "charge-discharge" scans of the CO_2 heat-treated CB electrode. Interestingly, the electrochemical behavior of both samples becomes very similar after 8 cycles suggesting that an effective surface passive layer eventually forms at carbon black.

A typical positive Li-ion composite electrode that consists of ~7% carbon black conductive additive. Considering a reversible capacity of NMC-based positive electrode at 170 mAh/g, these results would indicate that ~6.2% of the overall electrode charge capacity is consumed in the reversible processes on the carbon black during the first ten cycles. The use of CO_2 heat-treated carbon black additives can help reduce these irreversible losses to ~1.2%. These investigations provide more evidence of the importance of interfacial effects on passive electrode components for the overall performance and lifetime of Li-ion batteries.

TASK 2
Calendar & Cycle Life Studies

Project Number: 1.1, 2.4, and 3.3 (ES034)

Project Title: Life and abuse tolerance diagnostic studies and new electrolytes development for high energy density PHEV batteries

Task 1.1: Develop/Engineer PHEV Electrode Materials, Electrolytes, & Additives
Task 2.4: Life Diagnostics
Task 3.3: Abuse Behavior Modeling and Diagnostics

PI, Institution: Xiao-Qing Yang and Kyung-Wan Nam, Brookhaven National Laboratory

Barrier: Calendar and cycling life, Abuse tolerance

Project Start/End Dates: October 2012 / September 2013

Objects: The primary objectives of the efforts at BNL are: to determine the contributions of electrode structural changes, interfacial phenomena, and electrolyte decomposition to lithium-ion cell capacity and power decline, and abuse tolerance; to develop new diagnostic techniques (in situ and ex situ) for lithium-ion batteries; to collaborate with other ABR teams and the battery developers to understand the technical barriers, especially the voltage fading mechanism of high energy density Li and Mn rich NCM cathode materials during cycling; to explore new approaches to improve the abuse tolerance. The other objective is to design, synthesize and characterize new electrolyte for PHEV oriented lithium-ion batteries with better performance and safety characteristics. Special attention will be given to the new electrolytes for high voltage cathode materials.

Approach: Our approach is to use a combination of *in situ, ex situ* and time-resolved synchrotron based x-ray techniques to characterize electrode materials and electrodes taken from baseline ABR Program cells. *Ex situ* soft X-ray absorption spectroscopy (XAS) will be used to distinguish the structural differences between surface and bulk of electrodes using both electron yield (EY) and fluorescence yield (FY) detectors. Time-resolved X-ray diffraction (TR-XRD) technique will also be used to understand the reactions that occur in charged cathodes at elevated temperatures in the presence of electrolyte. In situ x-ray diffraction will be used to monitor the structural changes of the electrode materials during charge-discharge cycling at different conditions. A combination of TR-XRD, in situ soft and hard X-ray absorption (XAS), in situ transmission electron microscopy (TEM) techniques during heating will be applied to study the thermal stability of the electrode materials. These approaches developed at BNL will be utilized to study various cathode-anode chemistry pair systems of ABR projects through extended collaboration with other ABR members, such as Dr. Khalil

Amine, Dr. Daniel Abraham, Dr. Chris Johnson, and Dr. Zhengcheng Zhang at ANL. We will continue to develop new synchrotron based x-ray techniques such as combined in situ x-ray diffraction and mass spectroscopy during heating for the thermal stability of cathode material studies. We will continue to develop TEM based in situ diagnostic tools to study the structural changes at both surface and bulk of the electrode particles with high spatial resolution.

Milestones:

(a) By April 2013, complete the studies of thermal decomposition of charged $Li_{1.2}Ni_{0.15}Mno_{0.55}Co_{0.1}O_2$ (Toda HE5050) cathode materials during heating using combined Time-Resolved XRD and Mass Spectroscopy, **on schedule.** (b) By April 2013, complete the ex situ soft x-ray XAS studies of $Li_{1.2}Ni_{0.15}Mno_{0.55}Co_{0.1}O_2$ (Toda HE5050) cathode material during charge-discharge cycling to distinguish the structural change differences between the surface and the bulk, **on schedule.** (c) By September 2013, complete the in situ hard x-ray XAS studies of $Li_{1.2}Ni_{0.15}Mno_{0.55}Co_{0.1}O_2$ (Toda HE5050) cathode material for the voltage fading mechanism and structural instability during extended cycling, **on schedule.** (d) By September 2013, complete the studies of thermal decomposition of charged $Li_{1.2}Ni_{0.17}Mno_{0.53}Co_{0.1}O_2$ (ANL-HE) cathode materials with and without AlF_3 coating during heating using combined Time-Resolved XRD and Mass, **on schedule.**

Progress toward milestones for the first quarter of FY2013:

Summary of work in the past quarter related to milestone (a)

In the first quarter of FY2013, progress toward the mile stone (a) has been made. Using combined Time-Resolved XRD and Mass Spectroscopy, the thermal decomposition of charged $Li_{1.2}Ni_{0.15}Mno_{0.55}Co_{0.1}O_2$ (Toda HE5050) cathode materials during heating has been studied. The preliminary results of the combination of time-resolved XRD and mass spectroscopy of $Li_{1.2}Ni_{0.15}Mno_{0.55}Co_{0.1}O_2$ cathode material charged to $Li_{0.3}Ni_{0.15}Mno_{0.55}Co_{0.1}O_2$ level of Li content during heating from 25 to 550 °C are plotted in Figure 1 (left and middle panel). The crystal structure evolution is illustrated in the right panel of figure 1. It can be seen from Fig. 1 the crystal structural changes of charged $Li_{0.3}Ni_{0.15}Mno_{0.55}Co_{0.1}O_2$ layered cathode material follow the similar path as the regular layered materials such as $Li_{1.0}Ni_{0.33}Mno_{0.33}Co_{0.33}O_2$ during heating: at about 220 °C, the layered structure start converting into disordered spinel structure. After completing this transition about 400 °C, it starts the second phase transition at about 450 °C from the disordered spinel to the rock-salt structure. Both of these two phase transitions are accompanied with the release of oxygen.

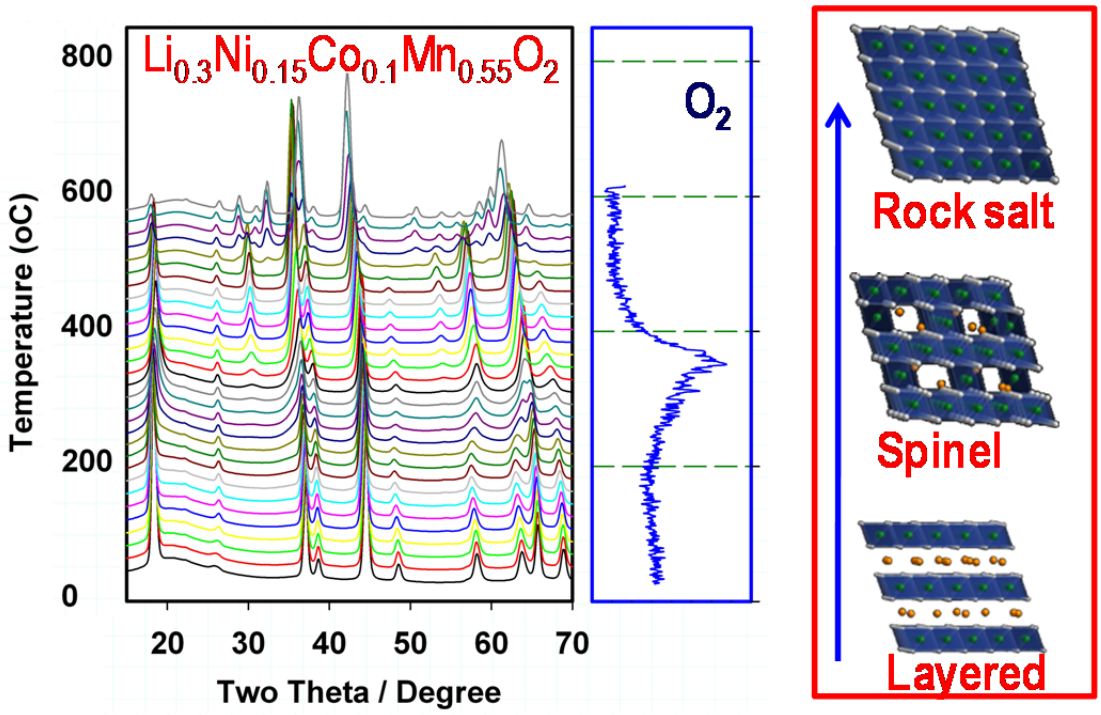

TR-XRD patterns and simultaneously measured mass spectroscopy (MS) for O_2 released from $Li_{0.3}Ni_{0.15}Co_{0.1}Mn_{0.55}O_2$ during heating to 550 ^{o}C. The right panel shows the models of ideal crystals with rhombohedral (layered), spinel, and rock-salt structures

TASK 2
Calendar & Cycle Life Studies

Project Number: CSP Project 18502, CSP Agreement 23060, ORNL FWP CEVT110 (ES165)

Project Title: Roll-to-Roll Electrode Processing NDE and Materials Characterization for Advanced Lithium Secondary Batteries

Project PI, Institution: David Wood, Oak Ridge National Laboratory

Collaborators: Argonne National Laboratory, Dow Kokam, Keyence, and Ceres Technologies

Project Start/End Dates: 10/1/11 to 9/30/14

Objectives: Due to high scrap rates of 10-20% or more associated with lithium secondary cell production, new methods of quality control (QC) must be implemented. Often flaws in the electrodes are not detected until the formation cycling when the entire series of manufacturing steps has been completed, and the associated scrap rates drive the costs of lithium secondary cells to an unacceptable level. If electrode flaws and contaminants could be detected in line near the particular processing steps that generate them, then the electrode material could be marked as unusable and the processing equipment could be adjusted to eliminate the defects more quickly. ORNL is considering in line analysis methods such as X-ray fluorescence spectroscopy (XRF) for electrode component uniformity and metal particle detection and laser thickness sensing of the electrode wet thickness measurement. In addition, on-line laser thickness measurement and IR imaging of wet and dry electrode coatings are being implemented for thickness uniformity and coating flaw detection. These methods have been effectively utilized in other industries such as photovoltaic, flexible electronics, and semiconductor manufacturing, but the equipment and measurement methods must still be tailored for lithium secondary cell production. The object of this project is to raise the production yield of lithium secondary battery electrodes from 80- 90% to 99% and reduce the associated system cost by implementing in line XRF and laser thickness control. In addition, ORNL is providing its diagnostics capabilities and expertise to address materials issues with ABR cathode materials.

Approach: Ceres Technologies has been identified as a top manufacturer of in line XRF instruments for roll-to-roll applications and has a great deal of experience with the photovoltaics industry. ORNL will work closely with them to establish this technology for the lithium secondary battery industry by producing tape casted and slot-die coated electrode rolls (anodes and cathodes) with deliberately introduced flaws to test the appropriateness of the method and the equipment modifications to the standard model. All key process parameters, such as line speed, coating thickness range, metal particle density, elemental homogeneity, etc., will be examined. In-line XRF data will also be

correlated with ex-situ XCT data to gain a complete chemical and structural picture of the electrode as it is coated and dried.

Keyence has been selected as the partner for developing a set of laser thickness sensors for lithium secondary battery electrode production. ORNL has purchased sensors with point scanning capability from Keyence and integrated them directly into the slot-die coating line for the proof-of-concept experiments. The next step is to implement sensors with the capability of scanning multiple points or a full line scan across the web.

The output data from the wet layer thickness measurements using the laser sensors will be used to mark regions that are out of specification during the coating process. The coated electrode rolls with markings will be fed into the in line XRF equipment to determine if wet regions out of specification match with dry regions that are determined to be out of specification. Ultimately a feedback mechanism will be designed that considers whether the wet or dry thickness is a better input for adjusting the dispersion flow rate into the slot-die coater. The IR imaging QC will be correlated with thickness variation data to determine any further systematic flaw formation mechanisms such as pinholes, divots, and large agglomerates.

ORNL characterization capabilities and offline diagnostics consisting of acoustic emission detection, in-situ and ex-situ X-ray diffraction, neutron scattering, magnetic property determination, and high-resolution microscopy will be utilized to investigate cathode materials issues with ABR developed materials (specifically TODA HE5050).

FY13 Milestones:

1) Determine feasibility of measurement of deliberately introduced metal contaminants into cathodes with in-line XRF using ORNL tape caster line (January 2013 – delayed to March 2013).
2) Correlation of wet and dry thickness using laser line-scan thickness measurement (wet thickness) and in line XRF (dry thickness) to within ±10% (April 2013).
3) Ceres Technologies to complete final design of in-line XRF system for secondary lithium battery electrode production (July 2013).
4) Transfer technology associated with each of the three techniques (in-line laser thickness, XRF, and IR imaging) to industry partner (TBD) pilot/production line (September 2013).

Financial data: $300k/year (FY12-FY13)

PROGRESS TOWARD MILESTONES

Summary of work in the past quarter related to milestone (2)

The Keyence laser system has been successfully mounted on the ORNL slot-die coater, which allows for point thickness measurement of the wet electrode along a line down the web (Figure 1). This setup has been utilized to measure the wet thickness of the ABR developed high-voltage cathode TODA HE5050 (composition: $Li_{1.2}Co_{0.1}Mn_{0.55}Ni_{0.15}O_2$) and ABR baseline graphite ConocoPhillips A12 anode to examine the feasibility of this technique. Before measuring the wet coating of the cathode, the laser sensors were

calibrated using Al foil (15 μm). The thickness data after calibration was collected for 5 minutes, and the average thickness was found to be 15.67 μm with a standard deviation of 0.23 μm (Figure 2a), which agrees well with the nominal thickness of the foil.

The thickness of a wet TODA HE5050 coating was measured at a line speed of 1ft/min (areal loading of 10 mg/cm^2) and data was collected for 20 minutes. Results are shown in Figure 2b where it is seen that the average thickness was 118.51 μm with a standard deviation of 2.75 μm (±2.3% thickness variation).

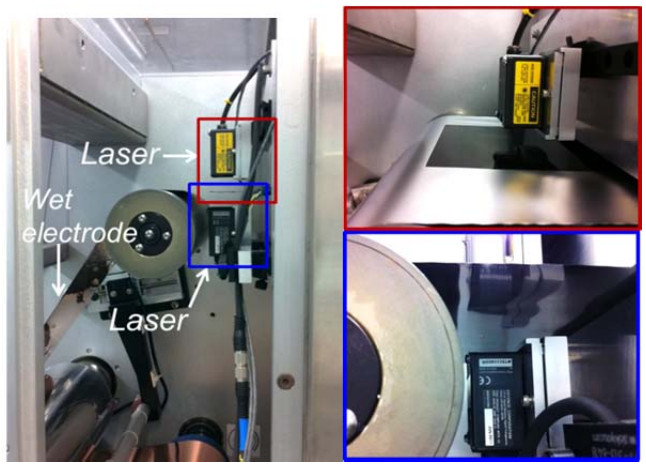

Figure 1. In-line laser thickness measurement setup on the ORNL slot-die coater.

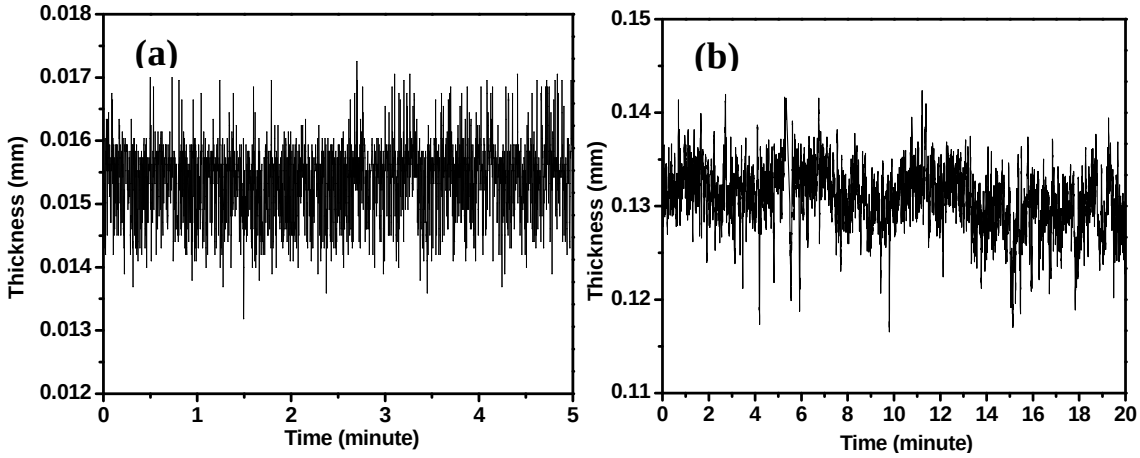

Figure 2. Measured thickness of (a) bare Al foil and (b) wet TODA HE5050 coating.

Similarly, we have also demonstrated this method with the ConocoPhillips A12 ABR baseline graphite anode coated on Cu foil. In Figure 3, the in-line thickness measurement of the bare Cu foil (Figure 3a) and wet anode (Figure 3b) are shown. The measured thickness for the Cu foil was 19.97 μm with a standard deviation of 0.76 μm (in excellent agreement with the nominal thickness of 20 μm) and that of the anode was found to be 96.99 μm with a standard deviation of 3.13 μm (±3.2% variation).

This method of measuring thickness has been shown to be highly accurate based on the bare foil measurements, and it is has also demonstrated that ORNL is producing electrode coatings with high thickness uniformity (no more than ±2-3% variation down the web). To correlate the thickness uniformity of the electrode coatings with electrochemical performance, we are performing systematic cycling experiments. Multiple pouch cells with TODA HE5050 cathodes and ConocoPhillips A12 graphite anodes were fabricated for capacity reproducibility and cycle life testing. An image of one of these pouch cells fabricated at ORNL Battery Manufacturing Facility (BMF) is shown in Figure 4.

In Figure 5, the electrochemical data from one of these cells is shown, which was cycled within the voltage window of 2.5-4.7 V at the rate of 20 mA/g. Prior to this testing, the cell underwent formation cycling by following the procedure reported by Abraham.[1] From

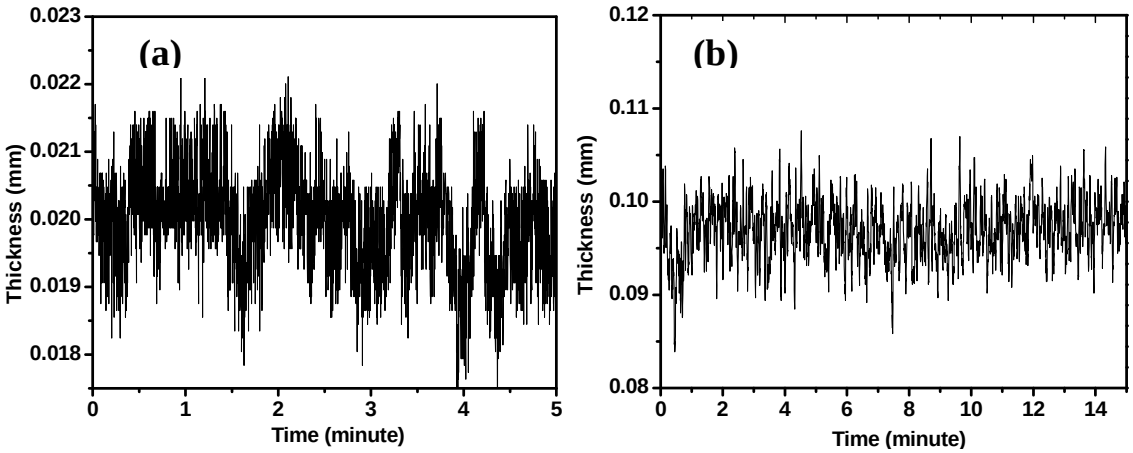

Figure 3. Measured thickness of (a) Cu foil and (b) wet ConocoPhillips A12 graphite coating.

Figure 5, it is evident that the cell exhibits the "voltage fading" phenomena after 25 cycles, and Figure 6 shows the corresponding trend in charge-discharge capacity (charge and discharge capacities are similar except the first cycle). After 25 cycles, ~85% of the discharge capacity was retained; however, significant voltage fade was observed (see the arrow marks in Figure 5).

[1] D. Abraham *et. al.*, *J. Electrochem. Soc.*, **159**(12), A2109-A2117 (2012).

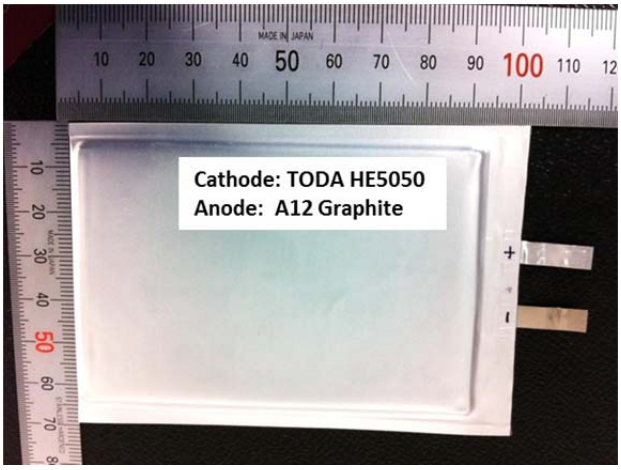

Figure 4. Representative image of a high-capacity pouch cell fabricated at the ORNL Battery Manufacturing Facility.

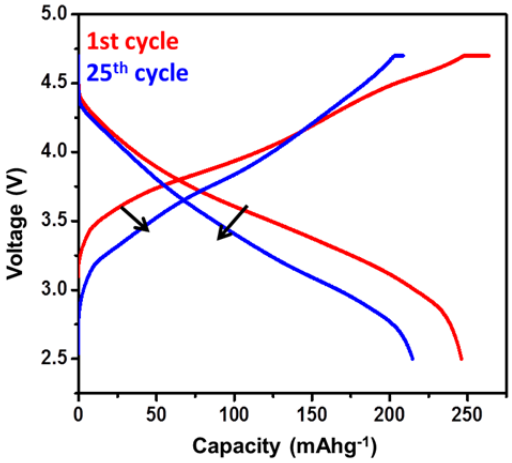

Figure 5. Charge and discharge voltage profiles for the 1st and 25th cycles showing the voltage fade

The electrochemical performance data obtained from this pouch cell was highly representative of the set of cells. One of the reasons for the observed reproducibility may be the homogeneous thickness of the anode and cathode coatings, which was confirmed by in-line laser thickness measurements. Currently we are examining individual performance of each of these pouch cells in order to correlate it with the measured in-line thickness data, and detailed analysis will be presented in next quarterly report. In addition, neutron diffraction experiments are scheduled at the Spallation Neutron Source (SNS) on these cycled pouch cells in order to shed light on the voltage fading phenomenon, and results will also be presented in the next quarterly report.

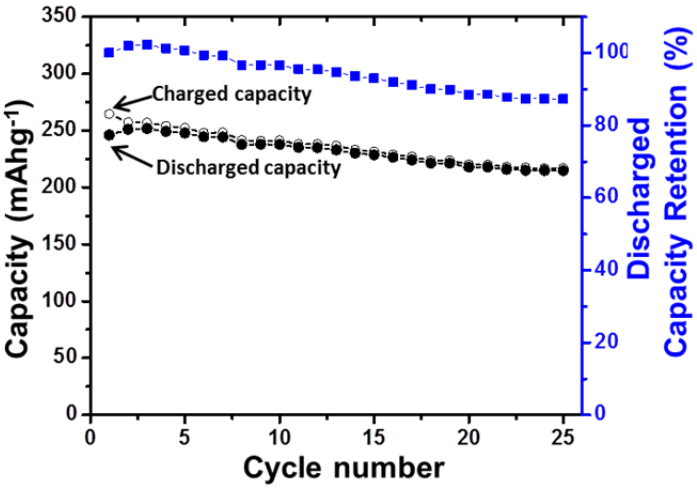

Figure 6. Charge-discharge capacity through 25 cycles for the ORNL BMF pouch cells with the TODA HE5050 cathode and ConocoPhillips A12 graphite anode.

Summary of work in the past quarter related to milestone (4)

In order to check for coating defects and homogeneity of the dried TODA HE5050 electrode, IR thermography was implemented at the exit of the slot-die coater (setup shown in Figure 7a). In Figure 7b, a representative IR image of this coating along with the temperature profile obtained along a line scan is shown. The temperature profile shows an increase at the defect region corresponding to an agglomerate or blister, which could not be detected optically. This finding demonstrates the effectiveness of IR thermography in detecting minute electrode coating defects, which could ultimately lead to cell failures. Because of limited space, the current IR camera could not be mounted at the exit of the slot-die coater oven. Hence, two mirrors were used in order to perform this measurement. Currently, the setup is being modified in order to obtain direct images of the electrodes using a new smaller IR camera, and these results will be discussed in the next quarterly report.

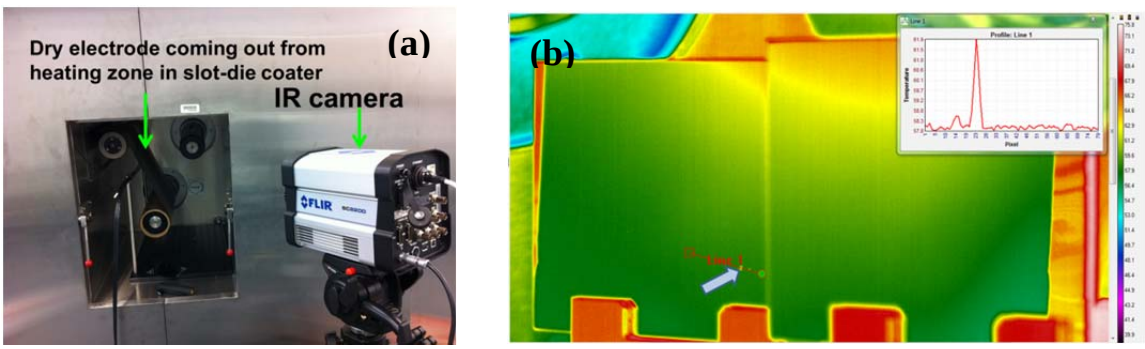

Figure 7. a) IR camera positioned at the exit of the slot-die coating line and b) processed IR thermography image where the inset shows the temperature profile across a line scan. The increase in temperature shows the presence defect corresponding to an agglomerate or blister (see arrow mark).

Summary of work in the past quarter related to HE5050 materials characterization

Key results previously reported:

- In-situ XRD was implemented to investigate and monitor the phase transformation of the TODA HE5050 Li-Mn-rich cathode, and the results showed the appearance of the spinel phase during low voltage discharge (3.5-2.4 V) after successive cycling.
- Magnetic susceptibility measurement (SQUID) provided information on the redox mechanism where the change in average transition metal ion oxidation state of the TODA HE5050 cathode during high-voltage (4.5 V *vs.* Li/Li^+) holding was determined.
- TEM and SQUID results were correlated to provide detailed insights to structural degradation pathways of TODA HE5050 during high-voltage (4.5 V *vs.* Li/Li^+)

holding; these results showed oxygen loss followed by migration of transition metal ions into the lithium layer during the hold.

In this report, recent results on magnetic susceptibility addressing the voltage fading issue in the Li-Mn-rich TODA HE5050 cathode material are presented. In order to understand this voltage fading mechanism, half coin cells were made and cycled at different cut-off voltages (4.2 V and 4.8 V cycled at 20 mA/g). In Figure 8, electrochemical cycling data to

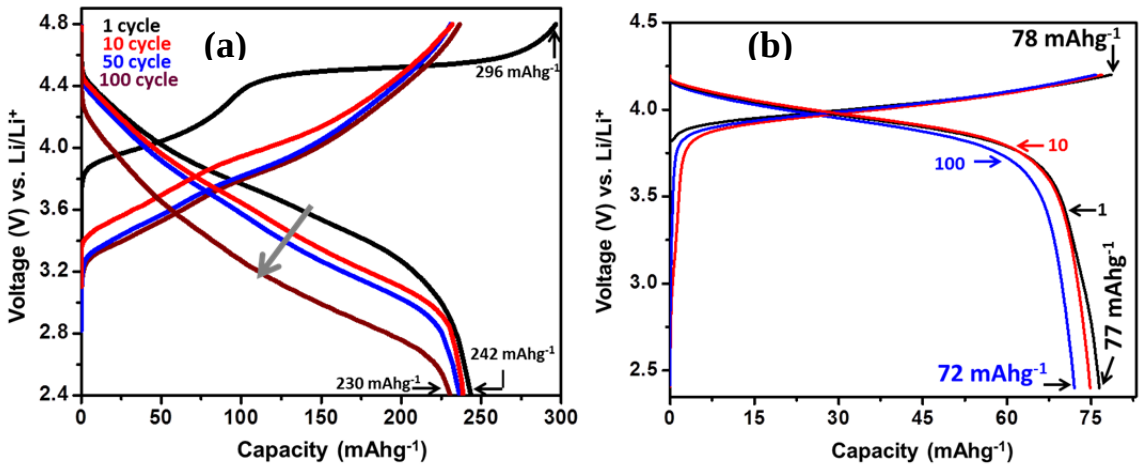

Figure 8. Charge-discharge profiles of TODA HE5050 cathode half coin cells at cut-off voltages of a) 4.8 V and b) 4.2 V.

4.2 V and 4.8 V is presented, which shows a substantial suppression of the voltage profile after 100 cycles when cycled to 4.8 V. Magnetic susceptibility data was collected from these cathodes after 100 cycles, and the results are shown in Figure 9. The DC magnetization was measured as a function of temperature using a Quantum Design Magnetic Property Measurement System. Each sample was first cooled to 5 K in zero field followed by application of a magnetic field of 100 Oe, and the data was collected from 5 K to 320 K (zfc). The samples were also cooled in the applied field from 320 K down to 5 K, while measuring magnetization (fc). Initially, magnetic ordering was detected in the starting electrode, which was attributed to the presence of cation ordering of Li^+ with Mn^{4+} and confirmed the presence of the Li_2MnO_3 phase.[2] Interestingly, after 100 charge-discharge cycles to 4.8 V, the magnetic ordering vanishes. However, magnetic ordering was still present even after 100 cycles to 4.2 V, which indicates that activation of Li_2MnO_3 did not occur. However, for activation, the cut-off voltage should be higher than 4.4 V in order to extract the Li^+ from the transition metal layer. Therefore, it can be concluded that the activation of Li_2MnO_3 plays an important role in the voltage fading mechanism. We are currently pursuing neutron diffraction experiments in order to investigate the mechanism of this voltage fading behavior of the TODA HE5050 cathode.

[2] David Wood; ABR program quarterly report Q3, FY2012

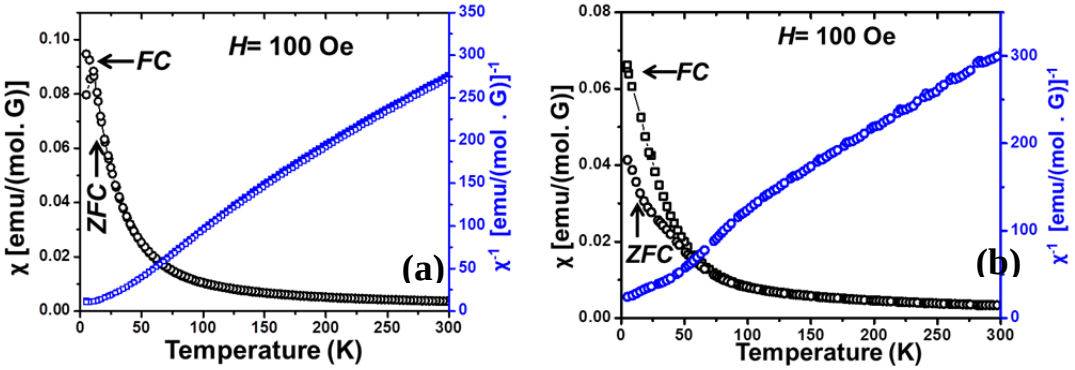

Figure 9. Magnetic susceptibility data from cycled TODA HE5050 cathodes after 100 cycles; cut-off voltages were a) 4.8 V and b) 4.2 V.

Publications, Reports, Intellectual Property or Patent Applications filed this quarter.

1. D. Mohanty, S. Kalnaus, R. Meisner, K. J Rhodes, E. A Payzant, D.L Wood, C. Daniel, "Structural Transformation of a Lithium-Rich $Li_{1.2}Co_{0.1}Mn_{0.55}Ni_{0.15}O_2$ Cathode During High Voltage Cycling Resolved by In Situ X-Ray Diffraction", *Journal of Power Sources* **229** (2013) 239.
2. D. Mohanty, S. Kalnaus, R. Meisner, A. Safa-Sefat, J. Li, K.J. Rhodes, E.A Payzant, D.L Wood, C. Daniel, "Structural Transformation in a $Li_{1.2}Co_{0.1}Mn_{0.55}Ni_{0.15}O_2$ Lithium-Ion Battery Cathode During High-Voltage Hold", *RSC Advances,* Under Review (2013).
3. D. Mohanty, A. Safa-Sefat, S. Kalnaus, J. Li, R.A. Meisner, E.A. Payzant, D.P. Abraham, D.L. Wood, and C. Daniel, "Investigating Phase Transformation in $Li_{1.2}Co_{0.1}Mn_{0.55}Ni_{0.15}O_2$ Lithium-Ion Battery Cathode During High-Voltage Hold (4.5 V) via Magnetic, X-ray Diffraction and Electron Microscopy Studies", *Journal of Materials Chemistry A*, Under Review (2013).
4. D.L. Wood, J. Li, D. Mohanty, C. Daniel, B. Armstrong, R. Dinwiddie, A. Safa-Sefat, H. Wang, R. Trejo, N. Gallego, C. Contescu, J. Howe, R. Meisner, J. Kiggans, and B. Brown, "Advanced Materials Processing and Novel Characterization Methods for Low-Cost, High Energy-Density Lithium-Ion Batteries" Advanced Automotive Battery Conference 2013, Pasadena, CA, February 4-8, 2013.
5. D. Mohanty, S. Kalnaus, R.A. Meisner, J. Li, E.A. Payzant, D.L. Wood, and C. Daniel, "Investigating the Voltage Fading Mechanism in $Li_{1.2}Co_{0.1}Mn_{0.55}Ni_{0.15}O_2$ Lithium-Ion Battery Cathode by *In-Situ* X-ray Diffraction Studies", ACS Spring 2013, New Orleans, LA, April 7-11, 2013.
6. D. Mohanty, A. Safa-Sefat, J. Li, S. Kalnaus, R.A. Meisner, D.L. Wood, and C. Daniel, "Investigating the Cation Ordering in $0.5Li_2MnO_3 - 0.5LiNi_{0.375}Co_{0.25}Mn_{0.375}O_2$ Cathode by Magnetic and Transmission Electron Microscopy Studies", ACS Spring 2013, New Orleans, LA, April 7-11, 2013. (Selected for ACS Presentation On Demand)

TASK 3
Abuse Tolerance Studies

Project Number: 3.2 (ES036)

Project Title: Abuse Tolerance Improvements

Project PI, Institution: Chris Orendorff, Sandia National Laboratories

Collaborators (include industry): ANL, INL, BNL, ORNL, NREL, Physical Sciences Inc.

Project Start/End Dates: 10/1/2012-9/30/2013

Objectives: The objective of this work is to develop inherently abuse tolerant lithium-ion cell chemistries. This involves understanding the mechanisms of cell degradation and failure, determining the effects of new materials & additives on abuse response, and cell level abuse testing and cell characterization to quantify improvements

Approach: Materials to full cell characterization to determine inherent safety and reliability of the most advanced lithium-ion chemistries. Approaches include a suite of battery calorimetry techniques (microcal, DSC, TGA/TDA, isothermal, ARC), abuse tests (electrical, mechanical, thermal), and analytical diagnostics (electrochemical characterization, optical spectroscopy, mass spectrometry, computed tomography, electron microscopy, etc.)

Milestones:
(a) LiF/ABA electrolyte development (ON GOING, on schedule)
(b) Cell prototyping optimization & collaboration with other Labs (ON GOING, on schedule)
(c) Overcharge shuttle evaluation in full cells (COMPLETED Q1 FY13)
(d) Ionic liquid electrolyte development (ON GOING, on schedule)

Financial data: Total budgeted $1.0M; received $500K

PROGRESS TOWARD MILESTONES

(a) LiF/ABA electrolyte development. As noted in Q3-Q4 of FY12, one challenge with LiF/ABA electrolyte is the fade observed at the negative electrode. One objective for FY13 is to improve capacity loss and SEI formation at the negative electrode with LiF/ABA. Figure 1 shows one example of improving the fade challenge with the addition of 2% VC in NMC523 cells with LiF/ABA electrolyte. Work is ongoing with different electrolyte additives to improve the performance of LiF/ABA electrolytes in cells and will be reported in Q2. Future work for FY13 will also focus on transferring the synthesis of ABA molecules to the ANL facility.

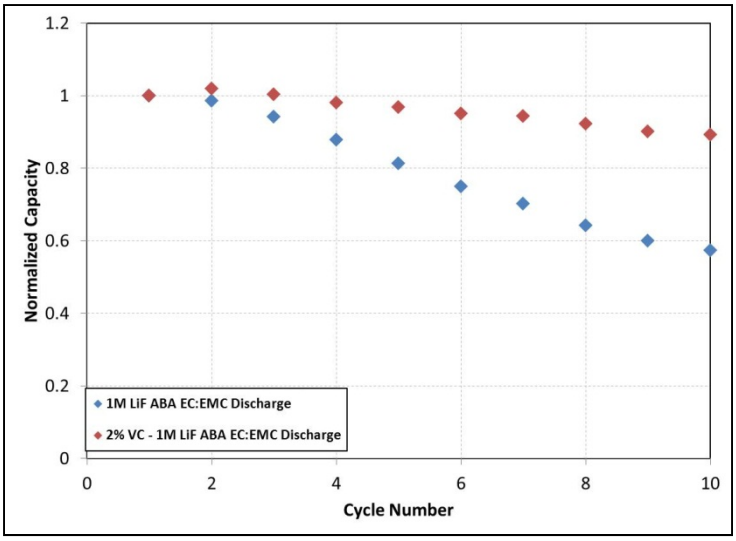

Figure 1. Discharge capacity of NMC523/Graphite cells + LiF/ABA electrolyte with (red) and without (blue) 2% VC additive.

(b) Cell prototyping optimization & collaboration with other Labs. One key difference in processing steps between SNL and the other Labs, is that SNL has traditionally used a milling step during the electrode slurry formulation step. This is largely historical because of particle in homogeneity of early generation active materials. Materials screening at ANL found that the milling step actually leads to particle fracturing of the Toda NMC523 (Figure 2). While no significant performance loss was measured using our electrodes over a relatively small number of cycles, the pulverized active material would likely impact long-term performance. As a result, the milling step has been removed from our electrode processing and will be evaluated for all new materials during the process development phase. This example highlights the collaborative nature of this interaction with other Labs to make overall improvements for ABR.

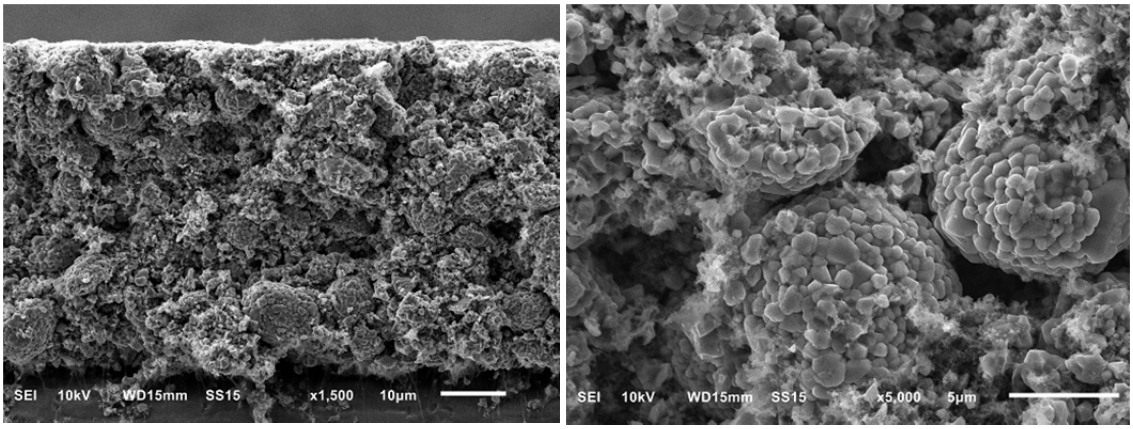

Figure 2. SEM images of a NMC523 electrode with milled and fractured NMC

(c) Overcharge shuttle evaluation in full cells. The bulk of the characterization of RS2 was completed in Q1 FY13. As part of this project, SNL worked to quantify the heat

output of cells with the shuttle at different charge rates, quantify the heat transfer efficiency of the shuttle activity, determined the cell balancing ability in batteries, and evaluated improvements in overcharge abuse of $LiFePO_4$ cells. At a 1C charge rate, cells can be overcharged to 260% SOC without any observable cell failure (cell cool to ambient temperature without incident post-test, Figure 3). To further demonstrate the effectiveness of the shuttle, cells were cycled after the overcharge test and show only an 8-10% capacity loss relative to fresh cells (Figure 3). This retention of electrochemical functionality is additional support for the efficacy of RS2 as an overcharge protection approach.

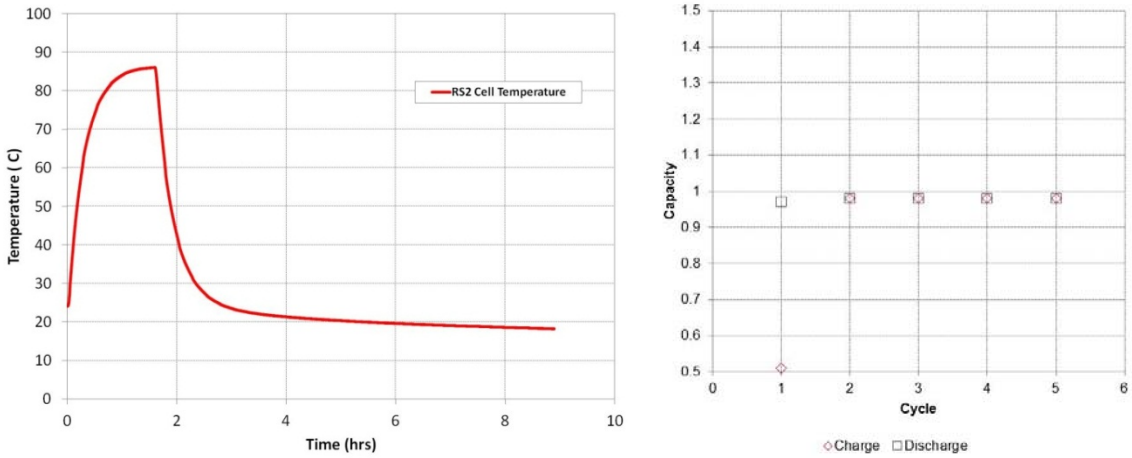

Figure 3. RS2 cell temperature during and after a 1C overcharge test (right) and charge/discharge capacity of a 1.070 Ah cell after overcharge to 260% SOC. Final capacity of the cell is 0.990 Ah

(d) Ionic liquid electrolyte development. Q1 focused on the development of useable electrolyte formulations of the candidate ionic liquids (ILs). While the viscosities of the three candidates developed under this program are on the order of 150-180 cP, they are significantly greater with the addition of lithium salt. The most successful formulations to date are mixtures with conventional carbonate solvents in large quantities (on the order of 1:1). Figure 4 show discharge curves for NMC523 cells with conventional electrolyte (green) and with 0.7 M LiTFSI in IL:EC:EMC (navy and blue, replicates) at room temperature. The ionic liquid electrolyte cells show modest performance and do have some measurable capacity loss compared to the conventional electrolyte cells. Work is ongoing in Q2 to optimize formulations and evaluate performance in cells.

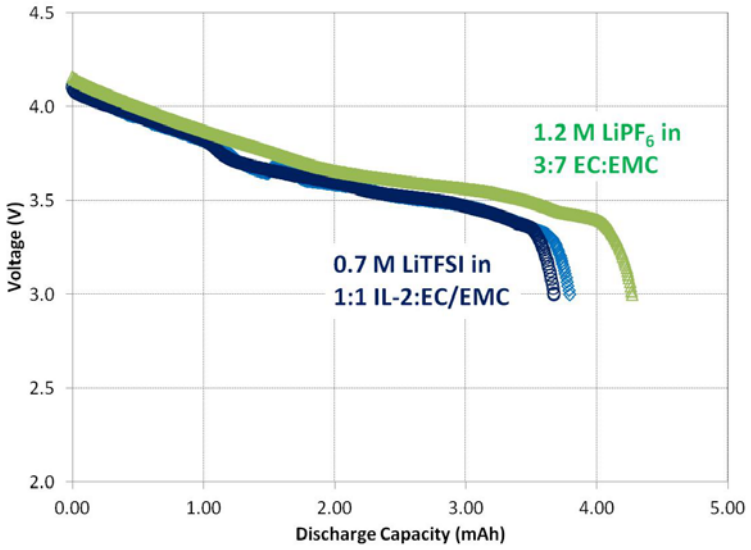

Figure 4. Discharge capacities for NMC523 2032 coin cells with conventional electrolyte (green) and ionic liquid containing electrolytes (navy and blue).

TASK 3
Abuse Tolerance Studies

Project Number: 3.3 (ES037)

Project Title: Overcharge Protection for PHEV Batteries

Project PI, Institution: Guoying Chen, Lawrence Berkeley National Laboratory

Collaborators: Robert Kostecki, John Kerr, Vince Battaglia, Marca Doeff, Gao Liu, Quy Ta and Brian Nguyen (American Dye Source, Inc.).

Project Start Date: March 2009

Objectives: Develop a reliable, inexpensive overcharge protection system. Use electroactive polymers for internal, self-actuating protection. Minimize cost, maximize rate capability and cycle life of overcharge protection for high-energy Li-ion batteries for PHEV applications.

Approach: Our approach is to use electroactive polymers as self-actuating and reversible overcharge protection agents. The redox window and electronic conductivity of the polymer will be tuned to match the battery chemistry for non-interfering cell operation. Rate capability and cycle life of the protection will be maximized through the optimization of polymer composite morphology and cell configuration.

Milestones:

a) Investigate rate performance and cycle life of Li-ion cells protected by electrospun electroactive-fiber-composite separators (January 2013). **Complete**

b) Evaluate alternative placements of the fiber-composite membranes in battery cells (March 2013). **On schedule**

Financial data: $240K/FY2012

PROGRESS TOWARD MILESTONES

In this quarter, we prepared bilayer fiber membranes consisting of a high-voltage electroactive polymer, poly[(9,9-dioctylfluorenyl-2,7-diyl)] (PFO) on one side, and a low-voltage polymer, poly(3-butylthiophene) (P3BT) on the other. Chloroform solutions containing either PFO or P3BT were used for electrospinning, with a small amount of polyethylene oxide (PEO) added to adjust solution viscosity and to ensure the formation of polymer fibers during the process. After the initial deposition of PFO/PEO fibers on an aluminum collector, the P3BT/PEO polymer fibers were then directly electrospun onto the surface of the PFO/PEO film. The prepared composite membrane was peeled from the Al substrate and the PEO polymer was removed by sonication in water. Fig. 1 shows the top-view SEM images of a 50 μm-thick PFO/P3BT (weight ratio 3:1) fiber membrane

obtained from the PFO (Fig. 1a) and P3BT (Fig. 1b) sides, respectively. It is clear that both types of electroactive fibers are well-connected in a highly porous structure, which suggests that the membrane may be capable of rapid transport of both ions and electrons. The individual layer thickness is easily adjusted by controlling the amount of each polymer used during electrospinning.

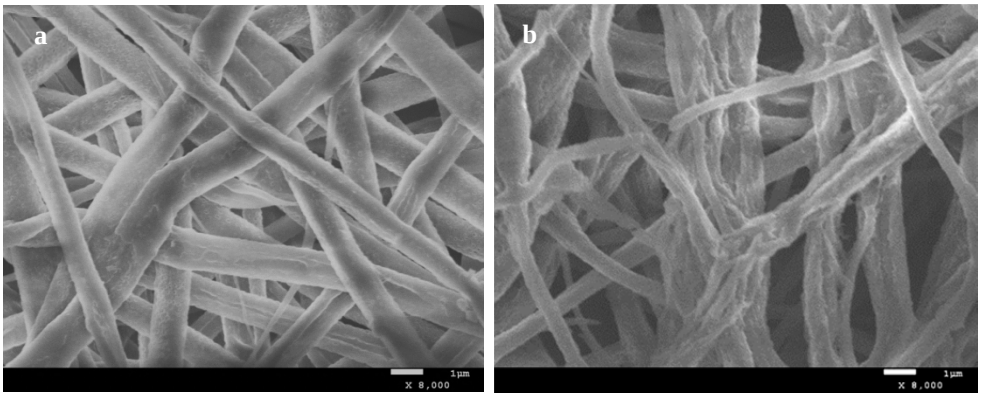

Figure 1. Top-view SEM images of an electrospun PFO/P3BT composite membrane: a) PFO side and b) P3BT side.

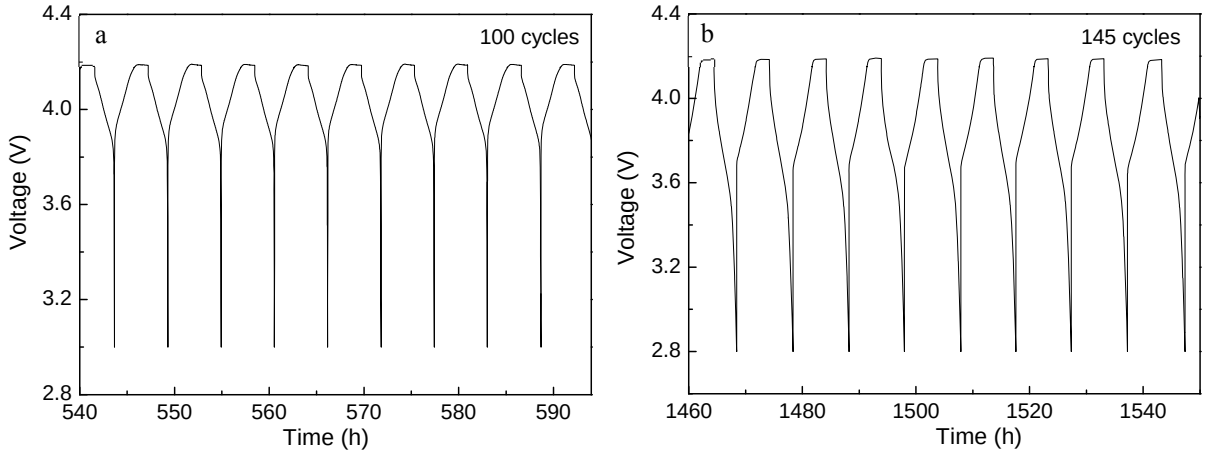

Figure 2. Cycling voltage profiles of a) $Li_{1.05}Mn_{1.95}O_4$ and b) $LiNi_{0.8}Co_{0.15}Al_{0.05}O_2$ half-cells overcharge protected by the electrospun PFO/P3BT composite separator.

The cycling performance of a spinel $Li_{1.05}Mn_{1.95}O_4$ half-cell overcharge-protected by the electrospun PFO/P3BT composite separator is shown in Fig. 2a. When cycled at a C/2 rate and 85% overcharge, a steady state was reached at 4.2 V, and the cell maintained its discharge capacity for more than 100 cycles. Fig. 2b shows the performance of a protected $LiNi_{0.8}Co_{0.15}Al_{0.05}O_2$ (Gen 2) half-cell. At C/4 rate and 65% overcharge, a constant voltage was reached at 4.2 V and the cell delivered steady performance for more than 145 cycles. In both cases, the upper limiting voltage is significantly lower compared to that of the previous cells protected by the PFO and P3BT composites with either a

microporous or glass-fiber membrane. This is consistent with reduced internal resistance and improved power density in the electrospun fiber separators. Further experiments on their rate capabilities are currently under investigation.

Publications, Reports, Intellectual property or patent application filed this quarter. (Please be rigorous, include internal reports--invention records, etc.)

1. Bin Wang, Thomas Richardson, and Guoying Chen, Stable High-Rate Overcharge Protection for Rechargeable Lithium Batteries, submitted to *Energy Environ. Sci.* (**2013**).